An auto-regulatory module controls fat metabolism in *Caenorhabditis elegans*

Inauguraldissertation

zur

Erlangung der Würde einer Doktorin der Philosophie

vorgelegt der

Philosophisch-Naturwisschenschaftlichen Fakultät

der Universität Basel

von

Cornelia Habacher

aus Österreich

Basel, 2018

Genemigt von der Philosophisch-Naturwissenschaftlichen Fakultät auf Antrag von:

Prof. Dr. Michael Hall

Dr. Rafal Ciosk

Dr. Hugo Aguilaniu

Basel, den 23. Mai 2017

Prof. Dr. Martin Spiess

(Dekan der Philosophisch-Naturwissenschaftlichen Fakultät der Universität Basel)

TABLE OF CONTENTS

SUMMARY

Obesity and obesity-related diseases such as type-2 diabetes or metabolic syndrome are on the rise word-wide (Ng et al. 2014). The negative aspects of obesity on the health of individuals is accompanied by an increasing financial burden for the global economy. Excess adipose tissue is often perceived as an indication of poor dietary choices and a sedentary lifestyle. However, compelling evidence from diverse model organisms and humans suggest that genetic make-up influences most aspects of fat metabolism and therefore the likelihood to develop obesity (Min, Chiu, and Wang 2013; Yazdi, Clee, and Meyre 2015). Hence, careful dissection of the underlying genetic regulations of fat metabolism to identify new putative targets for treatment is essential.

We successfully used *Caenorhabditis* elegans as a model organism to uncover and describe a novel auto-regulatory module, which we found is essential for wild-type levels of body fat. Utilizing cold-sensitivity as readout, we identified a hitherto uncharacterized gene, *C30F12.1*, which we named *rege-1* (REGnasE-1 homolog) after its mammalian homolog the PIN-domain endonuclease ZC3H12A/Regnase-1/MCPIP1. Regnase-1 negatively regulates pro-inflammatory cytokines via internal cleavage of their 3` untranslated region (3`UTR) (Iwasaki et al. 2011; Matsushita et al. 2009). Similarly, *C. elegans* REGE-1 targets the transcription factor ETS-4 and cleaves its mRNA within the first third of its 3`UTR. Knockout of *rege-1* causes a strong loss in overall body fat, developmental delay and a transcriptional upregulation of fat metabolic and innate immunity genes, depending on ETS-4. We also provide evidence that ETS-4 transcriptionally activates (directly or indirectly) *rege-1,* thereby forming an auto-regulatory feedback loop. REGE-1::GFP is mainly localized in the first four cells of the intestine adjacent to the pharynx and the ETS-4/REGE-1 module is transcriptionally upregulated upon re-feeding following long-term starvation. This, together with the observation that metabolic and immunity genes are induced upon loss of *rege-1* suggests that the ETS-4/REGE-1 module might have a role in bacteria clearance, nutrient uptake and/or defense against pathogens.

1. INTRODUCTION

1.1 Fat metabolism in *Caenorhabditis elegans*

Fat, carbohydrate and protein comprise the three macro nutrients essential to life. Fats are esters of a glycerol and three fatty acids (=triglyceride) and belong to the class of lipids. They are either stored, utilized for energy production or can serve structural and signaling purposes. In addition, dietary fats are essential for the uptake of fat-soluble vitamins such as vitamin A. Therefore, precise regulation of breakdown, storage and modification of lipids, together with their de-novo synthesis, known as fat metabolism, is indispensable for every organism. In mammals, fat is stored in designated adipose tissue that can be roughly subdivided into brown, white and beige fat. In contrast, the main metabolic tissue in *C. elegans* is the gut, in which the vast majority of fat is stored and processed (Srinivasan 2015; Watts 2009). Additionally, fat deposits are visible in the oocytes and the hypodermis (Chen et al. 2016; O'Rourke et al. 2009; Schneider 1996; Zhang, Trimble, et al. 2010). Although *H. sapiens* and *C. elegans* are separated by more than 600 million years of evolution (Ruvkun and Hobert 1998), many aspects of fat metabolism are shared and *C. elegans* has proven to be an excellent model organism to study the genetic influence on body fat (Lemieux and Ashrafi 2015; Zheng and Greenway 2012). Among the general advantages of this model organism are a short life cycle of about three days, high number of progeny (approximately 250 per animal) with negligible genetic variation, a transparent body, small size and low culture expenses. Its transparent body makes it fairly easy to study the influence of genetic mutations and chemical compounds on the distribution and quantity of fat. Lipophilic dyes, fluorescently labeled fatty acids (e.g. BODIPY), GFP-tagged proteins or staining-free methods can be used to visualize *C. elegans* fat stores. The most commonly utilized dyes are Oil red O, Sudan black and Nile red (Yen et al. 2010). The lipophilic dye Oil red O stains neutral lipids and was recently established in 96-well plate format, which makes it feasible to perform large-scale library screens of either chemical compounds or RNAi-knockdowns (Wahlby et al. 2014). The obvious downside of these dye-based methods is that they are unsuitable for live imaging as they require fixation of the specimen. To overcome this issue, different GFP tagged proteins which co-localize with lipid droplets (LDs) are used for live imaging of fat stores. DHS-3 was identified in a mass spectrometry analysis of LD resident proteins (Zhang et al. 2012). Consistently, DHS-3::GFP localizes to LDs, forming ring structures and can be used as a read out for number and size of these fat compartments (Zhang et al. 2012). Perilipin 1 (PLIN-1) is a lipid-droplet associated protein naturally not present in *C. elegans*, however when expressed in these animals it localizes to LDs and was successfully used to identify known and novel lipid associated proteins by extraction of LDs and follow-up mass-spectrometry (Liu et

al. 2014). Coherent anti-strokes raman scattering (CARS) microscopy is a staining-free method that uses the physical properties of fat to assess stores in living *C. elegans* (Hellerer et al. 2007; Tserevelakis et al. 2014). Another advantage of the *C. elegans* model system is that small chemicals such as fatty acids or pharmacological compounds can be conveniently administered by feeding. For example mutations in *fat-3,* an enzyme that catalyzes the rate limiting step in polyunsaturated fatty acid (PUFA) production, can be rescued by dietary supplementation of the missing PUFAs (Watts et al. 2003). Likewise exogenous serotonin mitigates neurological defects of loss of TPH-1, the enzyme that catalyzes the rate-limiting step in serotonin synthesis (Li et al. 2013). Biochemical assays can be limited due to the rigid cuticle and the fact that a whole animal lysis contains a mixture of different tissues. However, many tools for metabolic research have been adjusted to nematodes. Among the most important are: 1. whole lipid analysis (summarized in (Witting and Schmitt-Kopplin 2016)) 2. the extracellular flux technology, marketed by Seahorse, with which oxygen consumption and glycolysis can be measured (Koopman et al. 2016; Luz et al. 2015), and 3. whole animal metabolomics reviewed in (von Reuss and Schroeder 2015).

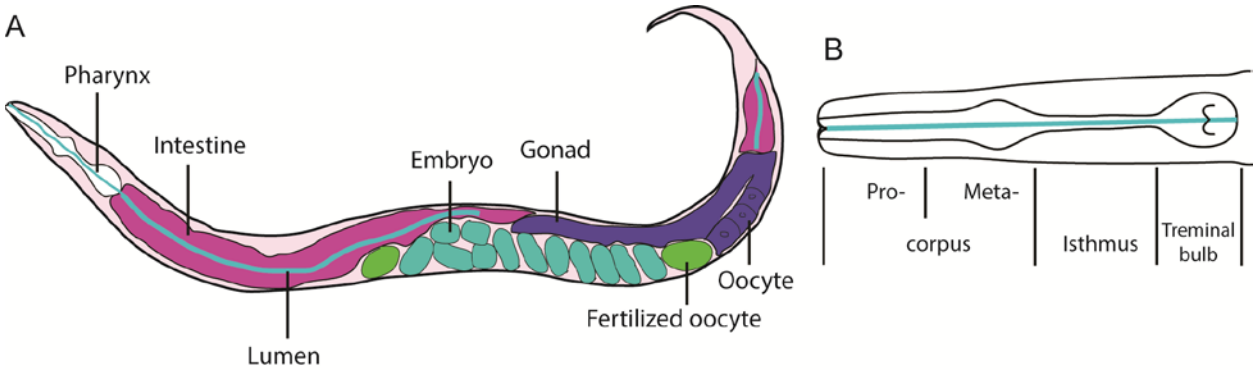

Figure 1: Schematic of a *C. elegans* body plan (A) and the pharynx (B).

1.1.1 Absorption of nutrients

The intestine of *C. elegans* is one of the largest tissues (Figure 1A) of the animal and fulfils a variety of tasks which are performed by distinct organs in higher organisms: digestion; synthesis and storage of macro and micro nutrients; defense against pathogens and, during adulthood, it provides the developing oocytes and embryos with nutrients. The intestine consists of 20 polyploid epithelia cells which are arranged in pairs and form a tube that reaches from the end of the pharynx-intestinal valve through the whole animal. *C. elegans* feed by contracting and relaxing the pharyngeal muscle, which can be subdivided into: procorpus, metacorpus, isthmus and posterior bulb/grinder (Figure 1B). At the beginning of one contraction/relation cycle the lumen of the corpus and the anterior isthmus are opened by contraction and bacterial suspension is sucked in, while at the same time contraction of the posterior bulb leads to

grinding of already trapped bacteria. During the relaxation state, liquid is expelled from the corpus into the environment while fresh bacteria are trapped and the crushed bacteria in the posterior bulb released into the pharyngeal-intestinal valve from where they enter the intestine (Avery and Shtonda 2003; Fang-Yen, Avery, and Samuel 2009). The crushing of bacteria serves a dual purpose: Firstly, to avoid any live bacteria entering the gut, thereby reducing the risk of infection and, secondly, to release nutrients. The lumen of the intestine, similar to the stomach in higher organisms, is slightly acidic (Chauhan et al. 2013), which facilitates digestion of macromolecules and provides a suitable environment for digestive enzymes. In addition, a whole range of different lysosomal enzymes, proteases and lipases are expressed by the intestinal cells and partially released into the lumen (McGhee et al. 2007) to facilitate digestion of bacterial content. Subsequently, nutrients have to pass through the intestinal cells membrane, either passively (e.g. free fatty acids) or are actively transported across the membrane. Di- and tri-peptides are taken up with the help of the high capacity/low affinity peptide transporter PEPT-1, which transports a wide range of up to 8000 different peptides (Spanier et al. 2009). Its functionality depends on the proton transporter NHX-1, which increases intestinal cell pH (Nehrke 2003). Loss of *pept-1* increases overall fat of the animals, which is likely facilitated by an accelerated absorption of free fatty acids from the intestine (Spanier et al. 2009). The transport of fatty acids across the membrane of intestinal cells might be facilitated by ACS-20 and ACS-22, both orthologs of the mammalian fatty acid transport protein 1 (FATP1) and FATP4. By homology, ACS-20 and ACS-22 likely serve dual functions: as Acetyl-CoA synthetases of very long fatty acids (ACSVL) and as fatty acid transporters. The role of ACS-20 and ACS-22 as ACSVL was confirmed recently and it was shown that human FATP4 can rescue *acs-20;acs-22* mutant phenotype, indicating high functional conservation of these proteins (Kage-Nakadai et al. 2010). ACS-22 is part of the TAG synthesis complex, is important for expansion of lipid droplets in *daf-22 (DAF-22* is a peroxisome-specific thiolase) mutants (Li, Xu, et al. 2016) and is required for iron-induced lipid uptake (Wang et al. 2016). Thus, although *acs-20 and acs-22* seem to be the only homologs of mammalian FATP (Dourlen et al. 2015; Kage-Nakadai et al. 2010), whether they really function as sole fatty acid transporters in *C. elegans* needs further investigation. Glucose transport is mediated by GLUT transporters in mammals. The *C. elegans* genome encodes eight genes with homologies to these mammalian proteins, however, only *fgt-1* (facilitated glucose transporter, isoform 1), localized in the basolateral membrane of intestinal cells seems to encode for a functional glucose transporter (Feng et al. 2013; Kitaoka, Morielli, and Zhao 2013). Loss of *fgt-1* leads to decreased glucose transport, reduced glucose metabolism and prolonged life span (Feng et al. 2013). The life span extension seen in the insulin/insulin-like signaling-defective *daf-2* mutants seems to partially depend on reduced FGT-1 glucose transport function observed in these mutants (Feng et al. 2013; Kitaoka,

Morielli, and Zhao 2016). In addition, like *daf-2* mutants, *fgt-1* mutants exhibit increased overall fat in the intestine (Kitaoka, Morielli, and Zhao 2013).

1.1.2 Lipid composition and fat accumulation

Triglycerides are the main form of stored fats in *C. elegans* and make up about 45% of the total fat content (Brock, Browse, and Watts 2006). In addition, but much less prominent, mono- and di-glycerides are found (Srinivasan 2015). Natural triglycerides are composed of an ester of glycerol and three fatty acid chains of varying length with an even number of carbon atoms. Fatty acids can be mono- or polyunsaturated and a sophisticated network of elongases (ELOs) and fatty acid desaturases (FATs) increase the complexity of the lipid composition (Kniazeva et al. 2003; Watts and Browse 2002). The ratio of mono-unsaturated fatty acids (MUFAs) and poly-unsaturated fatty acids (PUFAs) depend on species of bacteria in the diet as well as ambient temperature (Brooks, Liang, and Watts 2009; Tanaka et al. 1996). Misbalance can have severe consequences on the animals` physiology and behavior. The phenotypes range from neurological defects to developmental delay and, in case of total loss of PUFAs as seen in the *fat-5/fat-6/fat-7* triple mutants, to embryonic lethality (Kniazeva et al. 2003; Lesa et al. 2003; Watts et al. 2003). Very recently it was shown that an increase in MUFA, but not PUFA, seen in mutants of the H3K4me3 modifier, can extend the animals' lifespan (Han et al. 2017). In addition to triglycerides, the second major class of lipids present in *C. elegans* are phospholipids. This pool of lipids is mainly found in cellular membranes and comprises: 54.5% ethanolamine glycerophospholipid (EGP), 32.3% choline glycerophospholipid (CGP), 8.1% sphingomyelin and 5.1% others (Satouchi et al. 1993).

As *C. elegans* lacks specialized organs for catabolic and anabolic fat metabolism, digestion of dietary fats; fat synthesis and fat storage need to be spatially and temporally coordinated within the same gut cells. This can either be accomplished by high compartmentalization or temporal restriction of, for example, lipase expression. In the gut, most fat is stored in specialized lipid droplets (LDs) ranging from 50 nm to 3000 nm (Zhang et al. 2012), that are surrounded by a monolayer of phospholipids and are filled with neutral lipids such as triglycerides (Zhang, Box, et al. 2010). LDs are derived from the endoplasmic reticulum and expand depending on the need for fat storage (Zhang, Box, et al. 2010). The expansion of LD is accomplished by acetyl CoA synthase-22 and diacylglycerol acyl transferase-2, the *C. elegans* homologs of FATP1 and DGAT2, respectivley (Xu, Zhang, et al. 2012). These two well-conserved proteins co-localize on ER and LD membranes and a loss of either FATP1 or DGAT2 function blocks LD expansion. When LDs are filled with sufficient triglycerides, the lipid droplets bud off from the ER. This is facilitated by FIT (fat storage inducing transmembrane) proteins; the homolog in *C. elegans* is encoded by *fitm-2* and

its loss causes reduced LD size accompanied by muscular defects and high lethality (Choudhary et al. 2015). The final step of LD budding, fusion of the ER membrane to release the droplet, is aided by the GFPase atlastin (ATLN-1) (Klemm et al. 2013). Lysosome related organelles (LROs; also termed gut granules) which are compartments similar to lysosomes and peroxisomes contain neutral lipids, but do not represent a major site of fat storage in *C. elegans* (O'Rourke et al. 2009). As the amount of live Nile red staining (which marks LROs) increases upon fasting, LROs where suggested to be the site of initial lipid beak down (O'Rourke et al. 2009). In addition to the gut, fat staining can also be seen in the hypodermis. However, whether the hypodermis is a classical fat storage organ or if fat droplets are stored for local energy production is uncertain.

In order to ensure sufficient energy supply for the next generation, lipids and other nutrients from the gut are packed into yolk particles, secreted into the pseudocoelomic space and taken up by the oocytes via receptor-mediated endocytosis (Kimble and Sharrock 1983; Schneider 1996; Sharrock et al. 1990). This is accomplished by the vitellogenin (yolk proteins) proteins VIT-2, VIT-3, VIT-4,VIT-5 and VIT-6 (Spieth et al. 1991), which are distantly related to the mammalian lipid transport protein ApoB-100 (Smolenaars et al. 2007). As this process places a high burden on the animal, it is tightly transcriptionally and post-transcriptionally controlled (DePina et al. 2011; Goszczynski et al. 2016). In the long-lived mutant *daf-2*, *vit-2* expression is strongly decreased and thereby energy is conserved (Goszczynski et al. 2016; Mendenhall et al. 2017).

1.1.3 Lipid degradation

The lipase-mediated hydrolysis of dietary triglycerides (TAGs) into glycerol and free fatty acids (FAs) serves two major purposes: Firstly, free FAs are available as building blocks to form membrane lipids, lipid-based signaling molecules and triglycerides for storage and secondly, FAs can be degraded via β-oxidation in peroxisomes and mitochondria to provide energy. Most lipases are expressed in the intestinal cells and are either secreted into the gut lumen or retained within the cell to facilitate degradation of dietary lipids and stored lipids, respectively. The *C. elegans* genome encodes a variety of lipases, many of which have been investigated with respect to starvation; examples include the fasting induced lipases *(fil-1/2), lipl-1-7* (Lipase like) or the adipose triglyceride lipase *atgl-1*. Their regulation will be discussed in detail in the chapter “1.1.5 Regulation of fat metabolism and alteration during different physiological conditions”. After hydrolysis of TAGs, FAs are transported to either mitochondria or peroxisomes, depending on their length. Understanding of these transport mechanisms is incomplete and therefore conclusions about the involvement of certain genes in this process can only be made via study of their homologs in the

mammalian system. Putative fatty acid binding proteins (FABPs) are encoded by *lbp-1-9* and *EEED8.3* (Mullaney and Ashrafi 2009). All but *lbp-4* and *lbp-8* contain a secretion signal. *lbp-1, lpd-2* and *lpd-3* were shown to be localized in the perivitellin space (a liquid filled clear zone between the embryo and the eggshell) and in the body wall muscles after hatching (Plenefisch et al. 2000). A clear connection between a *C. elegans* FABP homolog and fat metabolism was made with studies of LBP-5, which is expessed in various tissues including the intestine and the hypodermis and binds fatty acids *in vitro* (Xu, Joo, and Paik 2011). Loss of *lbp-5* leads to reduced ATP and lactate levels as well as a reduced abundance of mitochondrial and β-oxidation proteins (Xu, Choi, and Paik 2014). The mammalian CD36 (cluster of differentiation 36) is an integral membrane protein that binds a diverse class of ligands including long-chain fatty acids (Baillie, Coburn, and Abumrad 1996; El-Yassimi et al. 2008). Circulating fatty acids serve as metabolic signal that is sensed by CD36 in the brain and loss of neuronal CD36 increases feeding, body weight, and fat mass in rats (Le Foll et al. 2013; Le Foll, Dunn-Meynell, and Levin 2015; Moulle et al. 2013). *C. elegans* encodes six SCAVenger receptor (CD36 family) related proteins: *scav-1-6.* So far only *scav-3* was studied more closely and was found to be involved in maintenance of lysosome integrity and longevity (Li, Chen, et al. 2016). Thus, it remains to be shown whether this class of proteins has a direct role in *C. elegans* fat metabolism. Long, medium and small chain fatty acids are oxidized in the mitochondria, whereas very long fatty acids (22 or more carbons) are exclusively oxidized in the peroxisomes. FAs can enter the mitochondria only as acyl carnitines, which are generated by the CPT I (carnitine palmotoyl transferase) complex. They are then transported through the outer and inner mitochondria membrane by translocases and the carnitine is removed by the CPT II complex, making the FA available for β-oxidation. Each round of oxidation reduces the fatty acid chain by two carbon atoms, producing Acetyl-coA, which is then used to generate energy in form of ATP via the Krebs cycle. A simplified overview of fat synthesis and β-oxidation pathways with indicated putative *C. elegans* homologs for the respective mammalian enzymes is shown in Figure 2.

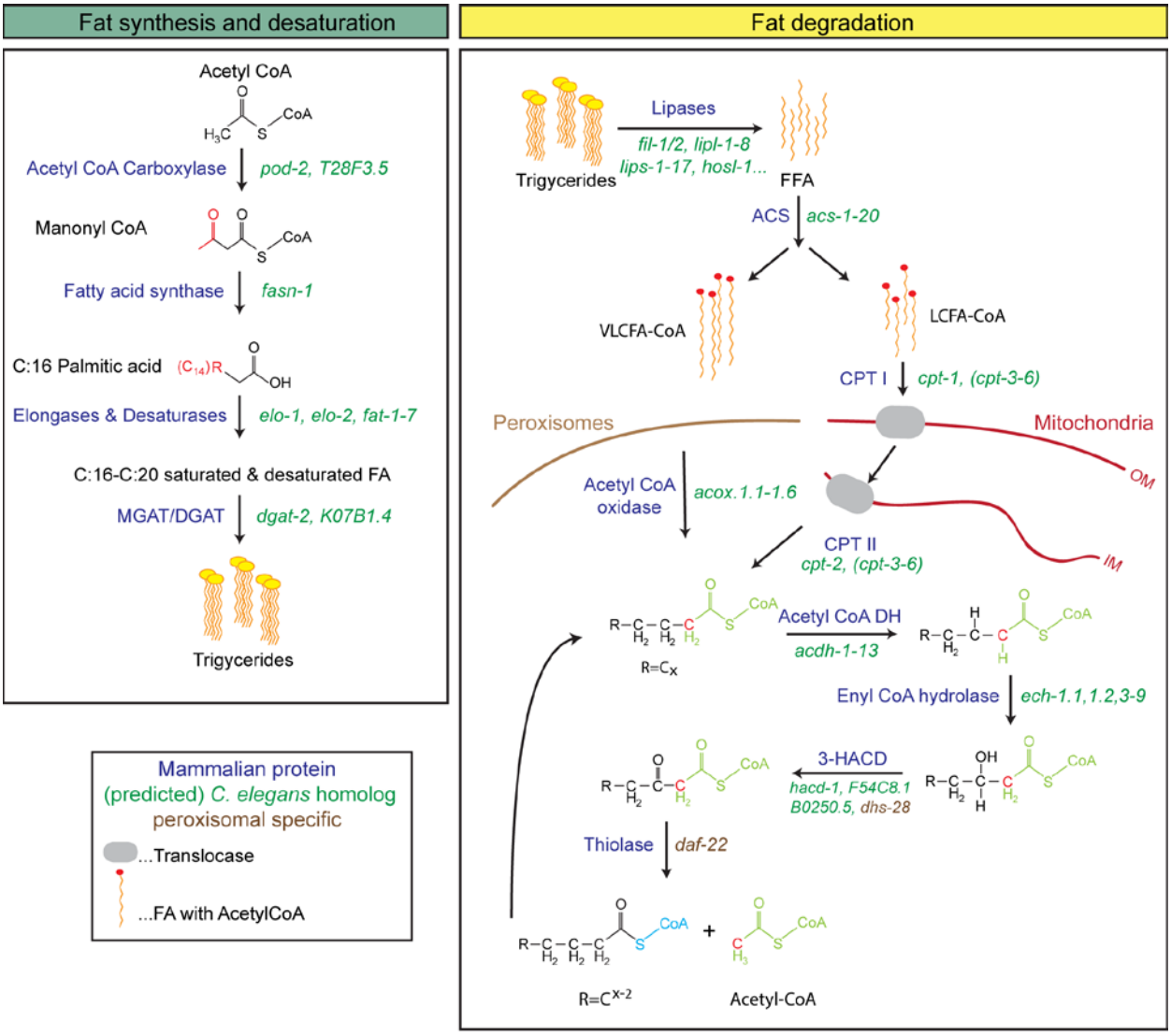

Figure 2: Schematic overview of the fat synthesis and degradation pathways.

Gene Ontology annotations from WormBase version WS258 (http://www.wormbase.org) were used to assign *C. elegans* homologs (in green) to the mammalian enzymes (in blue). Figure 3 of the review "Regulation of body fat in *Caenorhabditis elegans*" was used as basis for the graphic design (Srinivasan 2015). Abbreviations: ACS...acetyl CoA synthase, CPT-1/2...carnitine palmotoyl transferase, DH… dehydrogenase, 3-HACD...3-hydroxy acetyl CoA dehydrogenase, FFA...free fatty acid, (V)LCFA...(very) long chain fatty acid,M/DGAT...Mono-/Diacylglycerol acetyl transferase, OM…outer membrane, IM…inner membrane.

1.1.4 Signaling pathways regulating lipid metabolism

1.1.4.1 Insulin - daf-2

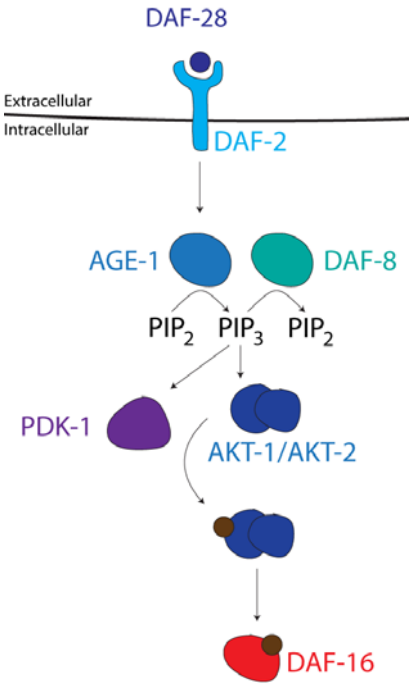

Figure 3: Insulin signaling pathway in fat metabolism: Activation of DAF-2 by an insulin-like peptide leads to the activation of a down-stream cascade, which ultimately causes DAF-16 inactivation by phosphorylation. See text for details.

The insulin-signaling-pathway is well-known for its influence on longevity; loss of function mutations in *daf-2*, the receptor for insulin, double the lifespan of *C. elegans* (Kenyon et al. 1993; Kenyon 2010). The signaling cascade downstream of DAF-2 is reviewed in (Altintas, Park, and Lee 2016; Murphy and Hu 2013). When DAF-2 is activated by binding to an insulin-like peptide (e.g. DAF-28), it recruits and activates the phosphoinositide 3-kinase, AGE-1, which coverts PIP_2 to PIP_3. PIP_3 leads to activation of the serine/threonine kinases PDK-1 and AKT-1/2, which cause the FOXO transcription factor DAF-16 to be phosphorylated. Phosphorylated DAF-16 is retained in the cytosol and prevented from entering the nucleus. Upon loss of *daf-2*, the phosphatase *daf-18*/PTEN which counteracts AGE-1 and AKT-1 activity, leads to an increase of dephosphorylated DAF-16 (Ogg and Ruvkun 1998). Consequently, DAF-16 is active and enters the nucleus to mediate the transcription of effector genes. Knock out of *daf-2* leads to an increase of overall body fat in *C. elegans*, which is mediated by *daf-16* (Ogg et al. 1997). How precisely loss of *daf*-2 mediates increased fat levels is, as yet, unknown.

1.1.4.2 TGFβ family - daf-7

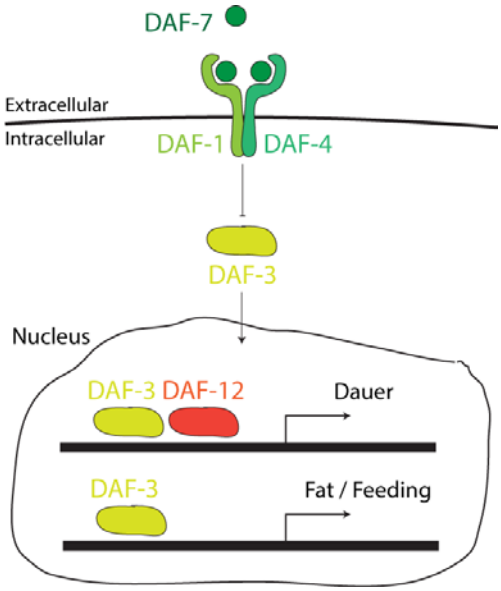

Figure 4: TGFβ signaling pathway in fat metabolism: Binding of DAF-7 to the receptors DAF-1/DAF-4 blocks DAF-3 activity and inhibits dauer entry. See text for details.

TGFβ (Transforming Growth Factor β) signaling mediates many aspects of development, cell specification, function and survival (Zhu and Burgess 2001). In *C. elegans* there are five ligands that belong to the TGFβ family: *dbl-1*, *unc-129*, *tig-2*, *tig-3*, *daf-7* (Gumienny and Savage-Dunn 2013). The latter was shown to be involved in fat metabolism. DAF-7 acts by binding to the receptors DAF-1 or DAF-4 (Estevez et al. 1993; Georgi, Albert, and Riddle 1990) which leads to inhibition of DAF-3, a receptor-associated coSMAD, and therefore blocks dauer-entry and promoted reproductive growth (Patterson et al. 1997). DAF-3 mediated dauer formation depends on the nuclear receptor (former: nuclear hormone receptor) DAF-12 (Antebi et al. 2000). Unlike the receptors DAF-1 and DAF-4 which are expressed in many neurons, DAF-7 only localizes in one specific pair of ASI sensory neurons (Ren et al. 1996) in the head. Mutation of *daf-7* (or *daf-1/daf-4*) leads to a 20-25% reduced feeding rate, accompanied by a 2.5-fold increase in total body fat (Kimura et al. 1997) and depend on *daf-3* (Greer et al. 2008). However, loss of *daf-12* does not rescue the increase of fat or feeding defect seen in *daf-7* mutants. Hence, fat and feeding related phenotypes are regulated independently from dauer entry (Greer et al. 2008). In addition, *daf-7* mutants exhibit increased de-novo fat synthesis by the fatty acid synthesis *fasn-1* (Antebi et al. 2000). Animals often leave their bacteria batch to find high quality food, which supports optimal growth and reproduction. This foraging behavior is, among others, also depending on *daf-7* (Milward et al. 2011). It is likely that DAF-7 under normal conditions controls normal fat accumulation whereas during unfavorable condition, which would lead to dauer formation, *daf-7* is inhibited and fat stores are increased to improve changes of survival.

1.1.4.3 Serotonin - tph-1

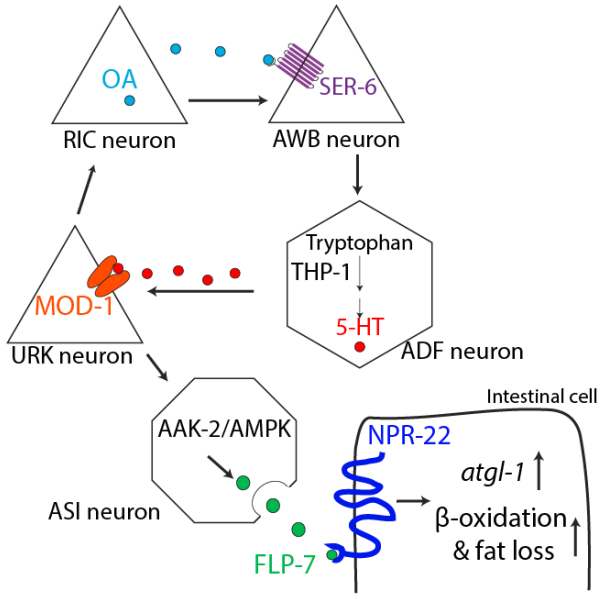

Figure 5: Serotonin signaling in fat metabolism See text for details. (Palamiuc et al. 2017) and (Srinivasan et al. 2008) were used as basis for the graphic design OA…Octopamine, 5-HT…5-hydroxytryptamine

Serotonin (5-hydroxytryptamine (5-HT)) is a potent neurotransmitter which, in *C. elegans*, is synthesized by the conserved tryptophan hydroxylase TPH-1. Many nutrition-related phenotypes such as feeding, egg laying, fat storage, reproductive life cycle and foraging are affected by loss of *tph-1* (Sze et al. 2000). In *tph-1* deletion animals, DAF-7::GFP fusion protein is strongly upregulated in the ASI neuron (i. e. TGFβ signaling is upregulated) and their increased fat storage partially depends on *daf-3*. Thus, the excess fat seen upon loss of *tph-1* can, to some extent, be explained by an increase of TGFβ signaling (Sze et al. 2000). Similar to mutants of the TGFβ pathway, serotonin modulates feeding behavior independent of fat accumulation (Noble, Stieglitz, and Srinivasan 2013). Serotonin is produced in the ADF chemosensory neurons and bound by MOD-1, a serotonin-gated chlorine channel (Ranganathan, Cannon, and Horvitz 2000). Activation of MOD-1 in the URX neurons ultimately induces lipid break down in the intestine, which leads to the accumulation of β-oxidation intermediates that modulate feeding behavior (Noble, Stieglitz, and Srinivasan 2013; Srinivasan et al. 2008). Thus, feeding is controlled by internal and external cues. After activation of MOD-1, FLP-7, a neuropeptide localized in ASI neurons (Palamiuc et al. 2017) is released depending on AMPK (AAK-29 signaling). When FLP-7 binds to NPR-22, a receptor expressed in the intestine, downstream signaling leads to transcriptional activation of the ligase ATGL-1 and increase of β-oxidation genes which diminishes fat stores (Palamiuc et al. 2017). In addition, MOD-1 activation also relays a signal to RIC neurons to release octopamine, the invertebrate analogue of adrenaline. Binding of octopamine by the G-protein coupled receptor, SER-6 in the AWB neurons a permissive cue to maintain 5-HT signaling by regulating *tph-1* expression (Noble, Stieglitz, and Srinivasan 2013).

1.1.5 Regulation of fat metabolism and alteration during different physiological conditions

During the course of an animals` life the availability of food and the way food is processed can vary tremendously. Depending on nutritional status, feeding is initiated or abandoned (Juozaityte et al. 2017) and while in young animals, only few ectopic fat reserves are visible, they become more pronounced in aged animals (Palikaras et al. 2017). These phenotypes are neither a passive consequence of time or the absence or presence of an outside stimulus (e.g. food density), but are actively regulated and can be genetically manipulated. Transcriptional regulation of fat metabolism is extensively studied in mammals and most key transcription factors have homologs in *C. elegans (Atherton et al. 2008; McKay, McKay, et al. 2003)*. The mammalian PPAR-γ (Peroxisome proliferator-activated receptor gamma) is a nuclear receptor expressed in adipose tissue (Fajas et al. 1997) where it stimulates lipid uptake and adipogenesis (Tontonoz, Hu, and Spiegelman 1994). The functional homolog in *C. elegans,* NHR-49 (Atherton et al. 2008), controls fat consumption and fatty acid composition (Taubert et al. 2006; Van Gilst et al. 2005) in *ad libitum* fed animals and activates β-oxidation upon food deprivation (Van Gilst, Hadjivassiliou, and Yamamoto 2005). Furthermore, *nhr-49* mutants exhibit a shortened life span, which is caused by their impaired expression of stearoyl CoA desaturase (Van Gilst et al. 2005). NHR-49 functions as transcriptional activator together with its co-activator MDT-15 (Taubert et al. 2008; Taubert et al. 2006) and represses transcription when paired with NHR-66 (Pathare et al. 2012). How exactly NHR-49 achieves target specificity and how its activity can be modulated depending on the cell's needs remain elusive. However, a recent study could show that distinct point mutations in the ligand binding domain affect NHR-49 target specificity suggesting that distinct ligands may influence NHR-49 activity (Lee et al. 2016).

Krüppel-like transcription factors have various roles in the regulation of an animal's physiology. In recent years, they have emerged as regulators of mammalian fat metabolism (Brey et al. 2009; Wu and Wang 2013). Similarly, in *C. elegans, klf-1* (Krüppel-like factor) is essential for fat metabolism, cell death and phagocytosis. (Hashmi et al. 2008). Loss of either *klf-1* or one of its orthologues *klf-2* or *klf-3* leads to an increase in overall body fat (Hashmi et al. 2008; Ling et al. 2017). KLF-2 and to some extent KLF-3, might influence lipid metabolism by regulating *lpd-1* (alternative name: *sbp-1*) and *lpd-2*, homologs of SREBP and NGDN (Neuroguidin), respectively (Hashmi et al. 2008). SREBPs (sterol regulatory binding protein) belong to a family of transcription factors that bind the conserved sterol element ATCACCCCAC (Kim et al. 1995) and regulate lipid metabolism in mammals (Eberle et al. 2004). SBP-1 together with its co-activator MDT-15 are needed for fatty acid homeostasis (Yang et al. 2006). Loss of *sbp-1* and *mdt-15* can be rescued by dietary supplementation with oleic acid, suggesting that their major physiological task is the regulation of oleic acid levels (Yang et al. 2006).

1.1.5.1 Starvation

Lack of food induces different behavioral and metabolic changes in animals. In *C. elegans,* depending on the developmental status, absence of nutrients can have life-changing consequences. L1 larvae hatch in an arrested state and only develop further in the presence of food (Baugh 2013). Later, when they reach L2 stage, the absence of food or high population density induces dauer formation, an alternative developmental stage associated with high fat stores, a thin needlelike body shape and high motility (Albert, Brown, and Riddle 1981; Gaglia and Kenyon 2009; Gems et al. 1998; Klass and Hirsh 1976; Ogg et al. 1997). Fat metabolism in dauer larvae is drastically altered and high fat content in the gut can be observed (Burnell et al. 2005). To avoid premature depletion of these fat deposits, AMPK monitors and inhibits the activity of the lipase ATGL-1 via phosphorylation (Narbonne and Roy 2009). This phosphorylation generates 14-3-3 binding sites which are recognized by PAR-5, a 14-3-3 protein orthologue, that sequesters ATGL-1 away from the lipid droplets, leading to reduced lipid hydrolysis and degradation of ATGL-1 (Xie and Roy 2015). Reduced AMPK signaling leads to an increase of ATGL-1-dependent lipolysis and consequently to reduced lifespan of dauer animals (Narbonne and Roy 2009). In contrast to this, during food deprivation in adulthood animals, increasing cAMP levels stimulate protein kinase A (PKA) to induce lipolysis via the lipid droplet protein LID-1 and ATGL-1 (Lee et al. 2014). AMPK signaling also induces lipid degradation via hormone-sensitive lipase HOSL-1 during cold-stress, which leads to glycerol accumulation and protection from cold-induced damage (Liu et al. 2017). Hence, the fine balance between lipid hydrolysis and retention is crucial for survival during certain stresses and dauer stage. After exit of dauer, animals enter L4 larval stage and develop into adults normally. When adult animals experience food depletion, they show increased motility while at the same time reducing their rate of pharyngeal pumping and in case of gravid adults, retaining eggs and embryos (Avery and Horvitz 1990; Hills, Brockie, and Maricq 2004; Sawin, Ranganathan, and Horvitz 2000). The latter is also known as adult reproductive diapause and protects germline stem cells at the expense of the rest of the germline cells, leading to an extension of the reproductive lifespan (Angelo and Van Gilst 2009). Genome-wide proteomics of adults that undergo acute starvation show, somewhat expected, that major fat metabolic enzymes are differentially expressed (Larance et al. 2015). Additionally, chromatin-associated proteins are misregulated, suggesting a more permanent influence on gene expression (Larance et al. 2015). During starvation, depletion of fat-deposits, and hence survival, depends on various fasting-induced lipases (FILs) (Jo et al. 2009; O'Rourke and Ruvkun 2013). The ER is an organelle closely associated with fat metabolism. IRE-1, an ER-resident transmembrane serine/threonine protein kinase, known to be induced by an accumulation of unfolded proteins in the ER, and HSP-4, an ER chaperone, regulate fat degradation by

influencing the expression of the fasting induced lipases FIL-1 and FIL-2 (Jo et al. 2009), which are related to the mammalian adipose triglyceride lipases (ATGL) (Zimmermann et al. 2004). When starvation is induced in *ire-1RNAi* or *hsp-4RNAi* animals, fat stores are maintained and life span during long-term starvation is compromised (Jo et al. 2009). *Lipl-1-5* are intestinal lipases that are induced upon starvation and *lipl-1* and *lipl-3* are responsible for lipolysis during starvation. During *ad libitum* feeding, the transcription factor MXL-3 represses *lipl-1, -2, -3,* and *lipl-5* (but not *lipl-4*), which are de-repressed as *mxl-3* levels decline during starvation (O'Rourke and Ruvkun 2013). In contrast to MXL-3, the transcription factor HLH-30 is a positive regulator of lipases during starvation and transcriptionally activates *lipl-2, -3* and *-5*. (O'Rourke and Ruvkun 2013). In the same study, it was shown that lipid accumulation also depends on the two autophagy genes *lgg-1* and *lgg-2*. Autophagy that serves in lipid hydrolysis is also termed lipophagy and plays an important role in lipid homeostasis. Loss of important autophagy genes such as *bec-1*, related to the mammalian autophagy gene Atg-6, leads to a decrease in overall lipid levels (Lapierre et al. 2013).

1.1.5.2 Variation of food source

Fat content of an animal is highly influenced by the dietary intake. In the lab the main source of nutrients for *C. elegans* is the *E. coli* strain OP50. However, it was shown that OP50 represents a rather low quality food judging by the time the animals spend quiescent on the bacteria lawn (You et al. 2008) and might even be slightly pathogenic (So et al. 2011). In their native environment the animals are associated with a species-rich microbiome dominated by variety of Proteobacteria (Dirksen et al. 2016). Furthermore, during RNAi knock down experiments, the *E. coli* strain HT115 is used for feeding. HT115 and HB101 have a higher carbohydrate content compared to OP50 and lead to a decrease of internal fat stores quantified via fixed Nile red staining (Brooks, Liang, and Watts 2009). This difference may be dependent on the uptake of peptides, because a mutation in *pept-1* (formerly known as *opt-2* or *pep-2*), an intestinal peptide transporter, abolishes the diet-dependent fat-change (Brooks, Liang, and Watts 2009). Lifespan, a readout for overall health of the animals, is only slightly increased. Further studies showed that feeding with *E. coli* strain HB101 leads to an increase of lifespan independent of *daf-2* and a 1.6- fold increase in the animals' body size, which is *daf-2* dependent (So, Miyahara, and Ohshima 2011; So et al. 2011).

1.1.5.3 Aging

In mammals, during the process of aging, lipid homeostasis is lost and consequently excess lipids are deposited in and around non-adipose tissues such as neurons and muscles. Consequences are overall decline of health, locomotion defects and eventually organ dysfunction and death, which can also be

observed in *C. elegans*. Deposition of ectopic fat is strongly delayed in long-lived mutants such as *eat-2(ad465)*, *daf-2(e1370)*, and *glp-1(e2141)* (Palikaras et al. 2017).

1.2 Regnase-1 and Regnase-1-related proteins

As described in chapter 2.1 "Ribonuclease-mediated control of body fat", we uncovered a hitherto uncharacterized RNase involved in *C. elegans* fat metabolism. We identified *rege-1* in a screen, using cold sensitivity as read out to uncover novel fat key factors in fat regulation. REGE-1 is important for wild type levels of fat and *rege-1* mutants exhibit a strong upregulation of fat metabolic and innate immunity genes, depending on the transcription factor ETS-4 (Habacher et al. 2016). REGE-1 is a close homolog of the mammalian Regnase-1, a well-studied regulator of innate immunity and potentially adipogenesis (reviewed in (Jura, Skalniak, and Koj 2012; Mao et al. 2017; Uehata and Akira 2013)). Previously to this study, high throughput research examined GFP under the control of the putative *C30F12.1* promoter and reported expression in the intestine, somatic gonad and head neurons (McKay, Johnsen, et al. 2003). Additionally, one genome-wide RNAi study found that knock down of *C30F12.1* causes a pale phenotype, a possible sign for reduced body fat (Simmer et al. 2003), another reported decreased Nile red live staining (Ashrafi et al. 2003), which reflects a decrease of lysosome related organelles (O'Rourke et al. 2009). Hence, the exact function and involvement in fat metabolism of *C30F12.1/rege-1* was elusive.

Following chapter was published in the journal "BioEssays": DOI: 10.1002/bies.201700051

THE (RNA) CUTTING EDGE OF ZC3H12A/MCPIP1/REGNASE-1–RELATED ENDONUCLEASES

Cornelia Habacher[1,2] and Rafal Ciosk[1,*]

ABSTRACT

The mammalian Zc3h12a/MCPIP1/Regnase-1, an extensively studied regulator of inflammatory response, is the founding member of a ribonuclease family, which includes proteins related by the presence of the so-called Zc3h12a-like NYN domain. Recently, several related proteins have been described in *Caenorhabditis elegans*, allowing comparative evaluation of molecular functions and biological roles of these ribonucleases. We discuss the structural features of these proteins, which endow some members with ribonuclease (RNase) activity while others with auxiliary or RNA-independent functions. We also consider their RNA specificity and highlight a common role for these proteins in cellular defense, which is remarkable considering the evolutionary distance and fundamental differences in cellular defense mechanisms between mammals and nematodes.

INTRODUCTION

With the exception of certain developmental stages and specific cell types, protein abundance is typically linked to the abundance of mRNA. This, in turn, is determined by the transcriptional output, mRNA modifications, and the association with regulatory RNA-binding proteins (RBPs) and non-coding RNAs. An important class of RBPs affecting RNA stability are ribonucleases (RNases), which catalyze RNA cleavage. These enzymes degrade RNA either from the 3' or 5' ends (exonucleases) or via internal cleavage (endonucleases). Depending on their mode of action and architecture, RNases are assigned to different families. Here, we focus on RNases belonging to the PIN- (PilT N-terminal) domain superfamily that are related to the endonuclease Zc3h12a/MCPIP1/Regnase-1, for brevity Regnase-1.

The PINendonuclease superfamily (CL0280), according to the Pfam protein database (www.pfam.xfam.org), includes eighteen families. Proteins related to Regnase-1 fall into two of these families, RNase_Zc3h12a (PF11977) and RNase_Zc3h12a_2 (PF14626), both of which are characterized by the presence of Zc3h12a-like NYN domains. Somewhat confusingly, proteins containing a related NYN domain (Anantharaman and Aravind 2006), originally named after the mammalian Nedd4-binding protein 1 (N4BP1) and bacterial YacP nucleases, belong to a distinct family. The Zc3h12a-like NYN domain is present in all three domains of life; in eukaryotes, the domain underwent functional diversification and fusion to additional functional domains. Regnase-1 is perhaps the most-studied protein carrying the Zc3h12a-like NYN domain; it is a critical regulator of inflammatory response, with additional roles in defense against viruses and various stresses, cellular differentiation and apoptosis (reviewed in (Jura, Skalniak, and Koj 2012; Mao et al. 2017; Uehata and Akira 2013)). Regnase-1 was first implicated in innate immunity when it was shown to be induced by the Monocyte chemoattractant protein-1 (MCP1), a chemokine that mediates inflammatory response – hence its other name, MCPIP1 (MCP1-induced protein 1) (Bidzhekov, Zernecke, and Weber 2006; Zhou et al. 2013). MCPIP1 was initially thought to be a transcription factor, but was later discovered to localize in the cytoplasm and regulate mRNA abundance by nucleolytic cleavage, which is why it was eventually re-named as Regnase-1 (regulatory RNase-1) (Iwasaki et al. 2011). Curiously, in addition to its RNA-cleaving function, the Zc3h12a-like NYN domain has been suggested to function as a deubiquitinase (Liang et al. 2010). However, how/whether these RNA and protein-regulatory functions relate to each other is not yet clear.

Recently, several reports have put the spotlight on *C. elegans* proteins related to Regnase-1. The closest homolog, REGE-1 (REGnasE-1), carries the same functional domains as Regnase-1, and, like its mammalian namesake, functions as a cytoplasmic endonuclease. By targeting mRNA encoding a

transcription factor, REGE-1 regulates the expression of genes involved in fat metabolism and and innate immunity genes (Habacher et al. 2016). A more distantly related *C. elegans* protein, RDE-8, together with several paralogs, has been implicated in RNA interference (RNAi) pathways (Tsai et al. 2015). With the recent description of nematode proteins REGE-1 and RDE- 8, the molecular functions and biological roles of proteins that belong to the Zc3h12a-like NYN domain family can be examined now from the evolutionary perspective. Here, we discuss potential molecular functions of these family members and highlight their, apparently ancient, roles in the regulation of cellular defense and homeostasis.

MAIN TEXT

The RNase activity and domain architecture of Regnase-1–related proteins

Proteins related to Regnase-1 share crucial structural and functional features. Towards the C-terminus of the Zc3h12a-like NYN domain, they typically contain four aspartic acids forming the catalytic center of the active site. These aspartic acids chelate a magnesium ion to activate a water molecule for nucleophilic attack at the phosphodiester bond of the RNA backbone (Anantharaman and Aravind 2006). Both, physicochemical properties and the spatial orientation of these residues relative to each other are crucial for the catalytic activity. Substitution of only one of the four charged aspartic acids (D141 of Zc3h12a) by a polar, uncharged asparagine abolishes the RNase activity (Matsushita et al. 2009). A representative structure of the Zc3h12a-like NYN domain from Regnase-1 (Protein Data Bank entry 3V34)is shown in Figure 1. In some of the Regnase-1–related proteins, the conserved aspartic acids are substituted by other amino acids, suggesting that these proteins no longer cleave RNA. The phylogenetic relationships of selected Regnase-1–related proteins, together with their domain architecture, are shown in Figure 2.

In vitro, the RNase domain of Regnase-1 alone binds to RNA inefficiently and, consequently, is incapable of RNA degradation (Xu, Peng, et al. 2012; Yokogawa et al. 2016) Hence, additional domains and/or co-factors are necessary for RNA binding and degradation. Specificity towards RNA can be achieved by RNA-binding domains (RBDs) or by interactions with RBPs. Most functional Zc3h12a-like NYN-domain proteins contain an RBD, such as a zinc finger (ZF) or a K-homology (KH) domain (Fig. 2). Regnase-1 harbors a CCCH-type ZF: *In vitro*, the CCCH ZF increases the binding strength of Regnase-1 to RNA, thereby increasing the efficiency of RNA cleavage (Yokogawa et al. 2016). An additional conserved domain, the N-terminal domain (NTD), increases the affinity to RNA and is necessary for efficient RNA cleavage *in vitro* (Yokogawa et al. 2016). Moreover, the Zc3h12a-like NYN domain appears to form a head-to-tail dimer, which, at least *in vitro*, is needed for the ribonuclease activity of Regnase-1 (Yokogawa et al. 2016). The conserved C-

terminal domain consists of a three-helical bundle and has been suggested to be expendable for degradation of most Regnase-1 mRNA targets (Yokogawa et al. 2016); however it may play a role during degradation of pre-mi RNA (Suzuki et al. 2011). Hence, both intra- and intermolecular interactions appear to govern Regnase-1 activity.

Regnase-1 activity is also influenced by other proteins. In T cells, Regnase-1 co-operates with another CCCH ZF RBP, Roquin (Jeltsch et al. 2014). This co-operation requires the nuclease activity of Regnase-1 as well as the RNA-binding ability of Roquin. A hybrid protein, harboring the RBP domain of Roquin fused to full-length Regnase-1, rescues mRNA regulation in cells devoid of endogenous Roquin and Regnase-1 (Jeltsch et al. 2014). These observations suggest that Roquin may recruit Regnase-1 to specific mRNA targets. However, a more recent study, using other cell types, suggests that, although Roquin and Regnase-1 control shared mRNAs, they do so in different sub-cellular compartments and by different mechanisms (Mino et al. 2015). According to this latter model, Regnase-1, with the help of UPF1 (a helicase functioning in nonsense-mediated RNA decay), degrades mRNAs during translation. Thus, the co-operation between Regnase-1 and Roquin is either cell-specific or incompletely understood.

Interactions with co-factors have been also demonstrated for family members lacking obvious RBDs. *C. elegans* RDE-8, which contains a functional Zc3h12a-like NYN domain but no obvious RBD, interacts with RDE-1, an Argonaute protein and a key player in RNA interference (RNAi) pathways (Tsai et al. 2015). RDE-1 is loaded with small interfereing RNAs (siRNAs), which guide RDE-1 and associated proteins to mRNA targets. Thus, the association with RDE-1 has been suggested to provide RNA specificity to RDE-8–mediated RNA degradation. Interestingly, RDE-8 also interacts with its paralogs NYN-1, NYN-2 and ERI-9 (Tsai et al. 2015). Although these paralogs carry subsitutions in the conserved aspartic acids of the Zc3h12a-like NYN domain, and so are thought be RNase-dead (Fig. 2), they are required for certain siRNA pathways (Tsai et al. 2015). In the absence of NYN-1 and NYN-2, immunoprecipitation of a catalytic-dead RDE-8 (D76N; allowing to capture the protein on RNA, which is otherwise rapidly degraded) showed reduced association between RDE-8 and its mRNA target (Tsai et al. 2015). Thus, although the precise role of the interaction between RDE-8 and its paralogs remains to be determined, these proteins have been proposed to serve structural functions, possibly promoting assembly of RNA-silencing complexes (Tsai et al. 2015).

Dynamic regulation of the RNase activity

Regulation of mRNA is a fast, and potentially reversible way of tuning gene expression to cellular demands, imposed by extracellular cues and intracellular fluctuations. As Regnase-1 functions in dosage-sensitive pathways, perhaps it comes as no surprise that its expression is tightly controlled: Regnase-1 is targeted to proteosomal degradation by IKB kinases or cleaved by the paracaspase MALT-1 (Iwasaki et al. 2011; Jeltsch et al. 2014; Uehata et al. 2013). It is also subjected to a sophisticated feedback regulation. For example, Regnase-1 cleaves its own transcript (Mizgalska et al. 2009; Uehata et al. 2013; Wawro, Kochan, and Kasza 2016) and its direct targets, IL-17 and IL-1β, induce Regnase-1 expression via different mechanisms (Garg et al. 2015; Mizgalska et al. 2009; Ruiz-Romeu et al. 2016; Somma et al. 2015). Presumably, these feedbacks ensure a correct dosage of the RNase activity, leading to a desired remodeling of the transcriptome. Interestingly, also *C. elegans* REGE-1 appears to be a subject of feedback regulation, as it degrades mRNA of its own transcriptional activator, ETS-4 (Habacher et al. 2016). In this, considerably simpler model, quantitative measurements and mathematical modeling of the feedback regulation may be more straightforward, potentially leading to a deeper understanding of the RNase function and regulation.

Features of RNA targets

Regnase-1 and its homolog REGE-1 cleave their mRNA targets within specific 3'UTR regions. Many 3'UTRs contain AU-rich elements (AREs) that, by recruiting RBPs, influence mRNA stability. Specifically CCCH ZF-containing proteins are known regulators of ARE-containing transcripts (Hudson et al. 2004; Lai, Kennington, and Blackshear 2002). In contrast, Regnase-1–dependent degradation of IL-2 and IL-6 mRNAs appears to be independent of the ARE sequences; instead, it requires RNA stem loops (Li et al. 2012; Matsushita et al. 2009). A large-scale study aiming at the identification of putative Regnase-1 targets revealed a three-nucleotide loop consensus motif (preferentially UAU or UGU) which was necessary for interaction with Regnase-1(Mino et al. 2015); whether these associated mRNAs are genuine targets remains to be determined. The stem loop within the IL-2 3`UTR consists of about 20 nucleotides and mutations that abolish formation of the loop render mRNA insensitive to Regnase-1-mediated cleavage. However, because additional mutations restoring the stem did not restore the cleavage, a combination of sequence and structure has been proposed to determine mRNA cleavage by Regnase-1 (Li et al. 2012). Similarly, while cleaving its own transcript, Regnase-1 appears to rely on both stem loops and the surrounding sequence (Wawro, Kochan, and Kasza 2016). In *C. elegans,* REGE-1 cleaves the 3'UTR of *ets-4* mRNA at a specific position within a roughly 100 nucleotide-long region. This region harbors many

potential stem loops (our unpublished observation). However, whether the requirement for stem loops is a conserved feature of RNA degradation by REGE-1 remains to be tested.

Besides targeting mRNA, Regnase-1 is reported to play a role in micro RNA (miRNA) processing. Initially, miRNAs are produced as primary miRNAs (pri-miRNAs) that can be several hundred nucleotides-long. Subsequently, pri-miRNAs undergo extensive processing to yield mature miRNAs, which are loaded onto Argonaute proteins, guiding them to specific mRNAs containing complementary sequences (Kim, Han, and Siomi 2009; Kobayashi and Tomari 2016). The biogenesis and maturation of miRNAs are tightly controlled. Regnase-1 was shown to cleave the terminal loop of pri-miRNAs, thereby inhibiting their maturation (Suzuki et al. 2011). Hence, in case of certain miRNAs, Regnase-1 appears to counteract Dicer and its mRNA-silencing function. This anti-dicer function was also observed in inflammation-induced angiogenesis, where Regnase-1 degrades the anti-angiogenic miR20b and miR34a (Roy et al. 2013). In addition, Regnase-1 was shown to degrade viral miRNAs, which, in turn, were shown to degrade Regnase-1 mRNA, potentially facilitating infection (Happel, Ramalingam, and Ziegelbauer 2016). However, the cleavage of pri-miRNA by Regnase-1 might depend on the specific context, as the same miRNAs that were reportedly degraded by Regnase-1 in HepG2 cells (human liver cancer cells) (Suzuki et al. 2011), were not affected by the depletion of Regnase-1 in mouse embryonic fibroblasts (Mino et al. 2015).

Control of protein ubiquitination

The amount, the type, and the position of ubiquitin linked to a target proteinhave diverse effects on protein stability, localization and activity. In general, chains of ubiquitin which are covalently linked via Lys48 (K48) to a target protein, mark it for degradation via the proteasome. In contrast, chains connected via Lys63 (K63) alter target protein activity. *In vitro*, Regnase-1 -is able to remove both types of chains, and a specific residue in the Zc3h12a-like NYN domain, C157 in Zc3h12a, is essential for deubiquitination but expendable for the RNase activity (Liang et al. 2010). *In vivo*, Regnase-1 has been reported to stabilize HIF1α (Roy et al. 2013) and modify the activity of TRAFs (Liang et al. 2010), by promoting de-ubiquitination. Thus, apparently through the same domain, Regnase-1 is capable of regulating the stability of either protein or RNA. Somewhat similar, a related protein, Nedd-4-binding partner 1 (N4BP1), predicted to have an RNase activity (Fig. 2), controls ubiquitin-mediated degradation by inhibiting a specific E3 ligase (Oberst et al. 2007). Interestingly, Roquin, functionally related to Regnase-1 as discussed above, contains a RING-type E3 ligase domain and promotes protein ubiquitination, potentially counteracting the de-ubiquitinating function of Regnase-1 (Ramiscal et al. 2015; Zhang, Fan, et al. 2015). Intriguingly, also the *C. elegans* homolog of Roquin, RLE-1, is reported to function as an E3 ligase (Li et al.

2007). However, whether RLE-1 contributes to REGE-1–mediated mRNA degradation, and whether REGE-1 controls protein stability, remains to be examined.

Biological roles of Regnase-1–related proteins

Regnase-1 negatively regulates pro-inflammatory transcripts, including IL-6 and IL-12p40, in resting T-cells (Matsushita et al. 2009). Upon T-cell activation, Regnase-1 is phosphorylated by IKB kinases (IKKs) and degraded in an ubiquitin-dependent manner (Iwasaki et al. 2011). In addition, the paracaspase MALT-1 directly cleaves Regnase-1, thereby stabilizing Regnase-1 targets (Jeltsch et al. 2014; Uehata et al. 2013). Mice lacking functional Regnase-1 develop auto-antibodies and die, postnatally, of systemic inflammation (Matsushita et al. 2009; Miao et al. 2013; Zhou et al. 2013). Regnase-1 knockout specifically in T-cells lead to a similar phenotype, suggesting that the phenotype is caused by the loss of Regnase-1 in these immune system cells (Iwasaki et al. 2011). Thus, Regnase-1 is crucial to suppress the autoimmune response under non-immunogenic conditions. Additionally, Regnase-1 exhibits broad-spectrum antiviral effects (Lin et al. 2013). Among others, it degrades RNAs of HIV (Human Immunodeficiency Virus) and HCV (Hepatitis C Virus), and restricts the replication of some DNA viruses such as adenovirus by an unknown mechanism (Lin et al. 2014; Liu et al. 2013). Additionally to Regnase-1, the mammalian genome encodes three more, less-studied, homologs Zc3h12b-d/Regnase-2–4. Zc3h12d is upregulated upon endotoxin exposure, and its knockdown leads to a strong increase in the levels of IL-1β, IL-6 and TNF-α, as well as other transcripts encoding additional inflammatory factors (Zhang, Wang, et al. 2015). Degradation of these mRNAs depends on the intact RNase domain of Zc3h12d (Wawro et al. 2017). Although Zc3h12a and Zc3h12d appear to target common transcripts and seem to interact by co- immunoprecipitation, they act independently in degrading IL-6 mRNA (Huang et al. 2015). Another family member, Zc3h12c, was shown to be induced by TNFα and overexpression of it represses pro-inflammatory signals, such as IL-8 and MCP-1, in HUVEC cells (Liu et al. 2013). Furthermore, overexpression and mutations in Zc3h12c have been linked to psoriasis (Munir et al. 2015; Tsoi et al. 2012). A more direct evidence for the involvement of the Zc3h12a-family in chronic skin inflammation comes from studies on Zc3h12a, which is both stimulated by IL-17 and degrades IL-17 mRNA during chronical skin inflammation (Monin et al. 2017; Ruiz-Romeu et al. 2016).

Among nematode proteins, the closest counterpart of Regnase-1, REGE-1, targets mRNA encoding a transcription factor, ETS-4, which in turn controls expression of target genes. Many of these genes have been implicated in nematode innate immunity (Habacher et al. 2016). Thus, although Regnase-1 directly controls mRNAs encoding immunity factors and REGE-1 appears to do so indirectly, both RNases play roles

in cellular defense. Also RDE-8, together with its paralogs described above, has a role in cellular defense, by functioning in RNAi pathways protecting against transposons; it may also defend against nematode viruses (Tsai et al. 2015). Thus, Regnase-1–related proteins play apparently ancient roles in cellular defense, which is remarkable considering major differences in the defense mechanisms between nematodes and mammals (Irazoqui, Urbach, and Ausubel 2010; Pradel and Ewbank 2004). It is tempting to speculate that this functional conservation might be due to a special relationship between cellular defense-oriented signaling pathways and their effector RNases, whose targets have changed over the course of evolution.

CONCLUSIONS

Recent publications on Regnase-1 and related proteins brought these important RNA regulators into focus. However, most family members, including proteins being studied in major animal models such as zebrafish and fruit fly, remain poorly or not characterized. Based on the critical functions of Regnase-1 in mammalian immunity and the essential functions of the nematode protein REGE-1 in fat metablism, other Regnase-related proteins may be expected to play important functions in defense and homeostasis. A defining feature of Regnase-1–related proteins is the Zc3h12a-like NYN RNase domain. However some family members carry substitutions in the active site, suggesting that they do not function as RNases. Although some of these proteins may have adopted entirely different functions, others appear to fulfill auxiliary roles in RNA regulation. For example, nematode NYN-1 and NYN-2 are dispensable for the RNase activity of RDE-8 *in vitro* but, *in vivo*, they are required for RDE-8–mediated RNA regulation, possibly by facilitating the formation of an RNA-silencing complex. Thus, dissecting precise functions of the pseudo-RNase proteins related to Regnase-1 is an important goal for the future.

A key feature of Regnase-1 and REGE-1 is their high RNA specificity, which, however, remains poorly understood. Most observations suggests that the RNase domain is insufficient for RNA specificity. Some of the proteins carry RBDs, such as the CCCH ZF of Regnase-1 or the KH domain of N4BP1, which were either shown or are expected to improve affinity to RNA as well as specificity. Others, which do not carry any recognizable RBDs, may interact with RBPs, similar to RDE-8, which is recruited to mRNA targets by RDE-1. However, RNA recognition of even stand-alone RNases, such as Regnase-1, may be more complicated than previously thought: To efficiently cleave RNA *in vitro*, Regnase-1 forms a homodimer, in which one of the proteins is cleaving RNA whereas the other might serve structural purposes (Yokogawa et al. 2016). Also understanding the functional relationship between Regnase-1 and Roquin needs further work, and studies on the closest homologs, like REGE-1, are expected to bring new insights. Finally, also

RNA features underlying the RNase's specificity remain to be further investigated. Regnase-1–dependent cleavage requires RNA stem loops: Whether these stem loops are needed for Regnase-1 binding and/or the cleavage remains unclear. Also, whether RNA structure is important for RNA regulation by other family members remains to be seen. Thus, understanding precisely how Regnase-1–related proteins achieve RNA specificity, which is expected to differ between family members, remains a top priority, necessary to fully understand their biological effects.

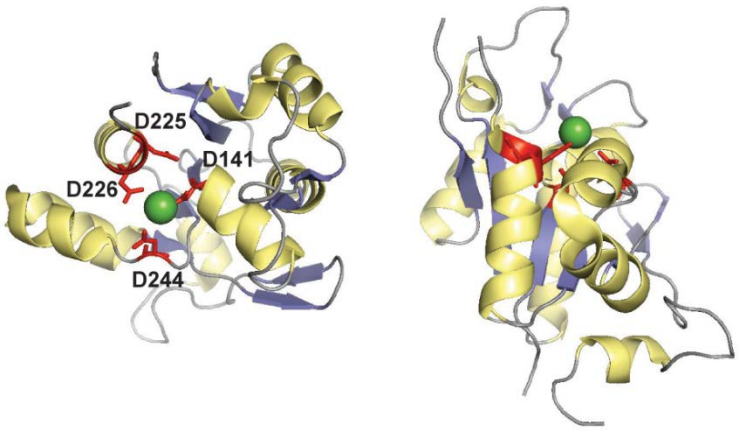

Figure 1: Representative structure of a Zc3h12a-like NYN domain.

The crystal structure of the RNase domain of human Regnase-1 is depicted as a cartoon model in two orientations, with α-helices in yellow and β- strands in blue (Protein Data Bank entry 3V34, (Xu, Peng, et al. 2012)). View from the "top" onto the active center (left) turned by 90° along the x- and y-axis on the right. Highlighted in red are the four aspartic acids (D141, D225, D226, D244), which chelate a magnesium ion (green sphere) in the active center. N- and C-termini are labelled and disordered loops which were not present in the structure are shown as dotted lines. Figures were prepared with PyMOL (www.pymol.org)

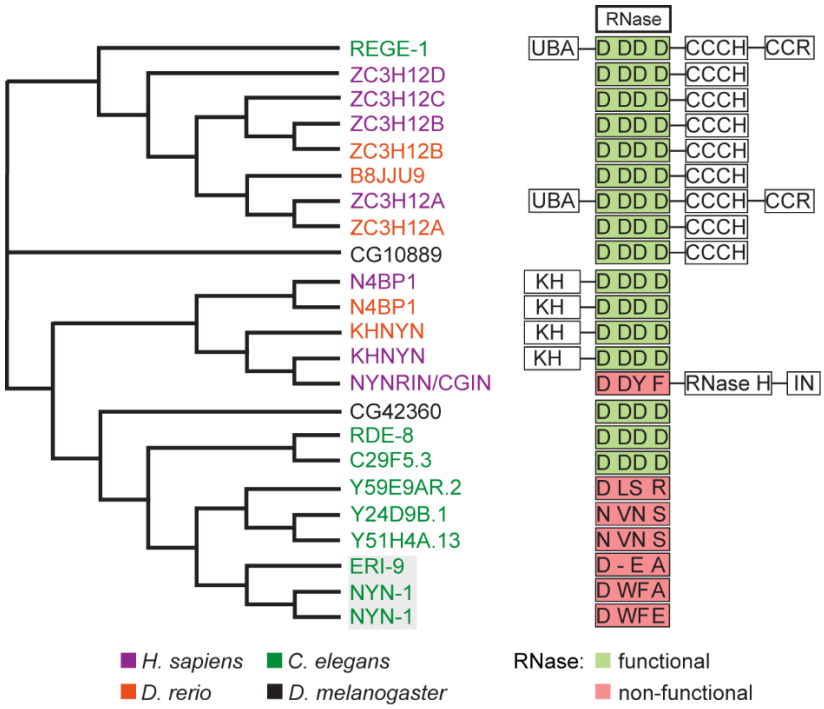

Figure 2: Proteins related to Regnase-1 from selected model organisms.

Left: Phylogenetic relationship of proteins related to Regnase-1 from *H. sapiens, C. elegans, D. melanogaster* and *D. rerio*. The alignment was constructed online with the multiple sequence alignment tool ClustalOmega (Goujon et al. 2010; McWilliam et al. 2013; Sievers et al. 2011). Default settings without tree branch corrections were used. Most of the proteins belong to the RNase_Zc3h12a family, with the exception of proteins on the light grey background, which belong to the RNase_Zc3h12a_2 family. Right: Domain architectures corresponding to the proteins on the left. "RNase" indicates the Zc3h12a-like NYN domain. The four aspartic acids (corresponding to D141, D225/225, D244 of the human Regnase-1, from left to right) of the active center are highlighted. The domains in green contain all four aspartic acids and thus likely display an RNase activity. The domains in red contain substitutions of the conserved residues and probably do not function as RNases. Additional domains are indicated, according to the annotation in the Pfam protein database (http://pfam.xfam.org/). The domains are positioned relative to the RNase domain as in the actual proteins (to the left is the N- and to the right the C-terminus of the protein). The size of the boxes is not proportional to the length of the actual domains. "UBA" indicates a predicted ubiquitin-binding domain; "CCCH" a CCCH-type zinc finger domain; "CCR" a C-terminal conserved region; "KH" a K-homology domain, "RNaseH" an RNase H domain, and "IN" a viral integrase domain.

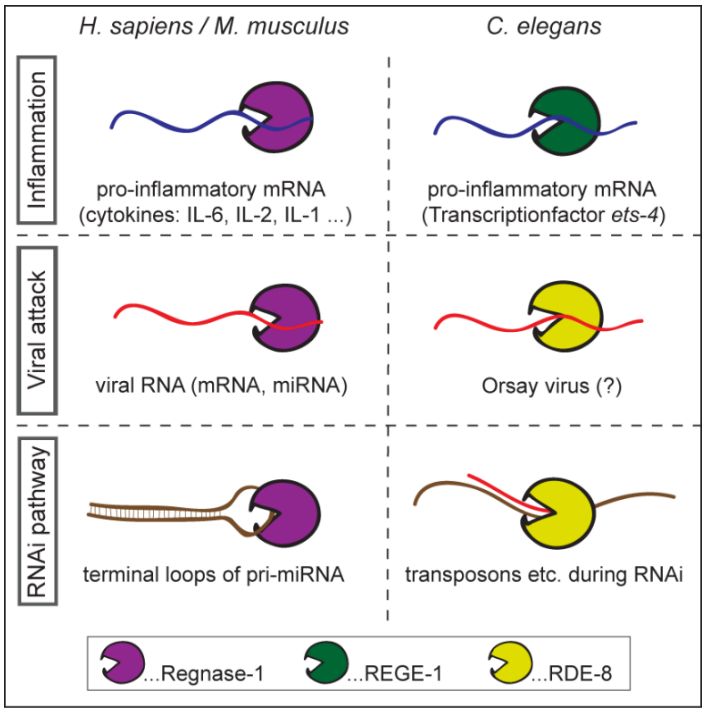

Figure 3: Biological roles of Regnase-1–related proteins connected to cellular defense.

A comparison between mammalian and *C. elegans* proteins, highlighting roles related to cellular defense mechanisms: Modulation of inflammation, direct degradation of pathogenic RNA, and function in RNAi pathways, which can also function in cellular defense against either exogenous or endogenous (such as transposons) pathogenic agents.

ACKNOWLEDGMENT

We thank Heinz Gut for comments on the manuscript and members of the Ciosk laboratory for discussions.

2. RESULTS

Chapter 2.1 was published in the journal “Developmental Cell”. DOI: 10.1016/j.devcel.2016.09.018

2.1 Ribonuclease-mediated control of body fat

Cornelia Habacher [1,2], Yanwu Guo [1], Richard Venz [1,2], Pooja Kumari [1], Anca Neagu [1], Dimos Gaidatzis [1,4], Eva B. Harvald [3], Nils J. Færgeman [3], Heinz Gut [1], and Rafal Ciosk [1]

SUMMARY

Obesity is a global health issue, arousing interest in molecular mechanisms controlling fat. Transcriptional regulation of fat has received much attention and key transcription factors involved in lipid metabolism, such as SBP-1/SREBP, LPD-2/C/EBP and MDT-15, are conserved from nematodes to mammals. However, there is a growing awareness that lipid metabolism can be also controlled via posttranscriptional mechanisms. Here, we show that a previously uncharacterized *Caenorhabditis elegans* RNase, REGE-1, related to MCPIP1/Zc3h12a/Regnase-1, a key regulator of mammalian innate immunity, promotes accumulation of body fat. Using exon-intron split analysis (EISA), we find that REGE-1 promotes fat by degrading the mRNA encoding ETS-4, a fat loss-promoting transcription factor. Because ETS-4, in turn, induces *rege-1* transcription, REGE-1 and ETS-4 appear to form an auto-regulatory module. We propose that this type of fat regulation may be of key importance when, faced with an environmental change, an animal must rapidly but precisely remodel its metabolism.

INTRODUCTION

Remodeling energy metabolism is critical for development, tissue homeostasis, and the etiology of numerous diseases including obesity and cancer (Folmes et al., 2012; Longo and Mattson, 2014; Ward and Thompson, 2012). Such remodeling can be induced by adverse environmental stimuli leading to a state of suspended animation or torpor. For example, hibernating animals use stored lipids, rather than carbohydrates, to fuel survival (Dark, 2005). In the wild, the *C. elegans* species populates temperate climates (Barrière and Félix, 2005), indicating that these animals are capable of surviving spells of cold. Indeed, when adapted to a decreasing temperature, *C. elegans* survives the exposure to near freezing temperatures (Murray et al., 2007; Ohta et al., 2014).

In this study, we observed that also *C. elegans* utilize fat while in cold. Using cold sensitivity as the readout, we identified a putative RNase, REGE-1, related to the mammalian MCPIP1/Zc3h12a/Regnase-1, as a factor critical for *C. elegans* body fat accumulation. The examples of posttranscriptional regulation of fat remain few and are limited to specific miRNAs, whose functionally relevant mRNA targets remain, in most cases, unclear (Arner and Kulyté, 2015; Rottiers and Näär, 2012). In animals, miRNAs repress their mRNA targets through translational repression and/or exonucleolytic degradation (Wilczynska and Bushell, 2015). By contrast, MCPIP1 is a PIN-domain endonuclease (Iwasaki et al., 2011; Matsushita et al., 2009; Xu et al., 2012), suggesting a possible requirement for the endonucleolytic mRNA degradation in *C. elegans* body fat regulation. Indeed, we demonstrate that REGE-1 controls body fat by targeting the 3'UTR of an mRNA encoding a fat loss-promoting transcription factor, ETS-4. Interestingly, while REGE-1 inhibits ETS-4, ETS-4 promotes the expression of REGE-1. Such an auto-regulatory module is particularly well suited for a dynamic control of gene expression. It may be of key importance when, faced in the wild with an environmental change, an animal must rapidly remodel its fat metabolism to maximize its chances for survival.

RESULTS

Cold-sensitivity screen reveals REGE-1 as a factor promoting body fat

Extending the initial observations by others that *C. elegans*, when adapted to a decreasing temperature, can survive the exposure to near-freezing temperature (Murray et al., 2007; Ohta et al., 2014), we found that the animals can do so for many days, without a major impact on fecundity or lifespan (Fig. S1A-C). To what degree the *C. elegans* response to cold is analogous to that of hibernating animals is not clear. Nevertheless, consistent with fueling cellular processes by fat in hibernators, we observed a gradual

decline in the fat levels in "hibernating" *C. elegans* (Fig. S1D). This observation prompted us to use cold sensitivity as a readout to uncover new regulators of fat stores. We performed a genome-wide RNAi screen, searching for genes essential at 4 °C but non-essential at 20 °C (Fig. 1A). This approach uncovered factors implicated in diverse cellular processes (Figs. 1B and S1E). Importantly, the depletion of several factors caused a "pale" appearance of animals already at 20 ºC, indicating reduced stores of body fat. Indeed, some of these factors have established roles in fat metabolism (Fig. 1B). For example, the mediator complex component MDT-15 regulates expression of many fatty acid metabolism genes (Taubert et al., 2006), and FAT-6/7 are fatty acid desaturases previously implicated in cold survival (Murray et al., 2007; Watts and Browse, 2000). Additionally, knockdown of the hitherto uncharacterized gene *C30F12.1* resulted in pale animals. C30F12.1 protein is a member of the CCCH-type zinc finger family (Liang et al., 2008) and is related to the mammalian MCPIP1/Zc3h12a/Regnase-1, a PIN-domain endonuclease (Xu et al., 2012), which directly degrades specific mRNAs such as those encoding proinflammatory cytokines (Iwasaki et al., 2011; Matsushita et al., 2009). Because the RNase and CCCH zinc finger domains are highly conserved between C30F12.1 and Zc3h12a/MCPIP1/Regnase-1 (Fig. S2 and 3A), we named C30F12.1 as REGE-1 (REGnasE-1). To verify that *C. elegans* lose fat upon *rege-1* RNAi, we stained the animals with Oil Red O (ORO) and enzymatically determined the levels of triglycerides (TAGs), which are the main storage form of lipids. By both approaches, we confirmed that the fat levels were reduced (Fig. 2A-B). Additionally, we examined lipid droplets in live animals by Coherent Anti-Stokes Raman Spectroscopy (CARS) and found that REGE-1–depleted animals had substantially reduced numbers of lipid droplets (Fig. 2C). Because germline plays an important role in fat homeostasis (Hansen et al., 2013), REGE-1 could affect body fat by functioning in the germline. However, the loss of fat also occurred in REGE-1–depleted, germline-less (*glp-1*) animals (Fig. 2D), suggesting that, to promote fat accumulation, REGE-1 functions in the soma.

REGE-1 is a putative RNase primarily expressed in the intestine

To study REGE-1 in more detail, we generated a deletion allele, *rege-1(rrr13)*, predicted to cause a severe truncation of the protein (Fig. 3A). Consistent with the RNAi-mediated depletion, *rege-1(rrr13)* animals were viable but displayed reduced fat (Fig. 3B). We also observed that they developed somewhat slower than wild type (Fig. S3). Both of these phenotypes were rescued by a single copy-integrated, GFP-tagged REGE-1, expressed under the control of endogenous promoter and 3'UTR (Figs. 3B and S3). This REGE-1::GFP was mostly expressed in the intestinal cells adjacent to the pharynx (Fig. 3C), suggesting that REGE-1 functions in the intestine – the primary fat-storing organ of *C. elegans* (Srinivasan, 2014; Watts, 2009).

Mammalian Regnase-1 is a cytoplasmic RNase that, by an internal cleavage, induces the degradation of specific mRNA targets (Iwasaki et al., 2011; Matsushita et al., 2009; Xu et al., 2012). Investigating the putative RNase domain of REGE-1, we noticed that the residues critical for the RNase activity of Regnase-1 are conserved in REGE-1 (Figs. S2 and 3D), suggesting that REGE-1 may also function as an RNase.

REGE-1 promotes body fat through the transcription factor ETS-4

Assuming that REGE-1 functions similarly to Regnase-1, depleting REGE-1 would be expected to primarily affect the levels of mature but not nascent transcripts. It has recently been shown that comparing exonic and intronic expression across conditions (Exon-intron-split analysis, EISA) can be used to quantify the levels of nascent and mature transcripts in standard RNA-seq experiments (Gaidatzis et al., 2015). We thus performed RNA-seq on animals subjected to control or *rege-1* RNAi and compared changes in the levels of nascent RNAs (Δintron) to the changes in mRNAs (Δexon). Although most of the observed changes in mRNA levels could be explained by differential transcription, we observed a small group of transcripts that were affected mainly at the level of mRNA, the most extreme example being *ets-4* mRNA (Figs. 4A-B, S4A and Tables S1-2). Consistent with REGE-1–mediated regulation, we found, by western blot, that the GFP and FLAG-tagged ETS-4 protein was more abundant upon *rege-1* RNAi (Fig. 4C). Importantly, we did not detect any obvious expression of this protein in wild-type animals, but observed its strong expression in the intestine nuclei upon *rege-1* knockdown (Fig. 4C), suggesting that REGE-1 and ETS-4 function in the same tissue. ETS-4 belongs to the ETS-domain family of transcription factors (Sharrocks, 2001). Prior to this work, ETS-4 was studied in the context of aging and ETS-4–regulated genes were reported (Thyagarajan et al., 2010). Interestingly, we found that transcripts reportedly activated by ETS-4 were enriched among the transcripts upregulated in REGE-1–depleted animals (data not shown). This suggested the possibility that the increased expression of ETS-4 may be largely responsible for the changes in gene expression observed in *rege-1* animals. To test this, we compared changes in transcript levels between *rege-1(rrr13)* and *rege-1(rrr13); ets-4(RNAi)* animals, to the changes in transcript levels between animals subjected to *rege-1* or mock RNAi. Impressively, we found that the majority of changes in gene expression observed in the absence of REGE-1 were reversed by the additional depletion of ETS-4 (Fig. 4D and Table 3), suggesting that ETS-4 is the major effector of REGE-1. If so, the depletion of ETS-4 would be expected to rescue the phenotypes observed in *rege-1(rrr13)* animals. Indeed, we found that the RNAi-mediated depletion of *ets-4* mRNA (but not of other putative targets marked in red in Fig. 4A), restored both fat and developmental timing in *rege-1(rrr13)* animals to the wild-type values (Figs. 4E and S4B). By examining gene ontology terms associated with transcripts induced by ETS-4 in *rege-1(rrr13)* animals (the transcripts

marked in red in Fig. 4D), we found two major classes of genes: genes implicated in lipid metabolism and responses to pathogens (Fig. S5A and Table S4). While the former category includes key genes functioning in the fatty acid degradation pathway (Fig. S5B), the latter category contains many genes induced upon infection with bacterial or fungal pathogens (Fig. S5C) (Engelmann et al., 2011).

REGE-1 regulates ETS-4 posttranscriptionally through the 3'UTR

Regnase-1 is an RNA-binding protein (RBP) that targets 3`UTRs of specific mammalian mRNAs. To test if REGE-1 regulates ETS-4 expression by targeting the 3'UTR of *ets-4* mRNA, we produced strains carrying a single copy-integrated *ets-4::gfp*, expressed from the endogenous *ets-4* promoter and fused to either endogenous (*ets-4*), or unregulated (*unc-54*) 3'UTR. We found that the depletion of REGE-1 caused increased expression of ETS-4::GFP only when this expression was controlled by the *ets-4* 3'UTR (Fig. 5A). Thus, *ets-4* 3'UTR is required for the REGE-1–mediated regulation. To examine this further, we produced a strain expressing a reporter GFP (fused to H2B to accumulate signal in the nucleus, facilitating quantification) from a ubiquitous promoter (*dpy-30*) under the control of the *ets-4* 3`UTR. In wild-type animals, we observed the expression of this reporter in various tissues and across development (reflecting promoter activity, data not shown) but not in the gut nuclei (Fig. 5B). In contrast, in *rege-1(rrr13)* mutants, this reporter GFP was additionally expressed in the gut nuclei (Fig. 5B). Thus, the *ets-4* 3'UTR is not only required but also sufficient for REGE-1–mediated regulation of ETS-4 expression. To examine which part of the *ets-4* 3'UTR is targeted by REGE-1, we produced strains expressing the reporter GFP under the control of truncated variants of the *ets-4* 3'UTR. We found that the fragment spanning the first one-third of the 3'UTR (fragment F1, 357 nt) was sufficient for the repression of the reporter GFP in the gut nuclei and this repression was alleviated upon *rege-1* RNAi (Fig. 5C). Examining this fragment more closely, we noticed a stretch of homology between the corresponding sequences from other nematode species (Fig. S6). To test the functional significance of this fragment (fragment F1S, 115 nt), we "transplanted" it into the otherwise unregulated *unc-54* 3'UTR. We found that this transplantation rendered the *unc-54* 3'UTR sensitive to the regulation by REGE-1 (Fig. 5D), suggesting that the RNA features required for REGE-1–mediated regulation are contained within the F1S fragment.

REGE-1 induces an endonucleolytic cleavage within the *ets-4* 3'UTR

To test if the putative RNase activity of REGE-1 is important for the regulation of *ets-4* mRNA, we mutated, by genome editing, conserved amino acids (indicated in Fig. 3D) in the RNase domain of the endogenous REGE-1 (generating the *rrr21* allele of *rege-1*). Expectedly, mutating these residues (D231N, D313A, D314A

and D332A) resulted in increased levels of *ets-4* mRNA (Fig. 6A). If REGE-1 is indeed an RNase, its association with *ets-4* mRNA is expected to be short-lived. To examine this putative association, we used GFP-tagged and RNase domain-mutated REGE-1 (corresponding to the *rrr21* allele). By immunoprecipitating this REGE-1 variant, followed by RT-qPCR–based detection of associated transcripts, we observed that, indeed, REGE-1 associated with *ets-4* mRNA (Fig. 6B). Based on the homology with Regnase-1 and the above experiments, REGE-1 is expected to induce an endonucleolytic cleavage within the F1S region of *ets-4* 3'UTR. Initially, we tested this by incubating immunoprecipitates of GFP-tagged, wild-type and RNase domain-mutated REGE-1 with *in vitro*-produced RNA, corresponding to the fragment F1S. We observed that the incubation with the wild-type, but not the RNase domain-mutated, REGE-1 resulted in the degradation of the F1S RNA, but had no effect on unrelated RNA (100 nt of *unc-54* 3`UTR) (Fig. 6C). Finally, although detecting mRNA cleavage intermediates can be difficult, we used a modified 5'RACE approach to amplify the 3'-terminal cleavage intermediates of *ets-4* mRNA. Rewardingly, this approach revealed that REGE-1 cleaves *ets-4* mRNA within the F1S fragment of its 3'UTR (Fig. 6D).

REGE-1 and ETS-4 may form a dynamic, auto-regulatory module

One advantage of posttranscriptional gene regulation is its speed and reversibility. Thus, the REGE-1/ETS-4 axis is potentially well suited to dynamically control ETS-4 levels. To test the dynamics of ETS-4 expression, we examined *ets-4* mRNA levels during starvation, which was followed by re-feeding. During starvation, *ets-4* mRNA levels remained low for several days, increasing somewhat on the sixth day (Fig. 7A). In contrast, upon re-feeding, *ets-4* levels were strongly increased. This increase was, however, transient, as the levels of *ets-4* were back to the pre-starvation values only one day after re-feeding (Fig. 7A). With the changing levels of *ets-4* mRNA, we expected to see the reciprocal changes in the levels of *rege*-1 mRNA. However, to our surprise, we observed similar, rather than opposite, changes of *rege-1* and *ets-4* mRNAs (Fig. 7A), suggesting their co-regulation. To test this further, we asked whether ETS-4 affects the levels of *rege-1* mRNA. Indeed, depleting ETS-4 resulted in reduced expression of *rege-1* (Fig. 7B). We observed this effect also using a GFP reporter, driven from the *rege-1* promoter and under control of unregulated (*unc-54*) 3' UTR (Fig. 7C), suggesting that ETS-4 induces (directly or indirectly) the transcription of *rege-1*. Thus, our findings suggest that REGE-1 and ETS-4 form an auto-regulatory module, which, upon an environmental change, is capable of rapidly adjusting its transcriptional output by altering ETS-4 levels.

DISCUSSION

We describe here a previously uncharacterized RNase, REGE-1, involved in the regulation of body fat. The mammalian Regnase-1 binds mRNAs by recognizing structured RNA, reportedly with the help of a distinct RBP, Roquin (Jeltsch et al., 2014). However, Regnase-1 and Roquin have been recently suggested to function in distinct subcellular compartments and by different molecular mechanisms (Mino et al., 2015). Moreover, in addition to the RNase and zinc finger domains, Regnase-1–like proteins contain two additional domains, of which one has been recently reported to contribute, at least *in vitro*, to the RNase activity of Regnase-1 (Yokogawa et al., 2016). Thus, the problems of how exactly Regnase-1–like proteins achieve specificity for selected mRNA targets and whether additional mechanisms contribute to mRNA regulation are only partly understood. Nevertheless, our results suggest that degradation, induced by an endocucleolytic cleavage, is the most plausible mechanism by which REGE-1 controls *ets-4* mRNA.

While REGE-1 degrades *ets-4* mRNA, ETS-4 stimulates (directly or indirectly) the transcription of *rege-1*. Such an auto-regulatory RNase/transcription factor module is well suited to a rapid and reversible regulation of gene expression. We hypothesize that, coupled to the positive transcriptional feedback, REGE-1–mediated degradation is more efficient at buffering changes in ETS-4 levels. Thus, upon an environmental cue, including but perhaps not limited to nutrient abundance, the reciprocal regulation of REGE-1 and ETS-4 might ensure a rapid but controlled change in the transcriptional output of ETS-4, eliciting desired metabolic remodeling (Fig. 7D). However, proving this model will require quantitative measurements of both ETS-4 levels and ETS-4–induced transcription, upon manipulating regulatory elements in the *rege-1* promoter and *ets-4* 3'UTR. Also, whether a particular environmental cue affects the module by primarily altering (levels or activity of) REGE-1 and/or ETS-4 will need to be established.

Finally, how precisely increased levels of ETS-4 stimulate fat loss remains an exciting problem for the future, with potential implications for obesity research. Our preliminary observations suggest that increased expression of ETS-4 does not alter feeding behavior, as monitored by pharyngeal pumping of *rege-1* mutants (our unpublished observation). Therefore, the loss of fat is unlikely caused by reduced food consumption. Interestingly, upon re-feeding (following long-term fasting), when the intestine is challenged with increased nutrient uptake and utilization, we observed a rapid upregulation of the REGE-1/ETS-4 module, possibly indicating a role for the module in accelerating food utilization. The observed induction of lipid genes by ETS-4, including genes in the fatty acid degradation pathway, is consistent with this hypothesis. Other scenarios are, however, possible. Whether the mammalian Regnase-1 impacts fat metabolism remains to be determined. In cultured adipocytes, where this possibility was addressed, the

reported results are contradictory (Lipert et al., 2014; Younce et al., 2009). In contrast, in innate immune cells, Regnase-1 is well established to inhibit pro-inflammatory cytokines (Iwasaki et al., 2011; Matsushita et al., 2009), which, in turn, can stimulate adipocytes to lose fat (Gregor and Hotamisligil, 2011; Guilherme et al., 2008). Curiously, through ETS-4, REGE-1 regulates expression of many nematode defense genes, suggesting a conserved function of Regnase-1–like proteins in innate immunity. Although ETS-4 may control lipid and defense genes separately, perhaps depending on a particular environmental cue, it is possible that ETS-4–dependent fat loss is linked to an inflammatory response. If, so, dissecting the underlying mechanism could provide important insights into the well-known, though insufficiently understood, connection between inflammation and lipid metabolism.

A

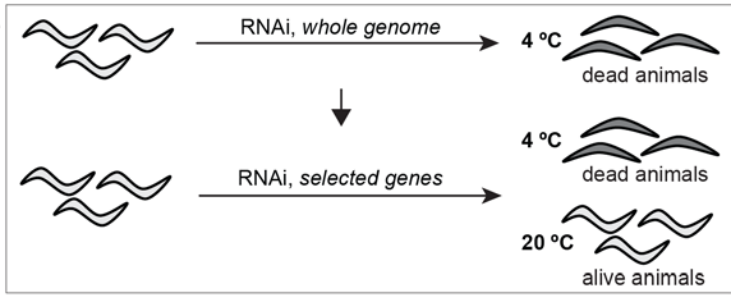

B

Gene	Molecular function	Human homologue
C30F12.1	Putative ribonuclease	ZC3H12A/B/C/D; Regnase-1
mdt-15	Mediator complex subunit	MED15; mediator of Pol II
vhp-1	MAPK Phosphatase, stress signaling	DUS16; dual spec. phosphatase 16
ptc-1	Predicted functions in protein, lipid and sterol transport	PTCH1; Patched homolog 1
paa-1	PP2A phosphatase structural subunit	PR65; Protein Phosphatase 2A, subunit A α isoform
inos-1	Predicted function in de novo inositol biosynthesis	ISYNA1; Inositol-3-phosphate synthase 1
pbs-6	Proteasome subunit	PSMB1; Proteasome sub. β type-1
R03E1.2	Unknown	ATP6AP2; Renin receptor
fat-6 & -7	Fatty acid desaturation	SCD; Acyl-CoA desaturase
R02F11.2	Unknown, nematode-specific	None

Figure 1.

A. Genome-wide RNAi screen for cold sensitivity uncovers a conserved RNase as a factor promoting accumulation of body fat. A. Schematic description of the genome-wide RNAi screen for cold sensitivity. Only those RNAi clones that induced death following the incubation at 4 °C, but not at 20 ºC, were investigated further. **B.** Factors identified in the cold-sensitivity screen. In bold: factors whose depletion results in "pale" animals, suggesting reduced fat levels. This group includes a putative RNase, C30F12.1. See also Figure S1.

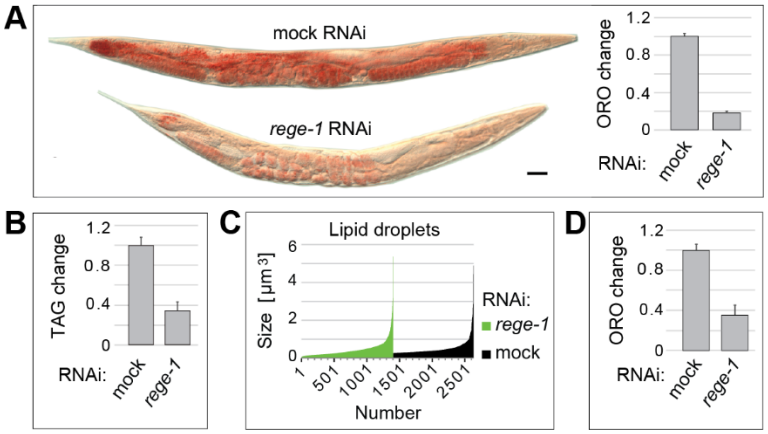

Figure 2. REGE-1 promotes fat accumulation under normal growth conditions.

A. Left: DIC color micrographs of animals, subjected to control (mock) or *rege-1* RNAi, stained with the lipophilic dye Oil Red O (ORO) to reveal fat. Size bar: 50 µm, Right: quantification of changes in the ORO staining. 20-25 animals were measured per condition. Data presented as mean; error bars, here and in all the subsequent graphs, represent SEM. **B.** Change in *triacylglycerol (TAG) levels* upon *rege-1* RNAi. **C.** Size and numbers of lipid droplets quantified by CARS in control and *rege-1* RNAi-ed animals. **D.** Change in fat upon *rege-1* RNAi, in germline-less *glp-1(e2141)* animals, determined by the ORO staining. 10-15 animals were measured per condition.

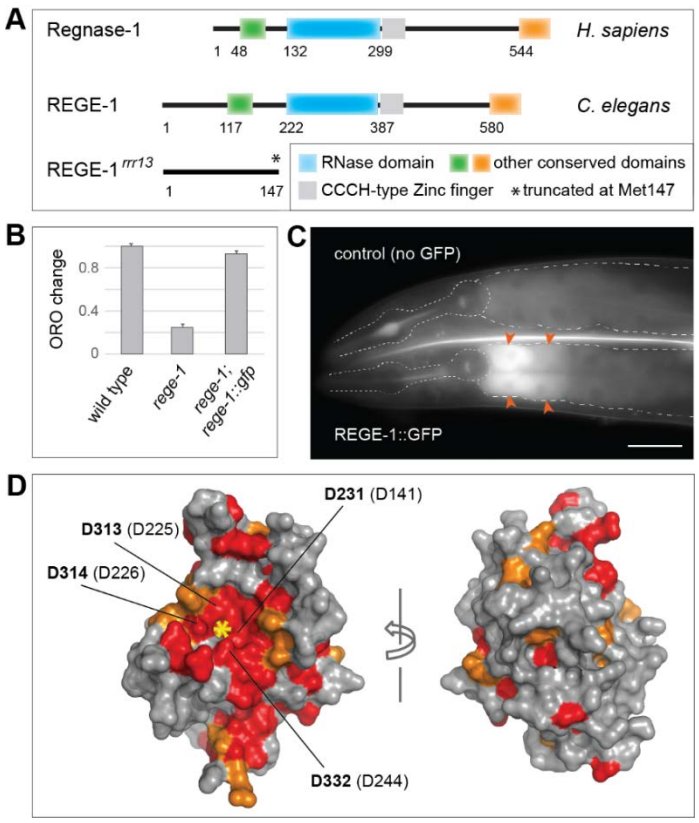

Figure 3. REGE-1 is a putative RNase expressed in the intestine.

A. Schematic view of Regnase-1/Zc3h12a/MCPIP1 and REGE-1 proteins, with the conserved domains indicated. The deletion allele of *rege-1, rege-1(rrr13)*, results in a truncated protein missing the RNase domain. **B.** The fat loss phenotype of animals subjected to *rege-1* RNAi is also observed in *rege-1(rrr13)* mutants, and is rescued by a transgenic GFP-tagged REGE-1. Fat levels were quantified with the ORO staining. 15-20 animals were measured per genotype. **C.** Partial view of representative live animals, either not (upper animal) or expressing (lower animal) the rescuing REGE-1::GFP. In order to reduce gut-specific autofluorescence, the animals carried the *glo-1(zu391)* mutation (Hermann et al., 2005). The pharynx and intestines are outlined, arrowheads point to the REGE-1::GFP-expressing intestinal cells adjacent to the pharynx. Scale bar: 50 µm. **D.** Homology model of the *C. elegans* REGE-1 RNase domain (surface representation), in two orientations, rotated around a vertical axis by 180°. Highly conserved residues computed by ConSurf (Glaser et al., 2003) are colored in red and orange (ConSurf color grades 9 and 8). Predicted active site (asterisk) and residues required for the RNase activity in the mammalian proteins are indicated. The numbers represent amino acid numbers in the *C. elegans* REGE-1 or, in parentheses, the human Regnase-1. See also Figure S2 and S3.

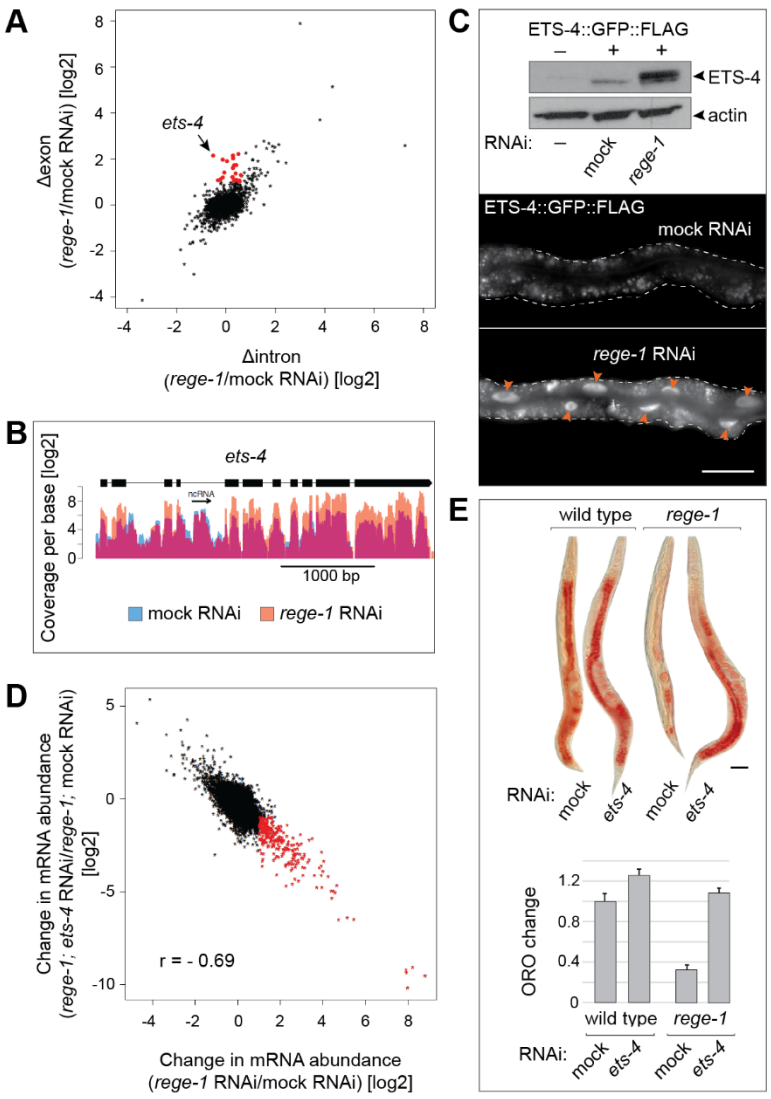

Figure 4. ETS-4 is the key effector of REGE-1.

A. Plot comparing changes in the intronic (*x* = Δintron) versus exonic (*y* = Δexon) RNA-seq reads (reflecting changes in nascent versus mature transcripts, respectively) upon *rege-1* RNAi. The Pearson correlation of r = 0.61 suggests that a substantial part of the observed changes in mRNAs may be explained by differential transcription. Red: putative REGE-1 targets that predominantly change (more than two fold) in the exonic (mature mRNA), but not the intronic (nascent RNA), reads. **B.** RNA-seq read coverage at the genomic *ets-4* locus, from animals subjected to either control (blue) or *rege-1* (orange) RNAi. Exons are represented by thick and introns by thin lines. The arrow indicates an annotated ncRNA. The samples were normalized for read depth and two replicate experiments were combined to increase the coverage. Note the increase in the exonic (but not intronic) reads upon the depletion of REGE-1. Changes in the exonic and intronic reads are quantified in Fig. S4A. **C.** Top: western blot of extracts from animals

expressing (+) or not (-) tagged ETS-4 (ETS-4::GFP::FLAG), which were subjected to mock or *rege-1* RNAi. The abundance of ETS-4::GFP::FLAG (for brevity ETS-4), detected with anti-GFP antibody, increased upon *rege-1* RNAi. Actin was a loading control. Bottom: partial view of live animals, subjected to mock or *rege-1* RNAi, with outlined intestines, expressing ETS-4::GFP::FLAG, visualized by the GFP fluorescence. Arrowheads point to the gut nuclei in a representative *rege-1* RNAi-ed animal, all of which contain increased levels of ETS-4::GFP::FLAG. Scale bar: 20 µm. **D.** Plot comparing changes in transcript levels upon *rege-1* RNAi on otherwise wild-type animals (*x*) versus *ets-4* RNAi on *rege-1* mutant animals (*y*). Transcripts that were induced two fold by ETS-4 in *rege-1* animals are marked in red. **E.** Upper panel: DIC color micrographs of representative wild-type and *rege-1(rrr13)* animals, subjected to either mock or *ets-4* RNAi, and stained by ORO to visualize fat. Depleting ETS-4 restored fat in *rege-1* animals to the wild-type levels. 15-20 animals were measured per condition. Scale bar: 50 µm. Lower panel: the corresponding ORO quantifications. See also Figure S4 and S5.

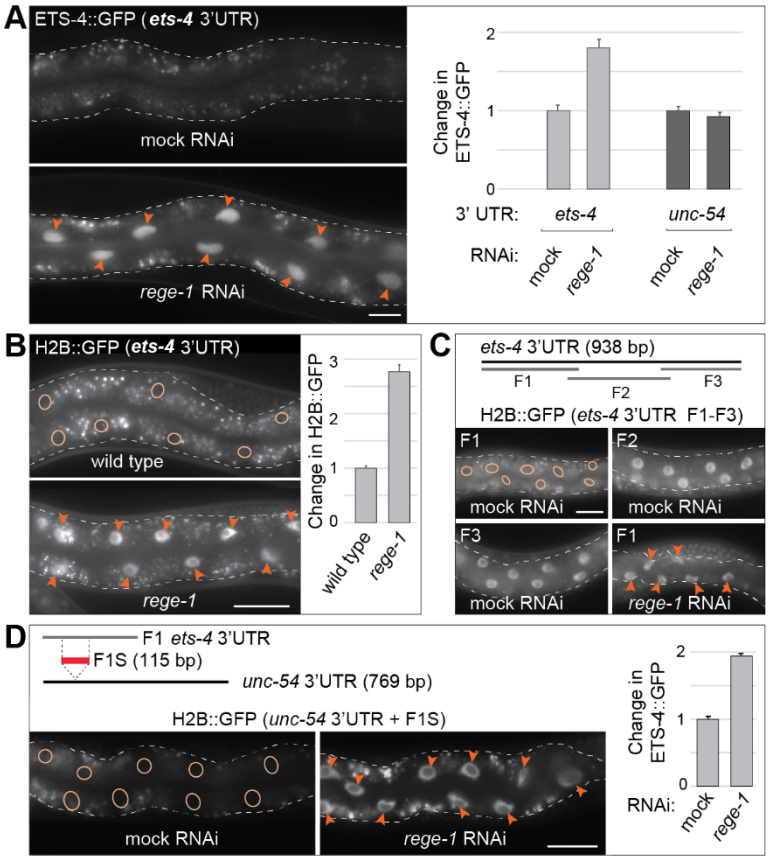

Figure 5. REGE-1 controls ETS-4 levels posttranscriptionally.

A. Left: partial view of live animals, with outlined intestines, expressing ETS-4::GFP from the endogenous *ets-4* promoter and under the control of *ets-4* 3'UTR, subjected to either mock or *rege-1* RNAi. Arrowheads point to the gut nuclei expressing ETS-4::GFP. Scale bar: 20 µm. Right: the corresponding quantification of changes in the GFP intensity, including in the control animals expressing ETS-4::GFP under the control of unregulated *unc-54* 3'UTR. The *ets-4*, but not *unc-54*, 3'UTR rendered the expression of ETS-4::GFP sensitive to REGE-1. Between 5-10 nuclei per animal, in at least 5 animals per condition, were analyzed. Error bars here and in subsequent panels represent SEM. **B.** Left: partial view of live, wild-type or *rege-1(rrr13)*, animals, with outlined intestines, expressing GFP::H2B reporter from a ubiquitous promoter (*dpy-30*) under the control of *ets-4* 3'UTR. Ovals in B-D indicate the positions of gut nuclei not expressing the reporter GFP in control animals. Arrowheads point to the gut nuclei expressing the reporter GFP in *rege-1* mutant (B) or *rege-1* RNAi-ed (C-D) animals. Scale bar: 50 µm. Right: the corresponding quantification of changes in the GFP intensity. Between 5-10 nuclei per animal, in at least 5 animals per condition, were analyzed. **C.** Top: schematic representation of the *ets-4* 3'UTR and three tested fragments (F1-3). Below: partial view of representative live, wild-type animals, with outlined intestines, expressing

the GFP::H2B reporter under the control of truncated *ets-4* 3'UTRs. The animals were subjected to either mock or *rege-1* RNAi, as indicated. Only the F1 fragment of *ets-4* 3'UTR caused repression of the GFP reporter. This repression was alleviated upon *rege-1* RNAi. Scale bar: 25 µm. **D.** Top: schematic representation of the F1 fragment of the *ets-4* 3'UTR and the shorter F1S fragment that was "transplanted" into an otherwise unregulated 3'UTR (*unc-54*; the fragment was inserted between bp 164 and 165 of the 3`UTR). Below, left: partial view of live, wild-type animals, with outlined intestines, expressing the GFP::H2B reporter under the control of the modified *unc-54* 3'UTR (containing the F1S fragment of *ets-4* 3'UTR). The animals were subjected to either mock or *rege-1* RNAi, as indicated. Insertion of the F1S fragment into the *unc-54* 3'UTR caused repression of the GFP reporter. This repression was alleviated upon *rege-1* RNAi. Scale bar: 25 µm. The corresponding quantification of changes in the GFP intensity is on the right. Between 4-8 nuclei per animal, in at least 8 animals per condition, were analyzed.

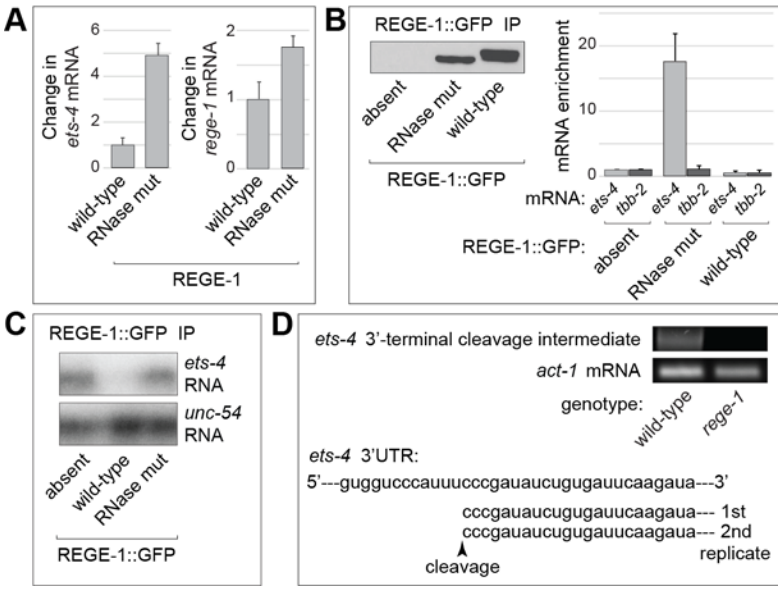

Figure 6. REGE-1 induces an endonucleolytic cleavage within the *ets-4* 3'UTR.

A. The levels of *ets-4* and *rege-1* mRNAs were measured, by RT-qPCR, in animals carrying either wild-type or mutated (RNase mut) alleles of *rege-1*. The RNase mut allele, *rege-1 (rrr21)*, was produced by changing four conserved residues in the RNase domain of REGE-1 (D231N, D313A, D314A and D332A; see Fig. 3D). Mutating these residues increased the levels of *ets-4* mRNA (left); this increase was not due to a lower expression of *rege-1* (right). The mRNA levels were normalized to the levels of *act-1* (actin) mRNA. Error bars here and in subsequent panels represent SEM. **B.** Extracts of wild-type animals, which either did not express GFP-tagged REGE-1, or expressed wild-type or the RNase mut GFP-tagged REGE-1, were subjected to immunoprecipitation (IP) using anti-GFP antibodies. Left: western blot of the IPs, showing that the RNase mut REGE-1::GFP was not expressed at a higher level than the wild-type. REGE-1::GFP was detected with REGE-1 antibody. Right: quantification of the indicated mRNAs, by RT-qPCR, in the IPs. As indicated by the enrichment of *ets-4* mRNA in the RNase mut REGE-1::GFP IP, REGE-1 associates with the *ets-4* mRNA. **C.** Immunoprecipitates, on beads, prepared as above, were incubated with labeled RNAs corresponding to either the F1S fragment of *ets-4* or a fragment of an unregulated (*unc-54*) 3'UTR. Only wild-type REGE-1 induced the degradation of *ets-4* but not *unc-54* RNA. **D.** A modified 5' RACE was performed to identify a 3'-terminal cleavage product of REGE-1 deriving from the *ets-4* mRNA. Shown is a partial sequence of F1S (beginning with the nt 89 of the *ets-4* 3'UTR, indicated by the star in Fig. S6) and sequences of two, independently amplified, 3'-terminal cleavage intermediates. Dotted lines represent sequences not shown for brevity. See also Figure S6.

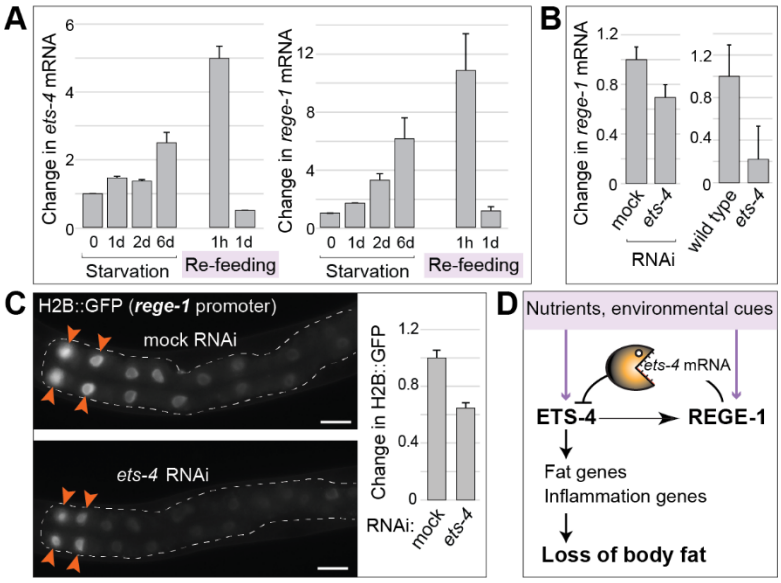

Figure 7. REGE-1 and ETS-4 form an auto-regulatory module.

A. Left: the levels of *ets-4* mRNA were measured, at indicated time points, by RT-qPCR, in wild-type animals subjected to starvation for 6 days, which was followed by re-feeding for 1 day. Right: the corresponding changes in the levels of *rege-1* mRNA. The mRNA levels, here and in B, were normalized to the levels of *act-1* mRNA. Error bars here and in subsequent panels represent SEM. **B.** The levels of *rege-1* mRNAs were measured, by RT-qPCR, in animals subjected to either control or *ets-4* RNAi (left), and in wild-type or *ets-4(rrr16)* mutants (right). **C.** Left: shown are representative fluorescent micrographs of intestines (outlined), expressing GFP::H2B reporter from the *rege-1* promoter, under the control of unregulated (*unc-54*) 3'UTR. The promoter was mostly induced in the first two pairs of intestinal cells (arrowheads). Upon *ets-4* RNAi, this expression was reduced. Scale bar: 20 µm. Right: the corresponding quantification of changes in the GFP intensity. Nuclei from the first two pairs of the intestinal cells, in 5 animals, were analyzed. **D.** A model for the REGE-1/ETS-4–mediated control of body fat. An environmental change, such as nutrient availability, is transmitted, by yet unknown mechanism(s), to alter the level of ETS-4 and/or REGE-1. Because REGE-1 inhibits ETS-4 (by degrading *ets-4* mRNA) and, conversely, ETS-4 promotes REGE-1 (by inducing, directly or indirectly, *rege-1* transcription), a change in either protein eventually alters the abundance of ETS-4. This leads to altered expression of ETS-4 target genes, including fat catabolic and innate immunity genes, consequently leading to either gain (when ETS-4 is low) or loss (when ETS-4 is high) of fat.

EXPERIMENTAL PROCEDURES

General animal handling and RNAi

Unless stated otherwise, animals were grown at 20 °C as described before (Brenner, 1974). RNAi of individual genes was performed by feeding animals with bacteria expressing dsRNA, beginning from the L1 or L4 larval stage.

Genome-wide RNAi screen

For the genome-wide RNAi screen, we used the Ahringer feeding library. The library was replicated in the 96-well format. Overnight cultures of this stock, supplemented with 2 mM IPTG, were used to seed 24-well plates. 10-15 staged L4 N2 animals were transferred per well. Knockdown was conducted for about 40 hours and, after inspection for death or sterile animals, the animals were adapted at 10 °C for 2 hours and then incubated at 4 °C for 3 days. Afterwards, the animals were incubated at 20 °C for several hours to recover. Dead animals were scored and clones with more than 4 dead animals were re-tested at least three times. The RNAi clones were sequenced.

Oil red O (ORO) staining, image processing and quantification

To visualize overall fat, ORO staining was performed essentially as described before (O'Rourke et al., 2009). All image-processing steps were done with the Fiji/imageJ software (Schindelin et al., 2012). RGB images were stitched with the Grid/Collection stitching plugin (Preibisch et al., 2009) and corrected for white balance by equalizing background mean values in the red, green and blue channels. After conversion from RGB to HSB color space and background subtraction, red pixels were selected by thresholding the "H" (Hue) channel (only pixels with a Hue value between 0 and 7 are kept). A binary mask was created with the Saturation channel and applied to the thresholded image. After conversion to 32-bit, zero pixel values were replaced by NaN. The integrated density of all remaining pixels was used as an index of the amount of red staining in the animals (Fiji/ImageJ macro available upon request).

Triglyceride (TAG) assay

Total triglyceride content was assayed essentially as before (Martorell et al., 2012), using the Triglyceride Quantification Colorimeric/Fluoromeric Kit from Biovision (Cat. no. K622-100). Animals were synchronized by hypochlorite treatment and grown on OP50 plates at 20 °C to the L4 stage. RNAi knockdown was performed for 48 h. After collecting 50 animals, and two washes in PBS, the animals were pelleted and re-suspended in 300 µl TAG buffer. Sonication was conducted with a Branson Digital Sonifier five times at 10

% power for 30 s. Worm debris were excluded by centrifugation and supernatant heated twice to 95 °C for 5 minutes. 50 µl and 25 µl of the supernatant were used to assess TAG content according to the protocol provided with the kit. Measurements were done in biological triplicates and technical duplicates.

Coherent Anti-Stokes Raman Spectroscopy (CARS)

Animals were grown at 20 °C from L1 to L4 stage and then transferred to RNAi plates. After 48 hours, animals were mounted on a slide with a drop of 2 % agarose with 20 mM levamisol. The animals were then examined by CARS microscopy on a Leica TCS SP8 system with a CARS laser picoEmerald (OPO, > 600 mW at 780 nm to 940 nm, pulse width 5 to 6 ps, 80 MHz; Pump, > 750 mW at 1064 nm, pulse length 7 ps, 80 MHz) and with LAS AF software. The lasers were adapted to the symmetrical C-H stretch range by tuning the pump beam to 816.4 nm while keeping the Stokes beam constant at 1064.6 nm. The output of both lasers was set to 1.3 W and the scan speed to 400 Hz. An image with the dimensions 145.31 µm x 145.31 µm (968 pixels x 968 pixels) and stacks of approximately 30-50 sections with a step size of approximately 0.6 µm were collected. Only signals from epi-CARS (E-CARS) and epi-SHG (E-SHG) detectors were collected. Animals were imaged just below the pharynx with one stack per animal and approximately 10 animals per conditions. Each experiment was repeated three times. The number and size of lipid droplets in each stack were examined with the Fiji software package with the Plugin DropletFinder.

Homology modeling of *C. elegans* REGE-1 RNase domain

The protein sequence of the REGE-1 RNase domain (Uniprot Q95YE2) was submitted to the HHPRED server for homology detection and structure prediction (Söding et al., 2005) in a search against known structures in the Protein Data Bank (www.rcsb.org). The structure of the human Regnase-1/MCPIP1 RNase domain (PDB 3V33; (Xu et al., 2012)) was the top hit (Score=360.7, E-value = 2.9e-57, 60% sequence identity) and its HHPRED alignment with the REGE-1 RNase domain was used for calculating a homology model encompassing residues 224-384 via the HHPRED MODELLER pipeline. Structural figures were prepared with PyMOL (www.pymol.org).

Mapping of conservation onto the REGE-1 RNase domain homology model

The homology model of REGE-1 RNase domain (residues 224-384) was uploaded to the ConSurf server (Glaser et al., 2003) using default parameters for mapping of conserved residues onto the structural model. The PSI-BLAST search for homologous sequences was done against the UniProt database and position specific conservation scores were calculated on 100 unique sequences.

Developmental timing assay

Animals were synchronized by bleaching and allowed to hatch in M9 buffer overnight. Around 200 staged L1 animals of each genotype were allowed to develop into L4s on RNAi knockdown and control plates. Picking L4s, the ratio of young adults/L4 (at least 35 animals per time point) was assessed every 2-3 h until all animals, of the respective strains, had reached adulthood. Development of vulva, alae and gonad were used to judge the developmental stage.

RNA extraction, RNA-seq and genomic data

Frozen pellets of about 6000 staged, young adults were subjected to RNA extraction with Trizol as described before (Arnold et al., 2014). Subsequently, RNA was depleted of rRNA using the Ribo-ZeroTM Magnetic kit (MRZ11124C) from epicenter and column purified with the RNA Cleanup & ConcentratorTM from Zymo research. Quality of RNA was monitored by Bioanalyzer RNA Pico chip. Library was prepared using ScriptSeqTM v2 RNA-Seq Library Preparation Kit (Epicentre).

Gene expression levels (exonic) from RNA-seq data were quantified as described previously (Hendriks et al., 2014). After normalization for library size, log2 expression levels were calculated after adding a pseudocount of 8 (y=log2(x+8)). The rege-1 and ets-4 RNAi experiments were normalized separately. Intronic expression levels were quantified as previously described (Gaidatzis et al., 2015). Exon-intron-split analysis (EISA) was performed for a subset of genes (n = 3093) that showed an average expression level (considering all samples) of at least 4.5 on the exonic as well as on the intronic level. Genes (n = 283) both up-regulated upon rege-1 RNAi and down-regulated upon ets-4 RNAi were subjected to GO overrepresentation analysis using PANTHER classification system (Mi et al., 2005), with default setting.

The genomic data has been deposited at the Gene Expression omnibus (GEO). Accession number: GSE75163. Also see Tables S1-3.

RT qPCR

RNA for RT-qPCR was extracted as described above. 300 ng of RNA was used for reverse transcription utilizing the QuantiTect Reverse Transcription Kit (Quiagen). The resulting cDNA was diluted 1:10 for further analysis. 5 µl of this dilution was used with equal volume of Express SYBR GreenER qPCR SuperMix w/ROX (Invitrogen) containing 0.2 µl of 10 mM of gen-specific primers. StepOne^{TM} RT-PCR system combined with StepOne^{TM} Software (Applied Biotechnologies) was used for analysis. The presented values are based on three biological replicates.

Western blot analysis

Western blot analysis was done as described before (Arnold et al., 2014). Primary antibodies diluted in 4 % milk/ PBS-T: mouse α-ACT-1 (MAB1501, Millipore) 1:2000, mouse α-GFP 1:1000 (Roche). Secondary antibodies: HRP coupled α–mouse from GM Healthcare, 1:4000. The REGE-1 polyclonal rabbit antibody was raised against the first 119 aa (SDIX), used at 1:1000.

Generation of rege-1(rrr13) and ets-4(rrr16) alleles, GFP-tagged REGE-1 and ETS-4, and GFP reporter lines

The rege-1(rrr13) and ets-4(rrr16) alleles were generated by CRISPR-Cas9 (Arribere et al., 2014; Katic et al., 2015). The mutations were verified by sequencing and outcrossed six times before analyzing. The ETS-4::GFP, REGE-1::GFP and 3'UTR reporter lines were constructed by MosSCI (Frøkjaer-Jensen et al., 2008). In constructing the ets-4::gfp, we used the est-4 promoter sequence (2634 bp), ets-4 genomic sequence fused to the gfp, and the ets-4 3'UTR (938 bp). In constructing the rege-1::gfp, the promoter sequence (2989 bp) was fused to rege-1 cDNA (1908 bp), gfp and rege-1 3`UTR (262 bp). To check whether the F1S sequence is sufficient for REGE-1–mediated regulation, we inserted it into an otherwise unregulated 3`UTR, unc54, between bp 164 and 165. The sgRNA sequences and primers used for construct generation are provided in the Supplementary Materials.

Quantification of the ets-4 3'UTR GFP reporter

Images for quantification of GFP intensity of reporter strains were acquired with an AxioImager.Z1 microscope (Zeiss, Jena, Germany) equipped with a 63x objective and an MRm camera (Zeiss). Signal intensity of a circular area of 52 pixels diameter of 5-7 gut nuclei of 5 animals per condition was measured in ImageJ and normalized to the background. In addition 30-35 animals per strain were visually inspected for GFP expression.

Generation of point mutations in the REGE-1 RNase domain

Four point mutations (D231N, D313A, D314A and D332A) were introduced at the endogenous locus of C30F12.1, by CRISPR/Cas9 genome editing performed by Knudra Transgenics. The editing was performed in two steps: in the first D231N and then, simultaneously, D313A, D314A and D332A. The obtained mutations, resulting in the rege-1(rrr21) allele, were verified by sequencing and the homozygous quadruple mutant was outcrossed three times to the wild type.

Starvation and re-feeding

The assay was modified after (Seidel and Kimble, 2011). Animals synchronized by hypochlorite treatment were hatched overnight in M9 and grown to young L4 stage. They were collected, washed two times with M9 buffer and transferred to plates devoid of bacteria. For re-feeding, the animals were transferred to bacteria-seeded plates. At indicated times, RNA was extracted and processed as described earlier.

REGE-1 IP / ets-4 RT-qPCR

Proteins were extracted from staged young adults as described for western blot analysis. 40 µl of Chromotek GFP Trap_A were washed twice in EB++ (EB + RNasin 5µl/ml form Promega) and 3 mg of protein was added to a final volume of 1 ml. After incubation overnight on 4 °C, the beads were washed four times with 600 µl EB++ and RNA was extracted directly from the beads by adding 500 µl Trizol. After RNA extraction and subsequent qPCR analysis, fold-enrichment was calculated as following: Enrichment IP over input: ΔCt [normalized RIP] = Ct [RIP] – (Ct[input]-Log2(input dilution factor)); normalized to control/non specific(NS) IP ΔΔCt [RIP/NS] = ΔCt [normalized RIP] – Δ [normalized NS] ; Fold- enrichment: 2^(- ΔΔCt [RIP/NS].

On-the-beads RNase assay

Radioactively labeled RNAs were transcribed from PCR products. Templates for transcription were generated by PCR with an extended phage T3 RNA polymerase promoter (AATTAACCCTCACTAAAGGGAGAA) appended to the 5' end of the 5' primer, and gel-purified. Transcription was performed in 3 µl reactions containing 0.5 µl template, 1.5 µl αP32 UTP (3 µM) and 0.6 µl 5X transcription buffer (Promega), 0.2 µl RNasin (Promega), 2.5 mM rATP, rGTP and rCTP, and 0.025 mM rUTP (Roche) at 37 ^{o}C for 3 h. The reaction was stopped by adding 30 µl TE and the RNA was purified on Spehadex G-25 columns (Roche) using manufacturer's instructions. REGE-1::GFP was immunoprecipitated as above. The beads were washed additionally once with RNase assay buffer (20 mM Tris-HCl pH 7.5, 150 mM NaCl, 5 mM MgCl2, 2 mM DTT). RNA (10^5 cpm) was suspended in RNase assay buffer and incubated with IP beads for 15 minutes at room temperature. The tubes were centrifuged and supernatant was loaded on a pre-run 6% denaturing polyacrylamide gel. After electrophoresis at 200 V for 90 min, the gel was dried and auto-radiographed.

Modified 5' RACE

To identify the 3'-terminal cleavage product of ets-4 mRNA, we employed a modified 5' RLM RACE protocol (Schmidt et al., 2015). 3-5 µg of total RNA was ligated with 0.8 µg of 5' RNA linker (GUUCAGAGUUCUACAGUCCGACGAUC) in a 10 µl reaction with 5U T4 RNA ligase in 1X RNA ligase buffer (NEB) and 1.5 mM ATP. The ligated RNA sample was reverse transcribed with a gene specific primer for ets-4 and SuperscriptIII reverse transcriptase (Thermo Fischer Scientific) using manufacturer's instructions. PCR was performed to obtain the cleaved product using a forward primer in 5' RNA linker and ets-4 reverse primer upstream of the RT primer. PCR products were sequenced to determine the cleavage site.

AUTHOR CONTRIBUTIONS

R.C. wrote the manuscript and designed the experiments. C.H. designed and performed majority of the experiments. Y.G. constructed *ets-4* transgenic lines, demonstrated the regulation of *rege-1* by ETS-4 and helped in analyzing the genomic data. R.V. performed the initial cold-sensitivity screen and analysis. P.K. assisted with the 5`RACE and on beads RNase assay. A.N. assisted with constructing some transgenic strains. D.G. analyzed the RNA-seq data. E.B.H. and N.J.F. performed the CARS experiment. H.G. did homology analysis and modeling of the *C. elegans* RNase domain. All authors contributed to interpretation of the data and provided comments on the manuscript.

ACKNOWLEDGMENTS

We thank Hugo Aguilaniu and Witold Filipowicz for comments on the manuscript, Ciosk lab members for discussions, Iskra Katic for technical help and Laurent Gelman for help with Oil red O quantification. Some of the strains were provided by the Caenorhabditis Genetics Center (CGC) funded by the NIH. Pooja Kumari has received funding for the research leading to these results from the EMBO Fellowship (ALTF 95-2015) co-funded by the European Commission support for Marie Curie Actions (LTFCOFUND2013, GA-2013-609409). FMI is sponsored by the Novartis Research Foundation.

REFERENCES

Arner, P., Kulyté, A., 2015. MicroRNA regulatory networks in human adipose tissue and obesity. Nat Rev Endocrinol 11, 276–288. doi:10.1038/nrendo.2015.25

Arnold, A., Rahman, M.M., Lee, M.C., Muehlhaeusser, S., Katic, I., Gaidatzis, D., Hess, D., Scheckel, C., Wright, J.E., Stetak, A., Boag, P.R., Ciosk, R., 2014. Functional characterization of C. elegans Y-box-binding proteins reveals tissue-specific functions and a critical role in the formation of polysomes. Nucleic Acids Res. 42, 13353–13369.

Arribere, J.A., Bell, R.T., Fu, B.X.H., Artiles, K.L., Hartman, P.S., Fire, A.Z., 2014. Efficient marker-free recovery of custom genetic modifications with CRISPR/Cas9 in Caenorhabditis elegans. Genetics 198, 837–846. doi:10.1534/genetics.114.169730

Barrière, A., Félix, M.-A., 2005. Natural variation and population genetics of Caenorhabditis elegans. WormBook 1–19. doi:10.1895/wormbook.1.43.1

Brenner, S., 1974. The Genetics of Caenorhabditis elegans. Genetics 71–94.

Dark, J., 2005. Annual lipid cycles in hibernators: integration of physiology and behavior. Annu. Rev. Nutr. 25, 469–497. doi:10.1146/annurev.nutr.25.050304.092514

Engelmann, I., Griffon, A., Tichit, L., Montañana-Sanchis, F., Wang, G., Reinke, V., Waterston, R.H., Hillier, L.W., Ewbank, J.J., 2011. A comprehensive analysis of gene expression changes provoked by bacterial and fungal infection in C. elegans. PLoS ONE 6, e19055. doi:10.1371/journal.pone.0019055

Folmes, C.D.L., Dzeja, P.P., Nelson, T.J., Terzic, A., 2012. Metabolic plasticity in stem cell homeostasis and differentiation. Cell Stem Cell 11, 596–606. doi:10.1016/j.stem.2012.10.002

Frøkjaer-Jensen, C., Davis, M.W., Hopkins, C.E., Newman, B.J., Thummel, J.M., Olesen, S.-P., Grunnet, M., Jorgensen, E.M., 2008. Single-copy insertion of transgenes in Caenorhabditis elegans. Nature genetics 40, 1375–1383. doi:10.1038/ng.248

Gaidatzis, D., Burger, L., Florescu, M., Stadler, M.B., 2015. Analysis of intronic and exonic reads in RNA-seq data characterizes transcriptional and post-transcriptional regulation. Nat. Biotechnol. doi:10.1038/nbt.3269

Glaser, F., Pupko, T., Paz, I., Bell, R.E., Bechor-Shental, D., Martz, E., Ben-Tal, N., 2003. ConSurf: identification of functional regions in proteins by surface-mapping of phylogenetic information. Bioinformatics 19, 163–164.

Gregor, M.F., Hotamisligil, G.S., 2011. Inflammatory mechanisms in obesity. Annu. Rev. Immunol. 29, 415–445. doi:10.1146/annurev-immunol-031210-101322

Guilherme, A., Virbasius, J.V., Puri, V., Czech, M.P., 2008. Adipocyte dysfunctions linking obesity to insulin resistance and type 2 diabetes. Nature Reviews Molecular Cell Biology 9, 367–377. doi:10.1038/nrm2391

Hansen, M., Flatt, T., Aguilaniu, H., 2013. Reproduction, fat metabolism, and life span: what is the connection? Cell Metabolism 17, 10–19. doi:10.1016/j.cmet.2012.12.003

Hendriks, G.-J., Gaidatzis, D., Aeschimann, F., Grosshans, H., 2014. Extensive oscillatory gene expression during C. elegans larval development. Mol Cell 53, 380–392. doi:10.1016/j.molcel.2013.12.013

Hermann, G.J., Schroeder, L.K., Hieb, C.A., Kershner, A.M., Rabbitts, B.M., Fonarev, P., Grant, B.D., Priess, J.R., 2005. Genetic analysis of lysosomal trafficking in Caenorhabditis elegans. Molecular biology of the cell 16, 3273–3288. doi:10.1091/mbc.E05-01-0060

Iwasaki, H., Takeuchi, O., Teraguchi, S., Matsushita, K., Uehata, T., Kuniyoshi, K., Satoh, T., Saitoh, T., Matsushita, M., Standley, D.M., Akira, S., 2011. The IκB kinase complex regulates the stability of cytokine-encoding mRNA induced by TLR-IL-1R by controlling degradation of regnase-1. Nat. Immunol. 12, 1167–1175. doi:10.1038/ni.2137

Jeltsch, K.M., Hu, D., Brenner, S., Zöller, J., Heinz, G.A., Nagel, D., Vogel, K.U., Rehage, N., Warth, S.C., Edelmann, S.L., Gloury, R., Martin, N., Lohs, C., Lech, M., Stehklein, J.E., Geerlof, A., Kremmer, E., Weber, A., Anders, H.-J., Schmitz, I., Schmidt-Supprian, M., Fu, M., Holtmann, H., Krappmann, D., Ruland, J., Kallies, A., Heikenwalder, M., Heissmeyer, V., 2014. Cleavage of roquin and regnase-1 by the paracaspase MALT1 releases their cooperatively repressed targets to promote TH17 differentiation. Nat. Immunol. 15, 1079–1089. doi:10.1038/ni.3008

Katic, I., Xu, L., Ciosk, R., 2015. CRISPR/Cas9 Genome Editing in Caenorhabditis elegans: Evaluation of Templates for Homology-Mediated Repair and Knock-Ins by Homology-Independent DNA Repair. G3 (Bethesda) 5, 1649–1656. doi:10.1534/g3.115.019273

Liang, J., Wang, J., Azfer, A., Song, W., Tromp, G., Kolattukudy, P.E., Fu, M., 2008. A Novel CCCH-Zinc Finger Protein Family Regulates Proinflammatory Activation of Macrophages. J. Biol. Chem. 283(10):6337-46. doi: 10.1074/jbc.M707861200

Lipert, B., Wegrzyn, P., Sell, H., Eckel, J., Winiarski, M., Budzynski, A., Matlok, M., Kotlinowski, J., Ramage, L., Malecki, M., Wilk, W., Mitus, J., Jura, J., 2014. Monocyte chemoattractant protein-induced protein 1 impairs adipogenesis in 3T3-L1 cells. Biochim. Biophys. Acta 1843, 780–788. doi:10.1016/j.bbamcr.2014.01.001

Longo, V.D., Mattson, M.P., 2014. Fasting: molecular mechanisms and clinical applications. Cell Metabolism 19, 181–192. doi:10.1016/j.cmet.2013.12.008

Martorell, P., Llopis, S., González, N., Montón, F., Ortiz, P., Genovés, S., Ramón, D., 2012. Caenorhabditis elegans as a model to study the effectiveness and metabolic targets of dietary supplements used for obesity treatment: the specific case of a conjugated linoleic acid mixture (Tonalin). J. Agric. Food Chem. 60, 11071–11079. doi:10.1021/jf3031138

Matsushita, K., Takeuchi, O., Standley, D.M., Kumagai, Y., Kawagoe, T., Miyake, T., Satoh, T., Kato, H., Tsujimura, T., Nakamura, H., Akira, S., 2009. Zc3h12a is an RNase essential for controlling immune responses by regulating mRNA decay. Nature 458, 1185–1190. doi:10.1038/nature07924

Mi, H., Lazareva-Ulitsky, B., Loo, R., Kejariwal, A., Vandergriff, J., Rabkin, S., Guo, N., Muruganujan, A., Doremieux, O., Campbell, M.J., Kitano, H., Thomas, P.D., 2005. The PANTHER database of protein families, subfamilies, functions and pathways. Nucleic Acids Res. 33, D284–8. doi:10.1093/nar/gki078

Mino, T., Murakawa, Y., Fukao, A., Vandenbon, A., Wessels, H.-H., Ori, D., Uehata, T., Tartey, S., Akira, S., Suzuki, Y., Vinuesa, C.G., Ohler, U., Standley, D.M., Landthaler, M., Fujiwara, T., Takeuchi, O., 2015. Regnase-1 and Roquin Regulate a Common Element in Inflammatory mRNAs by Spatiotemporally Distinct Mechanisms. Cell 161, 1058–1073. doi:10.1016/j.cell.2015.04.029

Murray, P., Hayward, S.A.L., Govan, G.G., Gracey, A.Y., Cossins, A.R., 2007. An explicit test of the phospholipid saturation hypothesis of acquired cold tolerance in Caenorhabditis elegans. Proceedings of the National Academy of Sciences 104, 5489–5494. doi:10.1073/pnas.0609590104

O'Rourke, E.J., Soukas, A.A., Carr, C.E., Ruvkun, G., 2009. C. elegans major fats are stored in vesicles distinct from lysosome-related organelles. Cell Metabolism 10, 430–435. doi:10.1016/j.cmet.2009.10.002

Ohta, A., Ujisawa, T., Sonoda, S., Kuhara, A., 2014. Light and pheromone-sensing neurons regulates cold habituation through insulin signalling in Caenorhabditis elegans. Nat Commun 5, 4412. doi:10.1038/ncomms5412

Preibisch, S., Saalfeld, S., Tomancak, P., 2009. Globally optimal stitching of tiled 3D microscopic image acquisitions. Bioinformatics 25, 1463–1465.

Rottiers, V., Näär, A.M., 2012. MicroRNAs in metabolism and metabolic disorders. Nature Reviews Molecular Cell Biology 13, 239–250. doi:10.1038/nrm3313

Schindelin, J., Arganda-Carreras, I., Frise, E., Kaynig, V., Longair, M., Pietzsch, T., Preibisch, S., Rueden, C., Saalfeld, S., Schmid, B., Tinevez, J.-Y., White, D.J., Hartenstein, V., Eliceiri, K., Tomancak, P., Cardona, A., 2012. Fiji: an open-source platform for biological-image analysis. Nat Meth 9, 676–682. doi:10.1038/nmeth.2019

Schmidt, S.A., Foley, P.L., Jeong, D.-H., Rymarquis, L.A., Doyle, F., Tenenbaum, S.A., Belasco, J.G., Green, P.J., 2015. Identification of SMG6 cleavage sites and a preferred RNA cleavage motif by global analysis of endogenous NMD targets in human cells. Nucleic Acids Res. 43, 309–323. doi:10.1093/nar/gku1258

Seidel, H.S., Kimble, J., 2011. The oogenic germline starvation response in C. elegans. PLoS ONE 6, e28074. doi:10.1371/journal.pone.0028074

Sharrocks, A.D., 2001. The ETS-domain transcription factor family. Nature Reviews Molecular Cell Biology 2, 827–837. doi:10.1038/35099076

Söding, J., Biegert, A., Lupas, A.N., 2005. The HHpred interactive server for protein homology detection and structure prediction. Nucleic Acids Res. 33, W244–8. doi:10.1093/nar/gki408

Srinivasan, S., 2014. Regulation of Body Fat in Caenorhabditis elegans. Annu. Rev. Physiol. doi:10.1146/annurev-physiol-021014-071704

Taubert, S., Van Gilst, M.R., Hansen, M., Yamamoto, K.R., 2006. A Mediator subunit, MDT-15, integrates regulation of fatty acid metabolism by NHR-49-dependent and -independent pathways in C. elegans. Genes Dev 20, 1137–1149. doi:10.1101/gad.1395406

Thyagarajan, B., Blaszczak, A.G., Chandler, K.J., Watts, J.L., Johnson, W.E., Graves, B.J., 2010. ETS-4 is a transcriptional regulator of life span in Caenorhabditis elegans. PLoS Genet 6, e1001125. doi:10.1371/journal.pgen.1001125

Ward, P.S., Thompson, C.B., 2012. Metabolic reprogramming: a cancer hallmark even warburg did not anticipate. Cancer Cell 21, 297–308. doi:10.1016/j.ccr.2012.02.014

Watts, J.L., 2009. Fat synthesis and adiposity regulation in Caenorhabditis elegans. Trends Endocrinol. Metab. 20, 58–65. doi:10.1016/j.tem.2008.11.002

Watts, J.L., Browse, J., 2000. A palmitoyl-CoA-specific delta9 fatty acid desaturase from Caenorhabditis elegans. Biochem. Biophys. Res. Commun. 272, 263–269. doi:10.1006/bbrc.2000.2772

Wilczynska, A., Bushell, M., 2015. The complexity of miRNA-mediated repression. Cell Death Differ. 22, 22–33. doi:10.1038/cdd.2014.112

Xu, J., Peng, W., Sun, Y., Wang, X., Xu, Y., Li, X., Gao, G., Rao, Z., 2012. Structural study of MCPIP1 N-terminal conserved domain reveals a PIN-like RNase. Nucleic acids ….

Yokogawa, M., Tsushima, T., Noda, N.N., Kumeta, H., Enokizono, Y., Yamashita, K., Standley, D.M., Takeuchi, O., Akira, S., Inagaki, F., 2016. Structural basis for the regulation of enzymatic activity of Regnase-1 by domain-domain interactions. Sci Rep 6, 22324. doi:10.1038/srep22324

Younce, C.W., Azfer, A., Kolattukudy, P.E., 2009. MCP-1 (monocyte chemotactic protein-1)-induced protein, a recently identified zinc finger protein, induces adipogenesis in 3T3-L1 pre-adipocytes without peroxisome proliferator-activated receptor gamma. J Biol Chem 284, 27620–27628. doi:10.1074/jbc.M109.025320

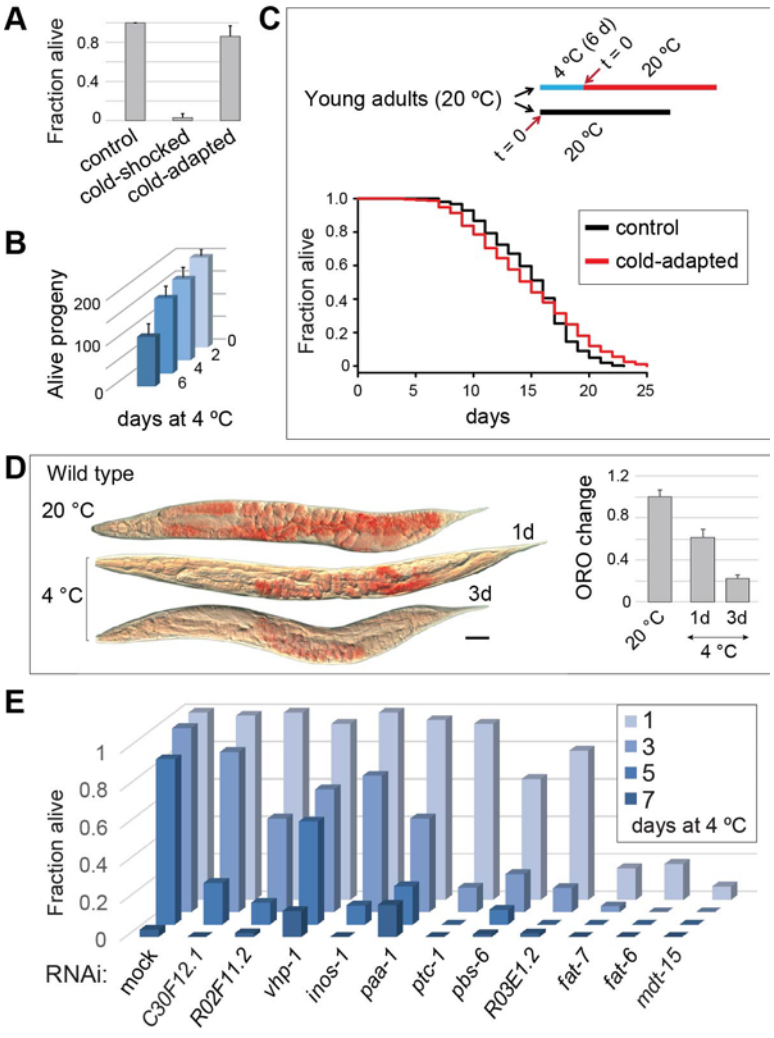

Figure S1. Characterization of cold-induced suspended animation in *C. elegans* and of factors required for cold survival

A. Shown are fractions of alive adults at 20 °C. Prior to this, the animals were incubated for 24 hours at either 20 °C (control), 4 °C (cold-shocked) or at 4 °C but following a prior incubation at 10 ºC for 2 hours (cold-adapted). Data presented as mean, error bars represent SD. **B.** Numbers of viable progeny per animal, based on analysis of at least 10 individual hermaphrodites. Following a 2 hours adaption at 10°C, the animals were incubated at 4 °C for the indicated number of days. Data presented as mean, error bars represent SD. **C.** Life span measurement. Top: schematic explanation of the experimental setup. Red arrows indicate the beginning of the life span measurement (t = 0). Blue line indicates the 6 days, prior to

the life span measurement, that the cold-adapted animals spent at 4 ºC. Bottom: Meier-Kaplan survival plot representing the life span of control (black line) and cold-adapted animals (red line). Analysis was done in triplicates, each with around 150 animals. P-value: 0.0349. **D.** ORO staining of control (20 °C) and cold-adapted animals that were incubated at 4 °C for the indicated number of days (d). Size bar: 50 µm. Quantification of the ORO changes is on the right. 5-10 animals were measured per condition. Data presented as mean, error bars represent SEM. **E.** Survival of animals, subjected to RNAi against the indicated genes (summarized in Fig. 1B), was examined, in a time course-like fashion, following their removal from 4 °C at the indicated time points. 50-100 animals were scored per time point and condition.

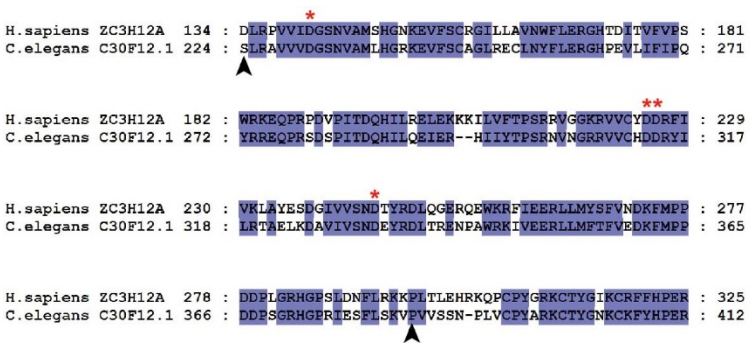

Figure S2. Conservation of the RNase domain of REGE-1, related to Figure 3: Sequence alignment of *H. sapiens* Regnase-1/ZC3H12A and *C. elegans* REGE-1, comprising RNase and CCCH zinc finger domains. The alignment was computed with HHPRED (Söding et al., 2005), or www. http://toolkit.tuebingen.mpg.de/hhpred, and used for modeling the *C. elegans* REGE-1 RNase domain. Arrowheads indicate the N- and C-termini of the human Regnase-1/MCPIP1 RNase 3D template (PDB 3V33, (Xu et al., 2012) and the *C. elegans* REGE-1 RNase homology model. Shaded are identical and similar amino acids. "*" indicate amino acids marked in Fig. 3D.

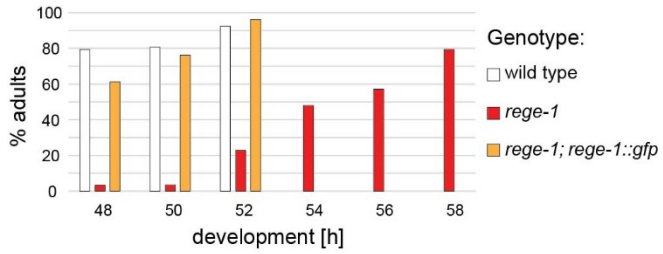

Figure S3. Rescue of the *rege-1(rrr13)* developmental delay by GFP-tagged REGE-1, related to Figure 3: Fraction of adults, among wild-type, *rege-1(rrr13)* or *rege-1(rrr13)* animals carrying the transgenic *rege-1::gfp*, determined at the indicated times (hours past the release from the L1 larval arrest; for details see experimental procedures). Note that the single copy-integrated *rege-1::gfp* rescued the developmental delay observed in *rege-1(rrr13)* animals. At least 30 animals were analyzed per time point and genotype.

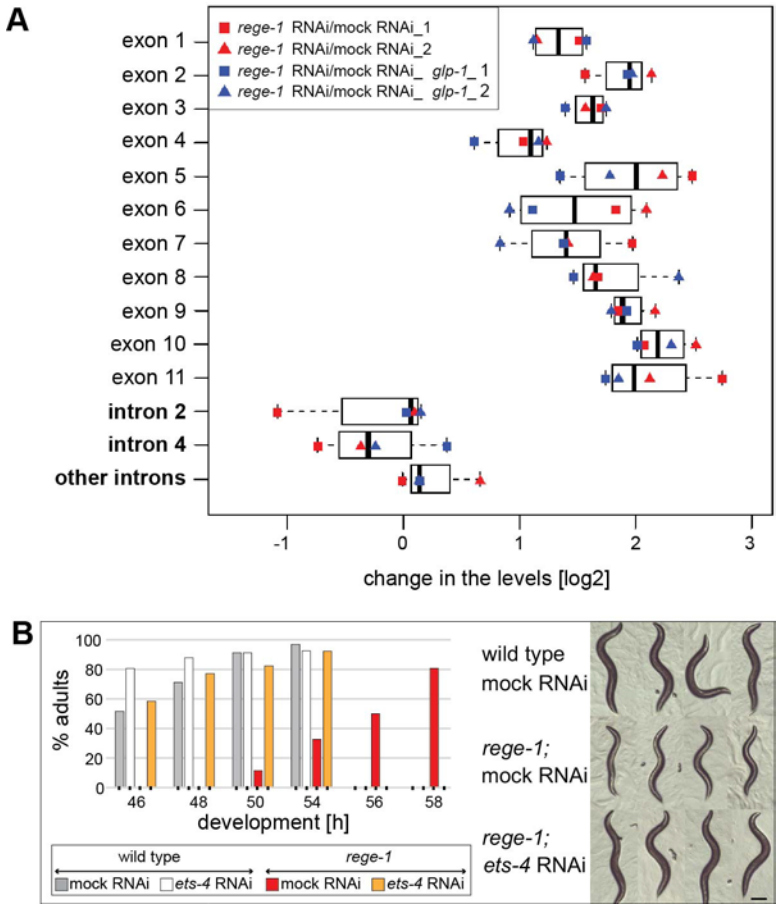

Figure S4. REGE-1 targets *ets-4* mRNA, related to Figure 4: A. Boxplot based on exon-intron split analysis, which was performed for each exon and intron of the *ets-4* gene. For introns shorter than 150 bp (other introns), mapped reads were summed before normalization with library size. Inset legend indicates the data points used for the boxplot from 4 experiments. The *glp-1* mutation results in germline-less animals. **B.** Left: % of adults among wild-type or *rege-1(rrr13)* animals, subjected to either mock or *ets-4* RNAi, was determined at the indicated times (past the release from the L1 larval arrest; for details see experimental procedures). At least 30 animals were analyzed per time point and condition. Right: representative micrographs of adults 65 h post the L1 stage. Note that depleting ETS-4 restored the wild-type size (reduced due to a developmental delay) in *rege-1(rrr13)* animals. Scale bar: 100 µm.

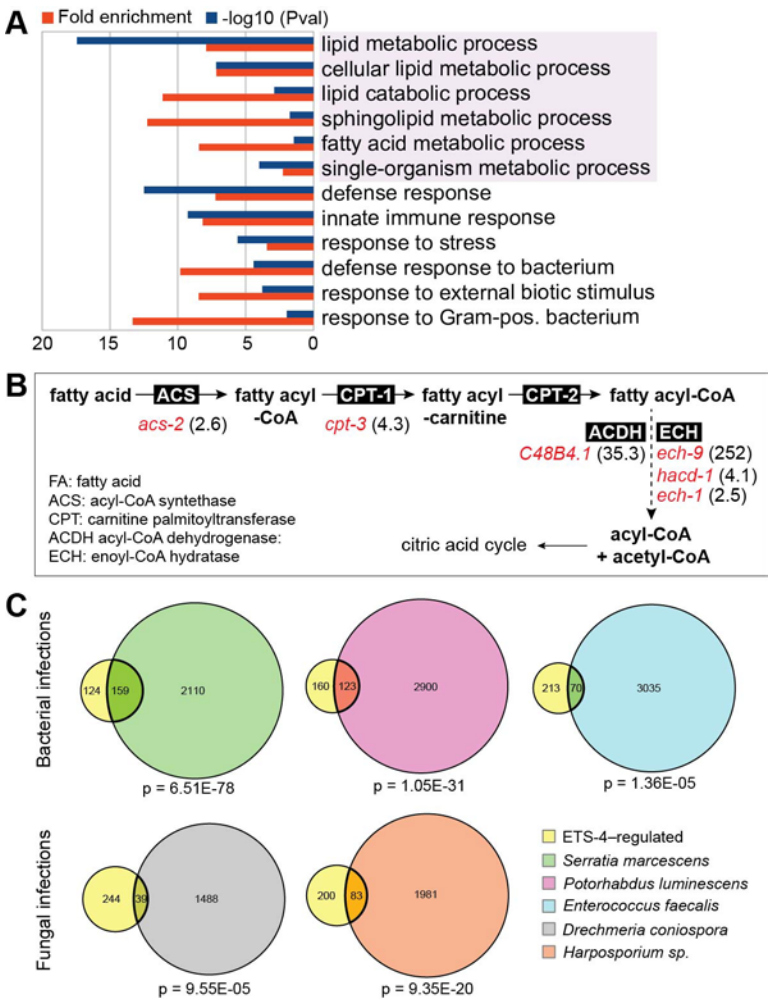

Figure S5. ETS-4 induces expression of lipid metabolic and defense genes, related to Figure 4: A. Gene ontology terms significantly enriched among the transcripts marked in red in Fig. 4D. The two major classes are fat metabolism (on colored background) and innate immunity. **B.** A simplified view of the fatty acid degradation pathway. Enzymes catalyzing the individual steps are indicated on the black background. In red are transcripts encoding the corresponding enzymes, which increase in abundance in *rege-1(rrr13)* animals (fold changes in parentheses). The first three steps in the pathway involve the delivery of fatty acyl-CoA into mitochondria. Dotted arrow collectively indicates beta-oxidation, resulting in the production of acyl-CoA and acetyl-CoA, which is further consumed in the citric acid cycle to produce energy. **C.** The relation between genes up-regulated by ETS-4 (red genes in Fig. 4D) and genes up-regulated upon pathogenic infections (Engelmann et al., 2011). Shown are proportional Venn diagrams showing the overlap between ETS-4–induced genes and genes induced by bacterial (*Serratia marcescens*, *Potorhabdus*

luminescens, *Enterococcus faecalis*) and fungal (*Drechmeria coniospora*, *Harposporium sp*.) infections. *D. coniospora* infects *C. elegans* via cuticle and epidermis, while others are able to infect through the intestine. The p values were calculated with hypergeometric test.

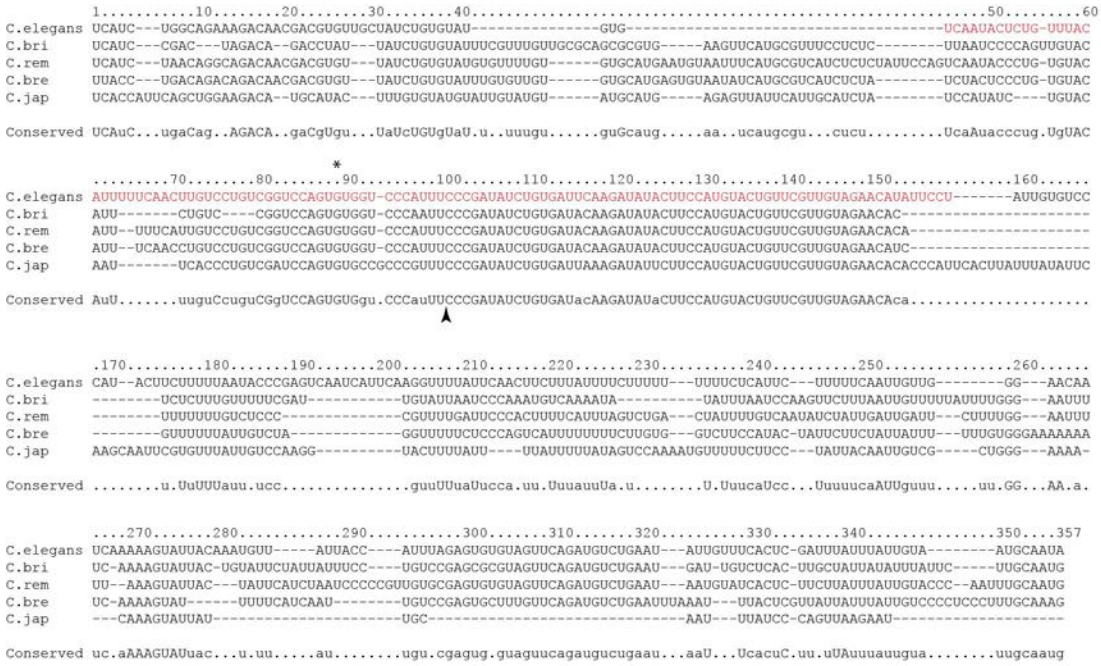

Figure S6. The F1 fragment of *ets-4* 3'UTR contains a stretch of highly conserved sequence, related to Figures 5 and 6: Shown is the sequence of fragment F1 (nt. 1-357), aligned to the corresponding sequences from other *Caenorhabditis* species (*briggsae*, *remanei*, *brenneri* and *japonica*). In red is the sequence of fragment F1S (nt. 45-159). "*" indicates the beginning of sequence shown in Fig. 6D and arrowhead points to the position of REGE-1–mediated cleavage.

Table S1. Related to Figure 4. Normalized exonic read counts (log2) from RNA-seq for mock and *rege-1* RNAi treated animals in N2 as well as in *glp-1* backgrounds.

Table S2. Related to Figure 4. Normalized intronic read counts (log2) from RNA-seq for mock and *rege-1* RNAi treated animals in N2 as well as in *glp-1* backgrounds.

Table S3. Related to Figure 4. Normalized exonic read counts (log2) from RNA-seq for mock and *ets-4* RNAi treated *rege-1* animals.

Abbreviation	Explaination
	TRUE
	FALSE
UpR	genes upregulated in *rege-1 (rrr13) vs.* N2 (log scale)
DnE	genes downregulated in *rege-1(rrr13);ets-4i vs.rege-1(rrr13)* (log scale)
Sma	Serratia marcescens
PL	Potorhabdus luminescens
Efa	Enterococcus faecalis
DC	Drechmeria coniospora
Har	Harposporium sp.

			GO term		Upregulated upon pathogen				
UpR	DnE	Gene	GO lipid	GO defense	Sma	Efa	PL	Dc	Har
7.98	-10.20	ech-9							
8.80	-9.55	spp-12							
7.92	-9.37	F21F8.4							
7.90	-9.20	ugt-18							
8.21	-9.08	clec-70							
4.73	-6.51	clec-52							
5.45	-6.49	clec-72							
5.14	-6.42	C48B4.1							
4.42	-5.34	F49C12.7							
4.57	-5.07	clec-69							
4.39	-4.98	clec-60							
4.48	-4.97	spp-9							
3.95	-4.79	clec-169							
3.70	-4.77	math-34							
2.27	-4.69	lys-4							
4.65	-4.67	Y65B4BR.1							
2.56	-4.58	cyp-13B1							
2.85	-4.42	fut-2							
2.67	-4.32	clec-125							
4.24	-4.19	F09C8.1							
3.06	-4.13	spp-23							
3.60	-4.13	clec-53							
3.91	-4.12	fil-1							
1.83	-4.10	Y39G8B.7							
3.99	-3.90	clec-71							
2.51	-3.86	T21H3.1							
2.55	-3.75	Y51H4A.5							
3.14	-3.72	K05B2.4							
3.82	-3.72	F55G1.13							
2.71	-3.70	F49F1.5							
3.03	-3.69	clec-81							
1.15	-3.64	cpr-1							
2.24	-3.63	F35E12.5							
3.91	-3.61	Y39B6A.1							
2.25	-3.57	Y39G8B.9							
2.74	-3.54	asp-6							
2.34	-3.52	F20G2.5							
2.59	-3.52	pmp-1							
2.47	-3.52	Y49E10.18							
2.85	-3.45	sru-40							
3.29	-3.44	clec-67							
2.40	-3.43	F23G4.1							
2.54	-3.37	cpr-3							
1.15	-3.37	F11D11.3							
2.71	-3.36	oac-5							
4.03	-3.36	lipl-1							
2.84	-3.31	spp-2							
1.67	-3.31	sulp-1							

			GO term		Upregulated upon pathogen				
UpR	DnE	Gene	GO lipid	GO defense	Sma	Efa	PL	Dc	Har
3.34	-3.29	cyp-13A12							
1.18	-3.27	W03F9.4							
2.63	-3.25	spp-18							
3.04	-3.24	C50F7.5							
1.76	-3.20	clec-4							
2.56	-3.20	C18A11.3							
3.00	-3.19	asp-3							
1.90	-3.15	B0035.13							
3.12	-3.09	B0244.7							
2.67	-3.09	W04C9.6							
1.83	-3.09	Y4C6B.6							
2.08	-3.08	cpr-4							
2.65	-3.03	Y37H2A.14							
2.69	-3.02	C33C12.3							
2.61	-3.02	clec-62							
2.91	-3.00	pcp-2							
3.12	-2.99	math-38							
2.10	-2.99	cpt-3							
2.80	-2.97	F55G1.12							
1.20	-2.97	clec-74							
1.69	-2.96	sodh-1							
2.69	-2.95	C31H5.6							
2.14	-2.93	clec-42							
1.10	-2.92	C49G9.1							
3.93	-2.88	F42A10.7							
2.59	-2.83	C17H12.6							
2.22	-2.78	T19D12.4							
2.55	-2.77	lact-3							
1.03	-2.76	ugt-35							
2.15	-2.74	clec-49							
2.40	-2.73	asp-2							
2.68	-2.72	fat-5							
2.36	-2.71	clec-80							
2.13	-2.70	Y68A4A.13							
1.91	-2.70	C49C3.9							
2.34	-2.70	W02B12.1							
2.79	-2.68	Y32B12A.3							
1.82	-2.68	K01A2.4							
2.28	-2.66	asp-1							
2.23	-2.64	C29F4.2							
1.95	-2.60	F28H7.3							
1.40	-2.58	F25A2.1							
1.61	-2.58	ZK896.5							
1.70	-2.56	nlt-1							
1.44	-2.52	clec-150							
2.33	-2.51	sptl-2							
2.53	-2.51	abt-4							
2.63	-2.51	trx-3							
2.86	-2.50	asm-2							
1.19	-2.47	oac-31							
1.70	-2.47	C54E4.5							
1.64	-2.46	fpn-1.2							
1.89	-2.46	clec-51							
2.78	-2.42	T24C4.9							
2.98	-2.42	spp-21							
1.15	-2.42	F46C5.1							
2.35	-2.41	clec-63							
1.27	-2.38	R07E3.2							
1.34	-2.37	clec-48							
1.25	-2.37	C17F4.7							
2.08	-2.35	cln-3.1							

			GO term		Upregulated upon pathogen				
UpR	DnE	Gene	GO lipid	GO defense	Sma	Efa	PL	Dc	Har
1.72	-2.35	M60.2							
1.16	-2.32	ins-7							
2.38	-2.31	F21H12.7							
2.06	-2.31	cat-4							
1.93	-2.31	C17F4.2							
1.52	-2.30	Y53G8AR.7							
2.08	-2.29	C18A11.1							
1.79	-2.28	F52H2.3							
1.56	-2.28	K02A11.4							
1.70	-2.26	ugt-34							
2.15	-2.25	ets-4							
1.91	-2.24	spp-4							
1.97	-2.24	ugt-37							
3.34	-2.24	W07B8.4							
1.10	-2.24	clec-66							
2.14	-2.23	W02G9.4							
2.05	-2.22	hacd-1							
1.21	-2.22	irg-3							
1.81	-2.22	Y49E10.16							
1.03	-2.21	F19C7.2							
1.27	-2.20	clec-50							
1.97	-2.19	asp-5							
1.29	-2.19	K10D11.5							
1.08	-2.17	cyp-37B1							
1.84	-2.17	nhx-2							
1.54	-2.17	T26H5.9							
1.99	-2.16	C14C11.4							
1.03	-2.16	F53A9.8							
1.08	-2.16	scav-5							
1.55	-2.15	Y46D2A.2							
3.49	-2.14	Y53G8AM.5							
1.57	-2.12	Y39B6A.24							
2.59	-2.11	C30F12.1							
1.92	-2.10	clec-172							
1.45	-2.10	F26G1.10							
2.07	-2.10	str-116							
1.95	-2.09	T28F3.8							
1.34	-2.08	ech-1							
1.59	-2.08	C24B9.3							
1.59	-2.07	F13D12.6							
1.42	-2.05	C49C8.5							
1.96	-2.03	dsc-4							
1.34	-2.03	Y9C9A.8							
1.66	-2.03	lys-8							
1.60	-2.01	C17H12.8							
2.30	-2.01	arrd-3							
1.18	-2.00	K12H4.7							
1.62	-2.00	F48G7.5							
1.34	-1.96	F48G7.8							
1.43	-1.94	F01D5.5							
2.94	-1.94	clec-47							
1.02	-1.93	clec-76							
1.03	-1.92	lipl-2							
1.76	-1.91	scav-4							
1.33	-1.89	C51E3.10							
1.49	-1.89	H20E11.1							
1.67	-1.87	fbxa-12							
1.73	-1.86	Y37E3.11							
1.57	-1.86	F57F4.4							
1.41	-1.84	Y73B6BL.31							
1.19	-1.82	F58A6.1							

			GO term		Upregulated upon pathogen				
UpR	DnE	Gene	GO lipid	GO defense	Sma	Efa	PL	Dc	Har
2.15	-1.82	spp-8							
1.82	-1.81	F55G1.15							
1.00	-1.81	K08D8.1							
1.68	-1.80	tag-244							
1.39	-1.80	Y51H4A.25							
1.16	-1.79	scav-1							
1.27	-1.79	M02H5.8							
1.33	-1.78	ads-1							
1.13	-1.78	R10H10.3							
1.87	-1.77	H02F09.3							
1.20	-1.77	twk-26							
1.30	-1.77	F25E2.3							
1.15	-1.74	nhr-168							
1.59	-1.74	F40F4.6							
1.38	-1.73	tmem-135							
2.04	-1.73	acl-1							
1.17	-1.73	Y71G12B.2							
1.53	-1.73	B0244.10							
1.22	-1.72	Y66D12A.13							
1.17	-1.72	Y32F6A.4							
1.12	-1.71	Y54G2A.45							
1.35	-1.71	F46G10.4							
1.29	-1.71	clec-33							
1.61	-1.69	Y106G6H.1							
1.35	-1.68	E02H9.5							
1.20	-1.68	pqm-1							
1.59	-1.67	sgca-1							
1.60	-1.65	H10E21.1							
1.48	-1.65	clec-205							
1.17	-1.65	pho-1							
1.87	-1.65	F47A4.5							
1.96	-1.64	ugt-44							
1.27	-1.63	K03H1.10							
1.26	-1.62	ddo-1							
1.34	-1.62	clec-31							
1.21	-1.61	T08B1.1							
1.12	-1.61	K11H12.4							
1.80	-1.61	gfi-1							
1.57	-1.60	M176.4							
1.42	-1.60	kgb-2							
1.36	-1.60	T22F3.11							
1.31	-1.59	ctl-2							
1.49	-1.58	Y46G5A.20							
1.17	-1.57	cln-3.3							
1.28	-1.57	F59F3.4							
1.46	-1.56	F07B10.4							
1.19	-1.56	F30H5.3							
1.28	-1.56	F54D7.2							
1.02	-1.54	lmp-2							
1.30	-1.52	C13C4.5							
1.90	-1.51	K10C2.1							
1.01	-1.51	glt-6							
1.27	-1.51	Y69A2AL.2							
1.25	-1.51	K06G5.1							
2.03	-1.50	F33H12.7							
1.40	-1.50	clec-204							
1.92	-1.50	asah-1							
1.29	-1.50	ZC328.3							
1.30	-1.49	B0281.3							
1.00	-1.49	C16D9.4							
1.00	-1.47	fbxa-66							

			GO term		Upregulated upon pathogen				
UpR	DnE	Gene	GO lipid	GO defense	Sma	Efa	PL	Dc	Har
1.04	-1.46	Y71G12B.32							
1.65	-1.46	B0280.2							
1.25	-1.45	C49A9.3							
1.34	-1.44	sma-5							
1.03	-1.44	Y23H5B.4							
1.06	-1.43	sptl-1							
1.16	-1.43	math-10							
2.32	-1.42	ghi-1							
1.03	-1.41	F59F4.1							
1.02	-1.41	K08F9.1							
1.37	-1.39	acs-2							
1.06	-1.39	W01C8.5							
1.01	-1.39	dhs-28							
1.20	-1.39	cyp-32B1							
1.01	-1.38	T05F1.11							
1.36	-1.37	Y48A6B.6							
1.25	-1.33	K10G4.3							
1.21	-1.33	pept-1							
1.59	-1.33	nhr-179							
1.07	-1.32	egl-44							
1.31	-1.32	K10D11.2							
1.32	-1.28	M04C9.4							
1.61	-1.27	T23F4.2							
1.13	-1.26	T16G12.1							
1.20	-1.26	pqn-32							
1.39	-1.25	T05F1.9							

			GO term		Upregulated upon pathogen				
UpR	DnE	Gene	GO lipid	GO defense	Sma	Efa	PL	Dc	Har
1.10	-1.24	E01G4.6							
1.07	-1.24	ZK180.6							
1.09	-1.23	R09H10.5							
1.65	-1.23	nhr-269							
1.13	-1.22	clec-84							
1.18	-1.18	C18H9.6							
1.20	-1.18	F09F7.5							
1.22	-1.16	ZK287.9							
1.38	-1.15	F42G4.5							
1.08	-1.14	peb-1							
1.27	-1.12	vha-6							
1.11	-1.11	fbxa-30							
1.35	-1.11	clec-17							
1.16	-1.10	F48G7.13							
1.13	-1.10	Y34B4A.6							
1.39	-1.09	C23G10.11							
1.14	-1.08	acl-7							
1.27	-1.08	C32D5.6							
1.13	-1.07	psd-1							
1.57	-1.07	nhr-99							
1.23	-1.06	F19C7.1							
1.59	-1.03	C12D12.1							
1.15	-1.02	F13H8.5							
1.56	-1.01	fbxa-8							
1.45	-1.01	F54H5.2							
1.03	-1.00	T25C12.3							

Table S4. Related to Figure 4 and Figure S5. Genes induced by ETS-4 (highlighted in red in Fig. 4D). Upregulation upon pathogenic infection is indicated by a green square. Lipid or defense-related GO terms are also indicated.

Supplementary Experimental Procedures

Strains used in this study

Strain	**CGC/** Ciosk lab No.
N2 bristol	**N2**
glp-1(e2141) III.	**CF1903**
glo-1(zu391) X.	**JJ1271**
glo-1(zu391) X.; rrrSi411 [Prege-1::rege-1(cDNA)::gfp::rege-1 3'UTR; unc-119(+)] II.	1761
rege-1(rrr13) I.	1657
rege-1(rrr13) I.; rrrSi411 [Prege-1::rege-1(cDNA)::gfp::rege-1 3'UTR; unc-119(+)] II.;unc-119(ed3)III.	1667
wgIs509 [ets-4::ty1::egfp::3xflag ; unc-119(+)]; unc-119(tm4063) III;	**OP509**
rrrSi400 [Pets-4::ets-4::gfp::ets-4 3'UTR] II.; unc-119(ed3) III.	1713
rrrSi403 [Pets-4::ets-4::gfp::unc-54 3'UTR] II.; unc-119(ed3) III.	1716
rrrSi412 [Pdpy-30::gfp::h2b::ets-4 3'UTR; unc-119 (+)] II.;unc-119(ed3) III.	1740
rrrSi412 [Pdpy-30::gfp::h2b::ets-4 3'UTR; unc-119 (+)] II.; rege-1(rrr13) I.; unc-119(ed3) III.	1762
rege-1(rrr21) I. [D231N, D313A, D314A, D332A]	1790
ets-4(rrr16) X.	1758
rrrSi413[Pdpy-30:: gfp::h2b::ets-4 3'UTR (F1); unc-119(+)] II; unc-119(ed3) III.	1792
rrrSi416[Pdpy-30:: gfp::h2b::ets-4 3'UTR (F2); unc-119(+)] II; unc-119(ed3) III.	1795
rrrSi418[Pdpy-30:: gfp::h2b::ets-4 3'UTR (F3); unc-119(+)] II; unc-119(ed3) III.	1797
rrrSi428[Pdpy-30:: gfp::h2b::unc-54 3'UTR with transplanted (F1S) of ets-4 3`UTR; unc-119(+)] II; unc-119(ed3) III.	1844
rrrSi431 [Prege-1::rege-1(cDNA [D231N, D313A, D314A, D332A])::gfp::rege-1 3'UTR; unc-119(+)] II.;unc-119(ed3) III.	1816
rrrSi423 [Prege-1::gfp::h2b::unc54 3'UTR; unc-118(+)] II. ; glo-1(zu391) X.	1807

Oligos used in this study

Purpose	**Name**	**Sequence**
Amplification of *rege-1* promoter	CH 84 (fw)	**GGGGACAACTTTGTATAGAAAAGTTG**ATTGCAGGTTACTGTACTCCGG
	CH 83 (rv)	**GGGGACTGCTTTTTTGTACAAACTTG**TCTTGAAATTTTGTGGTTTGG
rege-1 gene amplification (cDNA)	Reg-CDS+3UTR_fw	GGGGACAAGTTTGTACAAAAAAGCAGGCTATGGATTCAACGGCTCGTGGCCA
	Reg-E-rv	**GGG GACCACTTTGTACAAGAAAGCTGGGT**CTTT TCGGTACTCTTTTTGAGCTCG
rege-1 3'UTR amplification	Reg-3UTR_fw	**GGGGCAGCTTTCTTGTACAAAGTGG**TTCAATCAATATTATTATTTATTACATATTCTCACCGAA
	Reg-3UTR_rv	**GGGGCAACTTTGTATAATAAAGT**TGTTTAAATACAAATGTTCATTACATTC
To fuse GFP to 3'UTR of r*ege-1*	GFP_regUTR-Fne	**GGGGACAGCTTTCTTGTACAAAGTGG**GAAGTAAAGGAGAAGAACTTTTCA
	GFP_regUTR-M1ne	CATGGATGAACTATACAAATAGTTCAATCAATATTATTATTTATTACATATTCTCA
	GFP_regUTR-M2ne	TGAGAATATGTAATAAATAATAATATTGATTGAACTATTTGTATAGTTCATCCATG
	egfpetsR	**GGGGACAACTTTGTATAATAAAGTTG**AGATTATGAGACCTTTGGACTTGCA
Amplification of *ets-4* promoter	Pets-4Fn	**GGGGACAACTTTGTATAGAAAAGTTG**GATAGGCAGCTCACAAAAAATTGCT
	Pets-4Rn	**GGGGACTGCTTTTTTGTACAAACTTGTG**ATGAAGAATCTAGAGTGACAAAA

ets-4 gene amplification	ecdsF	**GGGGACAAGTTTGTACAAAAAAGCAGGCT**ATGAACGGTACTGGCTCAGTCGGTC
	ecdsR	**GGGGACCACTTTGTACAAGAAAGCTGGGT**ACAAGTTATAAGGAGGCAGGAATTTG
ets-4 3' UTR amplification	est-4-3UTR-F	**GGGGACAGCTTTCTTGTACAAAGTGG**TCATCTGGCAGAAAGACAACGACGT
	est-4-3UTR-R	**GGGGACAACTTTGTATAATAAAGTTG**AGATTATGAGACCTTTGGACTTGCACA
To fuse GFP to 3'UTR of *ets-4*	GFP_regUTR-Fne	**GGGGACAGCTTTCTTGTACAAAGTGG**GAAGTAAAGGAGAAGAACTTTTCA
	egfpetsM1	ACATGGCATGGACGAACTATACAAATGATCATCTGGCAGAAAGACAACGACGTG
	egfpetsM2	CAC GTC GTT GTC TTT CTG CCA GAT GAT CAT TTG TAT AGT TCG TCC ATG CCA TGT
	egfpetsR	**GGGGACAACTTTGTATAATAAAGTTG**AGATTATGAGACCTTTGGACTTGCA
To fuse GFP to 3'UTR of *unc-54*	egfpuncM1	TACACATGGCATGGACGAACTATACAAATGAGATAAGAGCTCCGCATCGGCCGCTGTCA
	egfpuncM2	TGA CAG CGG CCG ATG CGG AGC TCT TAT CTC ATT TGT ATA GTT CGT CCA TGC CAT GTG TA
	egfpuncR	**GGGGACAACTTTGTATAATAAAGTTG**AAACAGTTATGTTTGGTATATTGGG
sgRNA site at D231		TTGAGAGCTGTGGTTGTTGA
sgRNA site at D231		GGATCCAAGTTTGAGAGCTG
Repair template for D231N		CACCATCCAAATACAACCCGGATCCAAGTTTGAGAGCCGTTGTAGTAAATGGATCAAATGTTGCAA TGTTGTA
sgRNA site at D313, D314, D332		TGAGAATATATCTATCGTCG
sgRNA site at D313, D314, D332		CACGTGAGAATCCTGCGTGG
Repair template for D313A, D314A, D332A		ATTTTCAGAAACGTTAACGGTCGTCGAGTTGTCTGCCACG**C**CG**C**TAGATATATTCTCAGGACTGCT GAACTAAAAGACGCTGTAATTGTGTCAAACG**C**CGAATATCGTGACTTGACACGTGAGAATCC**G**GC**A** TGGAGGAAGATTGTCGAGGAGAGACTTCTTATGTTCACTT
sgRNA used to generate *ets-4(rrr16)*	esg52F	AATTGCAAATCTAAATGTTT**GTTGACTCCGTTCCGGAATG**GTTTAAGAGCTATGCTGGAA
	esg52R	TTCCAGCATAGCTCTTAAACCATTCCGGAACGGAGTCAACAAACATTTAGATTTGCAATT
	esg31F	AATTGCAAATCTAAATGTTT**GCCGGAAAAGAAGCAGCGTT**GTTTAAGAGCTATGCTGGAA
	esg31R	TTCCAGCATAGCTCTTAAACAACGCTGCTTCTTTTCCGGCAAACATTTAGATTTGCAATT
sgRNA used to generate *rege-1(rrr13)*	CH 5	AATTGCAAATCTAAATGTTT*GGATCCAAGTTTGAGAGCTG*GTTTTAGAGCTAGAAATAGC
	CH 6	GCTATTTCTAGCTCTAAAACCAGCTCTCAAACTTGGATCCAAACATTTAGATTTGCAATT
	CH 7	AATTGCAAATCTAAATGTTT*GGTGTGGATGATGACGTGGC*GTTTTAGAGCTAGAAATAGC
	CH 8	GCTATTTCTAGCTCTAAAACGCCACGTCATCATCCACACCAAACATTTAGATTTGCAATT
qPCR primers	qPCR_ets-4_fw	CTGAGAACCCGAATCATCCA
	qPCR_ets-4_rv	TCATTCATGTCTTGACTGCTCC
	C30F12.1_2_fw	CGGCAAATGAATGTTTATCCAG
	C30F12.1_2_rv	ATCAGATCCAGTATTCACAGGTC
	tbb-2 qPCR rv	TGGTGAGGGATACAAGATGG
	tbb-2 qPCR fw	GCTCATTCTCGGTTGTACCA
	qPCR_act-1_fw	CTATGTTCCAGCCATCCTTCTTGG

	qPCR_act-1_rv	TGATCTTGATCTTCATGGTTGATGG
ets-4 3' UTR F1 amplification	etsF1F	**GGGGACAGCTTTCTTGTACAAAGTGG**TCATCTGGCAGAAAGACAACGACGTG
	etsF1R	**GGGGACAACTTTGTATAATAAAGTTG**TATTGCATTACAATAAATAAATCG A
ets-4 3' UTR F2 amplification	etsF2F	**GGGGACAGCTTTCTTGTACAAAGTGG**ATTTATTTATTGTAATGCAATATTTA
	etsF2R	**GGGGACAACTTTGTATAATAAAGTTG**CACAATGATATAAAAAAACACTGGGA
ets-4 3' UTR F3 amplification	etsF3F	**GGGGACAGCTTTCTTGTACAAAGTGG**TATTACAACAATGTGTAGTCCCAGT
	etsF3R	**GGGGACAACTTTGTATAATAAAGTTG**AGATTATGAGACCTTTGGACTTGCACA
To transplant *ets-4* F1S into *unc-54* 3`UTR	ets-4SF	TCTCTTAATTTCTTTGTGGTCAATACTCTGTTTACATTTTTCAAC
	ets-4SR	CTTAAAAGAAGCTAAAAAGGAGGAATATGTTCTACAACGAAC
RACE_RT	CH 191	AGTAAACAGGGGAAGGAGGC
RACE_PCR	CH 194	GTTCAGAGTTCTACAGTCCGA
	CH 192	GGTAAAGTATTTGGGAGAGAGG
ets-4 RNA transcription	Unc54T3Fw	**AATTAACCCTCACTAAAGGGAGAA**CCCACCCCCTATTTTTGTTATTAT
	Unc54Rev	TTGAATCTACACAATTTCATTGTTAGAG
unc-54 RNA transcription	Ets4-ReBS T3 Fw	**AATTAACCCTCACTAAAGGGAGAA**TCAATACTCTGTTTACATTTTTC
	Ets4-ReBS Rev	AGGAATATGTTCTACAACGAAC

Supplemental references

Engelmann, I., Griffon, A., Tichit, L., Montañana-Sanchis, F., Wang, G., Reinke, V., Waterston, R.H., Hillier, L.W., Ewbank, J.J., 2011. A comprehensive analysis of gene expression changes provoked by bacterial and fungal infection in C. elegans. PLoS ONE 6, e19055. doi:10.1371/journal.pone.0019055

Söding, J., Biegert, A., Lupas, A.N., 2005. The HHpred interactive server for protein homology detection and structure prediction. Nucleic Acids Res. 33, W244–8. doi:10.1093/nar/gki408

Xu, J., Peng, W., Sun, Y., Wang, X., Xu, Y., Li, X., Gao, G., Rao, Z., 2012. Structural study of MCPIP1 N-terminal conserved domain reveals a PIN-like RNase. Nucleic Acids Res. 40, 6957–6965. doi:10.1093/nar/gks359

2.2 Annex I: Phenotypical analysis of fat-loss in *rege-1(rrr13)*

2.2.1 Differences in food intake cannot explain the *rege-1* mutant phenotype

Feeding is regulated in accordance to food availability and sentient state of the animals (Luedtke et al. 2010). It represents a very complex behavior, which influences the amount of food available to the gut cells for processing, but does not always have an influence on the fat content of the animal (Srinivasan et al. 2008). To address if *rege-1(rrr13)* animals show any sign of altered food intake, we measured their pumping rate, intake of fluorescent agarose beads, and the processing of GFP-labeled bacteria. The latter to check if the bacteria that pass the pharyngeal muscle are properly crushed by the grinder in order to release their nutrients.

Pumping rate of *rege-1(rrr13)* is slightly increased

The pumping of the pharyngeal muscle is a very stereotypical behavior that can vary in its frequency, but is reproducible under stable in conditions. As this behavior is very stereotypical, the frequency by which the posterior bulb moves during the contraction/relaxation cycle can be used as an estimate of the number of pumping motions of the whole pharynx. We found that, on average, *rege-1* mutants pump slightly more frequent than wild type animals (Figure 8A). This observation might reflect an attempt to counteract their poor nutritional status, but cannot explain why *rege-1(rrr13)* exhibit reduced fat content.

Intake of fluorescent beads in *rege-1(rrr13)* is slightly decreased compared to wild type

If the coordination of the pumping motion is affected, the movement of the posterior bulb might not reflect the intake of bacteria reliably (i.e. the animals move their posterior bulb, but release bacteria back into the environment). To explore this option, fluorescent agarose beads of the size of an average bacteria (0.5µm) where mixed with normal OP50, fed to the animals and the intake of particles was monitored by measuring the fluorescence in the gut. A slight reduction of fluorescent signal can be observed in *rege-1* mutants *versus* wild type animals on average. However, as a large population of wild type animals exhibit quite weak signal and we find many *rege-1* mutants with high fluorescence signal, we think that alteration of bacteria intake between these two strains cannot explain the *rege-1(rrr13)* fat loss. (Figure 8B).

***rege-1(rrr13)* animals have a functional grinder**

The task of the terminal bulb is to reliably crush bacteria to: i) release their nutrient content into the intestinal lumen and ii) kill any potentially pathogenic bacteria to reduce the possibility of infection. Malfunctions of the grinder impair the uptake of nutrients and render animals more susceptible to infection (Labrousse et al. 2000). To investigate the functionality of the grinder, we fed GFP-expressing

bacteria and monitored their distribution within the pharynx and the intestine. In wild type animals GFP locates mainly in the pharynx and weakly in the intestinal lumen, thus the bacteria are crushed sufficiently to release their content. In contrast, in the negative control *eat-2,* mutants show hardly any visible GFP in the pharynx (reflecting their previously reported feeding defect (Raizen, Lee, and Avery 1995)), but very strong GFP signal in the gut. This drastic increase of GFP reflects the insufficient grinding of microbes and retention of live bacteria in the intestine previously reported (So et al. 2011). In *rege-1(rrr13)* animals GFP localizes in the pharynx and is absent from the intestine (Figure 8C). Thus, we conclude that the bacteria are properly crushed and their interior is available to the intestinal cells of the worms.

In summary, *rege-1* mutant animals do not exhibit any change in feeding-related behavior that could explain their strong fat loss. Thus, further assays need to be applied to elucidate the pathway(s) involved in this phenotype.

2.2.2 REGE-1 in relation to major fat regulatory pathways

Knock-down of *rege-1* leads to reduced fat in *daf-2*, *daf-7* and *tph-1* mutants

The three major signaling pathways involved in fat metabolism in *C. elegans* are insulin, TGFβ and serotonin signaling. Functional loss of any of these pathways leads to a strong increase of stored fat in the animals. Interestingly, knock down of *rege-1* in all tree mutant backgrounds causes a decrease of fat (Figure 9A-C) to a different extend. This indicates that REGE-1 acts downstream or in parallel to this pathways. If the *rege-1/ets-4* module is receiving any input from this signaling pathways, is yet to be tested.

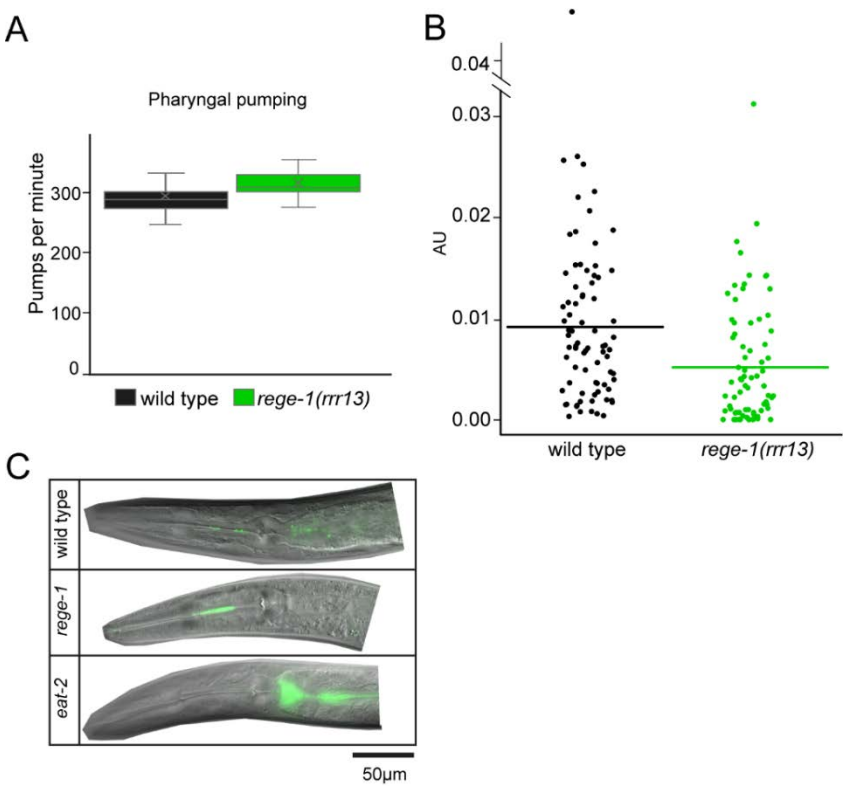

Figure 8: Food uptake in *rege-1(rrr13)* is comparable to wild type. A: Pharyngeal pumping of wild type and *rege-1(rrr13)* animals. Shown is the sum of two independent biological replicates with each 8-10 analyzed animals. **B:** Fluorescent beads assay. Each dot represents a single analyzed animal. Fluorescent intensity was normalized to the area of the worm body. **C:** Representative images of animals fed with GFP-expressing bacteria. Overlay of DIC and GFP to show localization of the bacteria. Scale bar: 50µm.

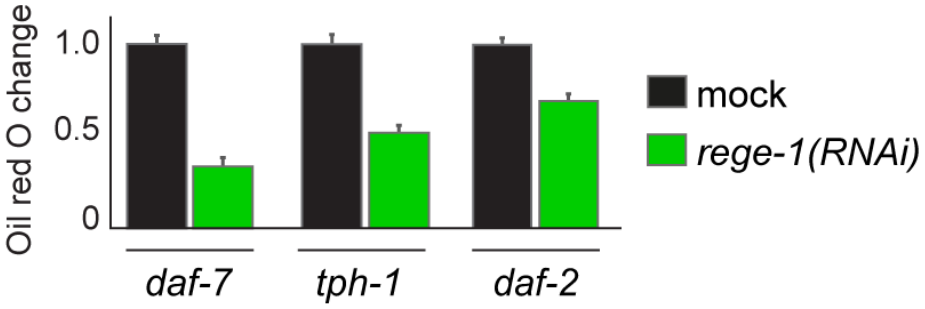

Figure 9: REGE-1 acts downstream or in parallel of major fat metabolic signaling pathways. Oil red O quantification of RNAi-mediated knock down of *rege-1* in the background of *daf-7(e1372)*, *tph-1(n4622)* or *daf-2(e1370)*. Changes in Oil red O intensity are normalized to the respective mock control. 8-10 animals were quantified per condition.

2.3 Annex II: Screens to identify ETS-4 targets that mediate *rege-1* fat loss

2.3.1 Targeted RNAi screen

Accelerated fat catabolism could be one possible explanation for the fat loss in *rege-1* mutants. Thus, knock-down of essential players of the fat pathway such as lipases and β-oxidation might reverse this phenotype. In order to identify genes, which are consequential for the fat-loss and developmental delay of *rege-1* mutant animals, we performed RNAi-mediated knock down of selected targets that fall in distinct categories: 1. Transcripts that are likely direct targets of *rege-1* as they exhibit upregulated exonic reads, but were unchanged intronic levels upon knock down of *rege-1i* highlighted in red in Figure 4A; among those we identified *ets-4*; 2. Transcripts that are upregulated upon knockdown of *rege-1* and have assigned GO terms related to lipid and fat metabolism; 3. Transcription factors that are predicted by HOMER analysis (Heinz et al. 2010) to regulate genes that are upregulated upon *rege-1* knock down; 4. Transcripts that are up-regulated upon knockdown of *rege-1* and down-regulated in the *rege-1(rrr13);ets-4i* double mutant (in red in Figure 4D) and have annotated GO terms related to lipid metabolism (4a) or innate immunity (4b) 5. Additional genes, previously reported to be important players of fat catabolism such as β-oxidation genes and lipases that were absent in the other categories. RNAi-mediated single gene knock-downs of more than 100 genes (Table 1) were conducted in *rege-1(rrr13)* background and animals were screened for increased fat and rescue of developmental delay. Only knock down of *ets-4* suppresses these phenotypes. Hence, it is likely that a distinct combination of *ets-4* targets is responsible for the fat loss. The reason why we were not able to identify these targets might have various reasons: 1. Redundancy in the fat metabolism might compensate for the loss of important fat metabolic genes and would make simultaneous knock down of two of more factors necessary; this would also be the case if multiple pathways would be affected by loss of *rege-1* 2. Inefficient knock down of the genes by RNAi.

2.3.2 Random mutagenesis screen by ethyl methanesulfonate (EMS)

To identify *ets-4* targets, which are responsible for the fat-loss phenotype of *rege-1(rrr13)*, we performed a random mutagenesis screen. EMS-based screens are widely and successfully used among *C. elegans* researches. Treatment with this alkalic agent leads to a chemical modification of guanine bases and causes them to miss-pair with an arginine; consequently introducing a heritable mutation in the next round of replication (Coulondre and Miller 1977; Brookes and Lawley 1961). The strain *rege-1(rrr13); ets4(rrr16)* containing a GFP tagged copy of ETS-4 to visualize ETS-4 levels, was subjected to EMS-based mutagenesis. Subsequently, we screened the F2 generation for a darker appearance of the gut, representing increased fat levels (screening scheme: Figure 10A). During two rounds of mutagenesis we screened roughly 50.000

haploid genomes in a semi clonal fashion and were able to recover five potential suppressors from four independent batches, representing independent mutations. (Figure 10B). Two (mut1 and mut4) of these exhibit a weak GFP signal during early larval stages and almost no GFP upon entering adult stage. Thus, they might represent a mutation in the transgene which alters its expression. However, as the expression is not completely vanished it is less likely that it is a simple loss of function allele. Furthermore, in the other three mutants (mutA, mutB, mutC) the strength of the GFP signal is similar the non-mutagenized strain. Thus, we speculate that these represent mutations in a locus distinct from the transgene. To identify genes that are causal for the suppression, we will backcross these mutants to the original strain (*rege-1(rrr13); ets4(rrr16); ets-4::GFP*) and subsequently perform deep sequencing as done before (Tocchini et al. 2014). Although the identity of the mutants is yet to be revealed, it is exciting to find that suppressors of the fat-loss of *rege-1(rrr13)* exist.

mock *versus rege-1RNAi*

1		
Transcripts with changed exonic/intronic reads		
Gene	**exonic**	**intronic**
clec-49	2.15	0.28
ets-4	2.15	-0.52
F33H12.7	2.03	0.29
ugt-37	1.97	-0.13
K10C2.1	1.90	0.04
M60.2	1.72	0.33
ZK896.5	1.61	0.28
C49C8.5	1.42	-0.07
F42G4.5	1.38	0.38
B0252.1	1.22	0.26
pqm-1	1.20	-0.13
clec-84	1.13	-0.21
R09H10.5	1.09	0.39
C01B10.6	1.08	-0.32
Y54G2A.11	1.06	0.32

2	
Upregulated transcripts GO term lipid	
Gene	**log2**
clec-70	8.25
clec-72	5.56
clec-52	4.71
clec-60	4.50
clec-71	4.20
F42A10.7	3.93
clec-53	3.56
clec-67	3.29
sru-40	3.27
math-38	3.00
asp-3	2.99
fut-2	2.91
C31H5.6	2.72
lact-3	2.59
C18A11.3	2.58
cpr-3	2.57
spp-4	1.95
clec-51	1.93
nlt-1	1.74
lys-8	1.71
Y53G8AR.7	1.57
clec-204	1.45
E02H9.5	1.39
twk-26	1.24
F19C7.2	1.09

3
TFs
Gene
elt-3
pha-4
che-1

rege-1(rrr13) over rege-1(rrr13);ets-4RNAi

4a	
Upregulated transcripts GO term lipid	
Gene	**log2**
ech-9	-10.20
ugt-18	-9.20
C48B4.1	-6.42
Y65B4BR.1	-4.67
cyp-13B1	-4.58
F09C8.1	-4.19
fil-1	-4.12
T21H3.1	-3.86
Y51H4A.5	-3.75
pmp-1	-3.52
Y49E10.18	-3.52
lipl-1	-3.36
cyp-13A12	-3.29
W03F9.4	-3.27
B0035.13	-3.15
W04C9.6	-3.09
gba-4	-3.09
gba-1	-3.02
cpt-3	-2.99
ugt-35	-2.76
fat-5	-2.72
W02B12.1	-2.70
F28H7.3	-2.60
F25A2.1	-2.58
sptl-2	-2.51
abt-4	-2.51
asm-2	-2.50

4a	
Upregulated transcripts GO term lipid	
Gene	**log2**
ugt-34	-2.26
hacd-1	-2.22
Y49E10.16	-2.22
cyp-37B1	-2.17
ech-1	-2.08
dsc-4	-2.03
lipl-2	-1.92
Y37E3.11	-1.86
ads-1	-1.78
nhr-168	-1.74
acl-1	-1.73
F46G10.4	-1.71
pho-1	-1.65
ipla-2	-1.65
ugt-44	-1.64
T22F3.11	-1.60
F54D7.2	-1.56
Y69A2AL.2	-1.51
asah-1	-1.50
sptl-1	-1.43
F59F4.1	-1.41
acs-2	-1.39
dhs-28	-1.39
cyp-32B1	-1.39
pept-1	-1.33
acl-7	-1.08
psd-1	-1.07

4b	
Upregulated transcripts GO term immunity	
Gene	**log2**
asp-12	-9.37
F20G2.5	-3.52
F11D11.3	-3.37
spp-18	-3.25
asp-3	-3.19
clec-62	-3.02
T19D12.4	-2.78
C49C3.9	-2.70
comt-2	-2.68
endu-2	-2.35
clec-66	-2.24
irg-3	-2.22
K12H4.7	-2.00
F01D5.5	-1.94
tag-244	-1.80
fbxa-30	-1.11
F19C7.1	-1.06

5
Additional genes
atgl-1
cpr-1
cpr-2
cpr-3
fil-2
ech-9/ech-1.1
ech-9/ech-1.2

Table 1: Candidate genes for the targeted RNAi-knock down screen.

Numbers on yellow background refer to the categories described in section 2.3.3. 1: "Transcripts with changed ratio in exonic/intronic reads" are transcripts, which show an increase concerning their exonic reads, but unchanged levels of intronic reads upon knock down of *rege-1* (highlighted in Figure 4A). 2: "Upregulated genes GO term lipid" contain genes that are more than two fold upregulated compared to the control (mock *versus rege-1i*) and have annotated GO terms related to lipid metabolism. 3: "TFs" are transcription factors predicted to bind the regulatory regions of transcripts which are upregulated in mock *versus rege-1* RNAi. 4: Transcripts that are upregulated upon knock down of *rege-1* (i.e. *mock versus rege-1i*) and down-regulated upon loss of *ets-4* in the background of *rege-1(rrr13)* (i.e. *rege-1(rrr13) versus rege-1(rrr13);ets-4*)) more than two-fold. For simplicity, only the transcriptional changes of *rege-1(rrr13) versus rege-1(rrr13);ets-4i* are shown for this category. 4a: "Upregulated genes GO term lipid" and 4b:"Upregulated genes GO term immunity" are genes that are more than two fold upregulated compared to the control and have annotated GO terms related to lipid metabolism and innate immunity, respectively. 5: "Additional genes" are selected lipid catabolic genes which are not already present in other lists.

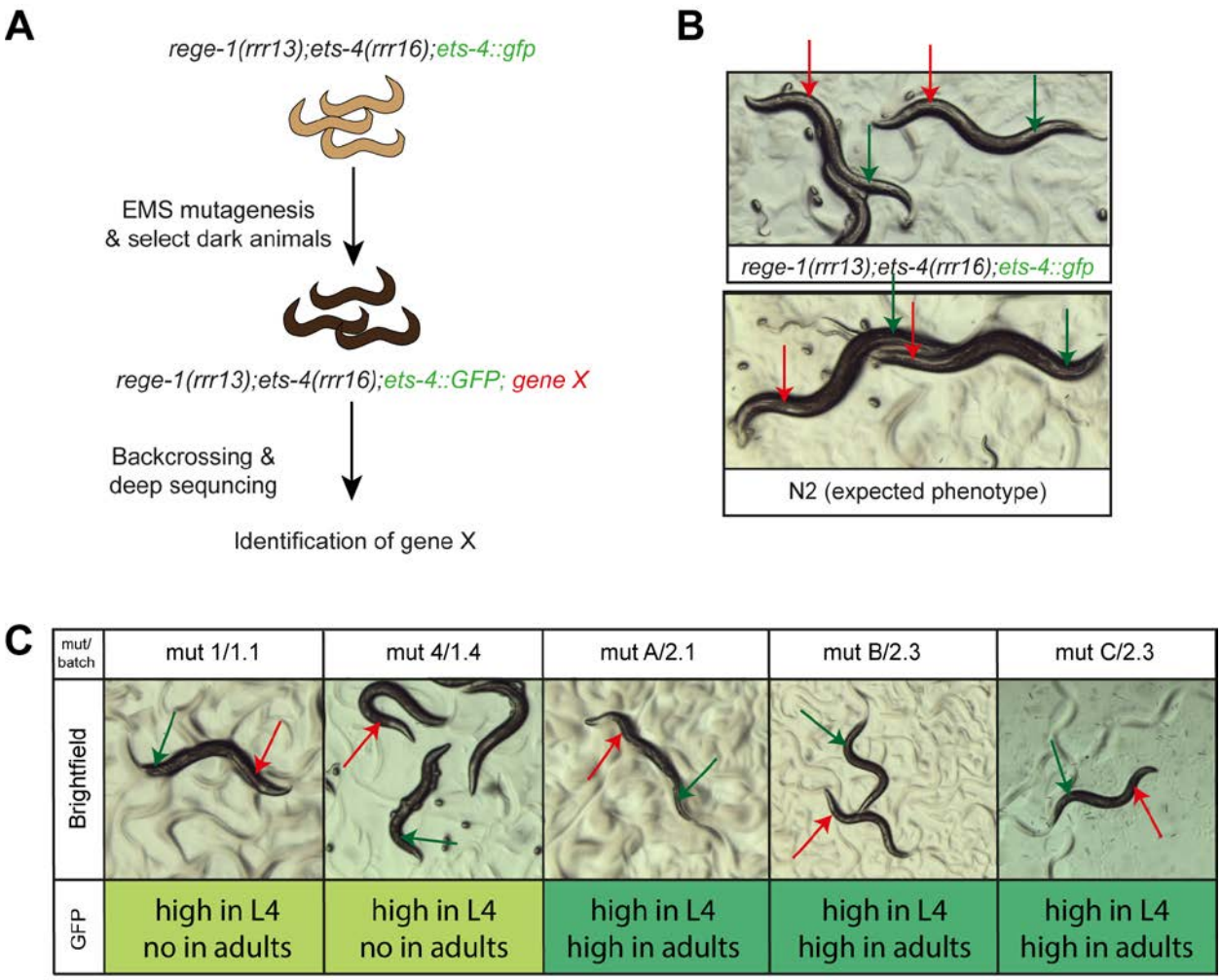

Figure 10: Random mutagenesis screen to identify *ets-4* targets that are responsible for *rege-1(rrr13)* loss of fat. A: Screening scheme. **B:** Representative pictures of the strain used for EMS-based screening *rege-1(rrr13);ets-4(rrr16);ets-4::gfp* exhibiting a pale phenotype and wild type (N2) animals with a dark gut representing the desired suppressor phenotype. Red and green arrows point to regions behind the pharynx and close to the tail, respectively, where changes in fat content in the animals are most visible **C:** representative pictures of mutants obtained from the screen and indicated GFP expression. Mutant name and the batch number is indicated "1"= first round of screening "2"= second round of screening. mut B/2.3 and mut C/2.3 were found in the same batch.

Experimental procedures of additional results

Pumping rate

Animals were bleached and grown to L4 stage. 20-30 L4 were picked to fresh plates and incubated overnight to develop into young adults. Animals were given some acclimation time under the light microscope (few minutes), then pumping of individual animals was recorded 3x for about 1 minute. To determine the pumping rate, 15 second videos of continuous pumping were slowed down to 0.5x speed and movement of the terminal bulb was counted manually; the 15 sec videos were used to estimate the pumping rate per minute. Each video was counted three times to ensure reliability. From each strain, 8-10 worms were used and their pumping rate was assayed from 3 different videos (i.e. 3 different minutes); two biological replicates were summed.

Beads assay

Staged and washed L4 are pipetted into wells of a 384-well plate (15 worms/well) that contain S-basal with OP50 (final 6mg/ml) and acclimated overnight. Fluorescent beads (Sigma, L3280 – 1 ml) were added: 50 µl of a 1:500 dilution in S-basal. Suspension was mixed, plate covered and incubated 15 minutes at RT. Animals were then transferred to a 1.5ml tube, washed twice, and immobilized with 10µl of 0.04M levamizol. Images were taken under 10x magnification with 50ms exposure in the red channel. Images were analyzed using a cell profiler file "Measuring ingested beads RFP levels with Area". This pipe-line applies a threshold that eliminates the average background and normalizes to the size of the animal (area).

Feeding of GFP bacteria

Young adults were collected, washed two times with M9 to remove residual OP50 bacteria and placed on plates seeded with GFP-expressing OP50 bacteria. After incubation for 20 minutes, animals were mounted on agarose pads and GFP distribution was observed under 40x magnification.

EMS-based screen

Animals were staged by hypochlorite treatment and grown to mid L4 stage. As the used strain exhibits developmental asynchrony, a batch of animals that displayed about 70-80% L4 stages animals was used. Animals were collected, washed and using sterile glass pipettes, they were transferred to a 15 ml sterile plastic centrifuge tube und spun down. Supernatant was removed and animals were diluted to a total volume of 4ml with M9, 20µl EMS (methanesulfonic acid, ethyl ester, Sigma #M0880) was added and incubated for three hours on a rotator. Afterwards, the animals were washed twice in M9 and transferred to seeded plates. The next day P0 were bleached (in three batches) to release F1, which are grow to gravid adult stage and bleached. F2 were then screened for desired phenotype.

3. DISCUSSION

3.1 Physiological changes observed in *rege-1(rrr13)*

We found that the loss of *rege*-1 is accompanied by a transcriptional increase of fat catabolic genes, which might explain their decreased fat levels. However, knock down of major lipases and genes involved in β-oxidation were not able to rescue *rege-1(rrr13)* fat loss. Another reason for decreased body fat can be reduced intake of dietary fats. Thus, we analyzed aspects of food-intake. The alterations in pharyngeal pumping rate and overall uptake of fluorescent beads in *rege-1(rrr13)* compared to wild type animals are only minor and feeding of GFP-expressing bacteria indicate proper grinding of the bacteria. Hence, we conclude that the observed changes do not account for the strong fat loss observed in *rege-1(rrr13)* and it is very likely that sufficient amount of nutrients are available to the gut cells. However, reduction in number, physical damage or alterations to the surface integrity of gut microvilli can lead to impaired transport of the nutrients form the gut lumen into the intestinal cells. To investigate this possibility, we plan to perform electron microscopy (EM) to inspect the surface of the lumen on a subcellular level. Nutrient uptake is influenced by additional factors such as proton concentration of the intestinal cells. The internal intestinal pH regulated by the Na^+/H^+-exchanger NHX-2 and was shown to influence the uptake of intact peptides form the lumen into the intestinal cells (Nehrke 2003). Loss of NHX-2 leads to decrease of intracellular pH in these epithelia cells. This disturbs the function of the peptide transporter *pept-1* (old name: *opt-2*) and consequently leads to shortage of available peptides and a pale phenotype (Nehrke 2003). To get an insight into nutrient transport across the apical epithelia cells of the intestine, fluorescently labeled fatty acids (BODIPY) can be utilized. Unfortunately, so far the quantification for this assay proved to be challenging and needs optimization before a definite statement can be made.

Perturbed defecation can cause decreased retention of bacteria content in the gut and consequential lead to fat-loss (Sheng et al. 2015). Over the length (45 seconds on average) of one cycle, three distinct muscle contractions (pBocs aBocs and Exps (Thomas 1990)) can be observed and the presence of this district motions as well as their frequency will be assessed in wild type and *rege-1(rrr13)*.

So far, we have not tested the possibility that the mechanisms involved in the fat loss (or reduced fat uptake/synthesis) might only be observable in a restricted time window. For example, upregulation of β-oxidation reduces overall body fat, but as soon as the stored fat is utilized by the animals, a steady state of lipid degradation would maintain this low levels of fat. Hence, time course experiments in which a decrease of *rege-1* or increase of *ets-4* is induced and the gradual decline of fat stores are monitored while

examining the dynamic changes of different fat metabolic pathways and markers (e.g. major lipases such as ATGL-1). To address this, we are currently constructing a degron-GFP-tagged ETS-4 transgenic line. The fusion of the small peptide degron to a protein renders the target susceptible to auxin-induced degradation (Zhang, Ward, et al. 2015). This line will be crossed to *rege-1(rrr13),* leading to increase of ETS-4 protein and low body fat. Given that this approach is successful, ETS-4 levels would decline in the present of auxin and the increase of fat can be monitored. *Vice versa*, when animals are grown on auxin plates they presumably exhibit high fat levels and when shifted to auxin-less plates the controlled decrease of fat can be monitored.

Reduction of fat synthesis and/or desaturation can be a possible cause a misbalanced fat metabolism of. Depending on the type fatty acid (FA), *de novo* synthesis accounts for about 2-20% of total FA content (Perez and Van Gilst 2008). This proportion seems to be negligible, considering that *rege-1(rrr13)* lose about 70% of their total body fat, however, misbalance of certain groups of fatty acids can have a tremendous impact on the overall fat content of the animals. For example, the double mutant of *fat-6* and *fat-7*, two fatty acid desaturases, exhibits altered FA composition alongside with growth delay and reduction of overall body fat (Brock, Browse, and Watts 2007; Watts and Browse 2000) similar to that seen in *rege-1(rrr13)*. FAT-5, a delta-9 desaturase that catalyzes the conversion of stearic acid (16:0) to palmitoleic acid (16:1Δ9) (Brock, Browse, and Watts 2006), is upregulated upon *rege-1* knockdown and down regulated upon loss of *ets-4* (i.e. in *rege-1(rrr13);ets-4i*). However, knock down of *fat-5* in *rege-1(rrr13)* background has no effect on its fat levels.

3.2 Mediation of fat-loss by ETS-4 and its targets

The fat-loss and developmental delay in *rege-1(rrr13)* animals is mediated via the transcription factor ETS-4. Impressively, RNAi-mediated knockdown of *ets-4* in *rege-1(rrr13)* rescues transcriptional and phenotypical changes alike. Thus, to identify targets of ETS-4, which mediate the observed phenotypes, we utilized two different screening methods. The targeted RNAi screen, during which we knocked down selected putative ETS-4 targets and key regulators of fat metabolism, did not reveal any suppressor. This may reflect redundancy of enzymes and pathways in fat metabolism or insufficient knock down by RNAi. To our excitement, a random mutagenesis screen revealed five potential candidates that suppress the fat-gain in *rege-1(rrr13)*. These mutants might fall into different categories: 1. *ets-4* targets that influence fat content 2. Distinct genes or *ets-4* alleles that influence *ets-4* levels and/or activity 3. Genes, which act independently of the *rege-1/ets-4* module to regulate fat metabolism. Two of the recovered mutants

show altered GFP expression compared to the non-mutagenized strain and thus, either represent mutations within genes that influence *ets*-4 levels or mutations in the *ets-4:gfp* transgene. These might be useful alleles to study upstream signaling or transcriptional and post-transcriptional regulation of *ets-4*. In addition, three mutants with high expression of GFP likely represent mutations in regions district from the transgene. In addition it will be interesting to see if one or more mutants also rescue developmental delay or if these two phenotypes of *rege-1(rrr13)* can be genetically separated.

3.3 Regulation of the *ets-4/rege-1* module

In the lab, where food is plenty and pathogens are rare, simultaneous loss of *ets-4* and *rege-1*, to our knowledge, does not have negative consequences for the animals, however, this regulatory module might be more relevant in the animals' natural habitat where they frequently experience food shortage and encounter a species rich bacterial environment. We show that *ets-4* and *rege-1* are transcriptionally activated in wild type animals upon refeeding following long-term starvation (Figure 7). This suggests that the *ets-4/rege-1* module has an active role in food processing or bacteria clearance. Furthermore, whether different stimuli act first on *ets-4* or *rege-1* levels/activity remains elusive. We find that *rege-1* acts either downstream or in parallel of major fat signaling pathways (Figure 9A-C). If and to what extend these signaling pathways might affect *rege-1/ets-4* levels and/or activity is unexplored. Feeding behavior of animals reintroduced to food is influenced by serotonin signaling (Avery and Horvitz 1990). Thus, it will be interesting to see whether serotonin modulates *rege-1/ets-4* levels.

As various infection related genes are deregulated upon loss of *rege-1*, it is tempting to speculate that signaling pathways involved in innate immunity, pathogen sensing or bacteria clearance may play a role in the control of *rege-1* and *ets-4* levels. In *C. elegans*, at least four different pathways are involved in immune response: DBL-1, DAF-2/DAF-16, MAP kinase, toll-like receptors (summarized in (Ewbank 2006)). It will be interesting to explore whether any of this signaling pathways incluence *ets-4/rege-1* levels or activity.

Among the putative targets of *rege-1* (transcripts upregulated on their exonic but not intronic reads upon knock down of *rege-1;* highlighted in red in Figure 4A) is *clec-49.* C-type lectin-like (*clec*) genes belong to a superfamily of pattern recognition receptors, which are predicted to be involved in pathogen sensing and often show de-regulation upon infection (Pees et al. 2016). *clec-49* together with *clec-39*, is crucial for immunity against *Serratia marcescens* infection (Miltsch, Seeberger, and Lepenies 2014). Knock down

of *clec-49* is does not change fat content of *rege-1* mutants. Whether *clec-49* is a true target of *rege-1* and might have any influence on the susceptibility of *rege-1* mutants to pathogens remains to be tested. However, it is intriguing to speculate that *rege-1* might serve a conserved role in immunity by directly targeting genes involved in pathogen recognition.

The dynamic regulation of energy metabolism and defense against pathogens are closely interconnected. For example, in obese patients an infiltration of adipose tissue by pro inflammatory cells drives a constant state of systemic low grade inflammation (reviewed in (Johnson, Milner, and Makowski 2012; Sell, Habich, and Eckel 2012; Wensveen et al. 2015)). This putative crosstalk becomes even more obvious in the bacterivore *C. elegans,* where energy metabolism and defense against pathogens are simultaneously happening in one tissue. The *ets-4/rege-1* module regulates innate immunity and lipid metabolic genes alike. As the mammalian Regnase-1 degrades pro-inflammatory cytokines and might be involved in differentiation of pre-adipocytes (Lipert et al. 2014; Younce and Kolattukudy 2012), the function of Regnase-1-like proteins seems to be conserved to some extent. Certainly, loss of the Regnase-1 is accompanied by the occurrence of autoantibodies and is fatal postnatal. Hence, the simpler animal model *C. elegans* may be utilized to dissect downstream regulatory mechanism and help identify targets for treatment of either obesity or auto immune diseases.

4. ACKNOWLEDGMENT

First and foremost I want to thank my supervisor Rafal Ciosk for his support and for all the help with improving my writing and presentation style, also for the confidence & reassurance he gave me during stressful times. I also want to thank my PhD committee members Prof. Dr. Michael Hall, Dr. Hugo Aguilaniu and Dr. Witold Filipowicz for the fruitful discussions during committee meetings, their valuable feedback and guidance during this project. I want to thank all former and current members of the Ciosk lab for the fun we had inside and outside the lab. I was lucky to work with an exceptional selection of smart, helpful and entertaining people during my thesis. Thanks to: Anca for keeping this lab neat, organized and fed with your delicious brownies; also for your help with all the strains. Silvi for being an exemption example of self-motivation and being my fellow Austrian. Cris for the best day ever and so much more. Chrissy for an unforgettable holiday in the U.S. national parks. Andi for being one of the most honest, straightforward and reliable people I know. Ricky for starting the cold-project and leading the list of geekiest people. Sandra for all the help with protein work and the commitment to the "cell project". Jorge for sharing all your worm knowledge and making fun of everything and everyone. Tina for the hours and hours of discussions about science, life and everything. Pooja for all your wisdom and for helping me to stay sane during the revision process. Janosch for being just the kind and cheerful person you are. Yanwu for the strains he shared, his effort with trying to teach us bioinformatics and for making me look a little less confused in comparison. Vishal for joining the *rege-1*-project and keeping it alive. Specially thanks goes to Dani and Mel, for all their support, the after work-beers that ended with morning pommes, essentially for making Basel a not so awful place after all. I also want to thank Jeremy for proof-reading my thesis, giving me valuable feedback and for his impressive pub quiz knowledge. Thank you to the Grosshans group for their insights and discussion during our joint lab meetings. Iskra for all the help with strains and worm work, especially for helping me create my very first CRISPR mutant. I want to thank the genomics facility for help with the generation of the RNA-Seq data and Dimos for the analysis. Heinz: Thanks for all the insight into protein structures and for your valuable feedback on the review. "Thanks" also to the whole FAIM team, especially to Laurent, who helped a lot with imaging and the Oil red O quantification. All this work would have taken much longer, if it weren`t for the media kitchen, which provided me with countless numbers of growth plates for my worms and buffers whenever needed. I want to thank also Elida for being always cheerful and helping me through the jungle of forms and regulations, especially in the beginning and the end. Special thanks goes to my friends and family who have supported me throughout the years of this thesis; especially my Viennese crew, who I could always come back to and it felt like I was never gone. Last but not least I want to thank Felix, who pushes me when I lack motivation and flies with me instead of bringing me back to earth; S4S4.

5. REFERENCES

Albert, P. S., S. J. Brown, and D. L. Riddle. 1981. 'Sensory control of dauer larva formation in Caenorhabditis elegans', *J Comp Neurol*, 198: 435-51.

Altintas, O., S. Park, and S. J. Lee. 2016. 'The role of insulin/IGF-1 signaling in the longevity of model invertebrates, C. elegans and D. melanogaster', *BMB Rep*, 49: 81-92.

Anantharaman, V., and L. Aravind. 2006. 'The NYN domains: novel predicted RNAses with a PIN domain-like fold', *RNA Biol*, 3: 18-27.

Angelo, G., and M. R. Van Gilst. 2009. 'Starvation protects germline stem cells and extends reproductive longevity in C. elegans', *Science*, 326: 954-8.

Antebi, A., W. H. Yeh, D. Tait, E. M. Hedgecock, and D. L. Riddle. 2000. 'daf-12 encodes a nuclear receptor that regulates the dauer diapause and developmental age in C. elegans', *Genes Dev*, 14: 1512-27.

Ashrafi, K., F. Y. Chang, J. L. Watts, A. G. Fraser, R. S. Kamath, J. Ahringer, and G. Ruvkun. 2003. 'Genome-wide RNAi analysis of Caenorhabditis elegans fat regulatory genes', *Nature*, 421: 268-72.

Atherton, H. J., O. A. Jones, S. Malik, E. A. Miska, and J. L. Griffin. 2008. 'A comparative metabolomic study of NHR-49 in Caenorhabditis elegans and PPAR-alpha in the mouse', *FEBS Lett*, 582: 1661-6.

Avery, L., and H. R. Horvitz. 1990. 'Effects of starvation and neuroactive drugs on feeding in Caenorhabditis elegans', *J Exp Zool*, 253: 263-70.

Avery, L., and B. B. Shtonda. 2003. 'Food transport in the C. elegans pharynx', *J Exp Biol*, 206: 2441-57.

Baillie, A. G., C. T. Coburn, and N. A. Abumrad. 1996. 'Reversible binding of long-chain fatty acids to purified FAT, the adipose CD36 homolog', *J Membr Biol*, 153: 75-81.

Baugh, L. R. 2013. 'To grow or not to grow: nutritional control of development during Caenorhabditis elegans L1 arrest', *Genetics*, 194: 539-55.

Bidzhekov, K., A. Zernecke, and C. Weber. 2006. 'MCP-1 induces a novel transcription factor with proapoptotic activity', *Circ Res*, 98: 1107-9.

Brey, C. W., M. P. Nelder, T. Hailemariam, R. Gaugler, and S. Hashmi. 2009. 'Kruppel-like family of transcription factors: an emerging new frontier in fat biology', *Int J Biol Sci*, 5: 622-36.

Brock, T. J., J. Browse, and J. L. Watts. 2006. 'Genetic regulation of unsaturated fatty acid composition in C. elegans', *PLoS Genet*, 2: e108.2007. 'Fatty acid desaturation and the regulation of adiposity in Caenorhabditis elegans', *Genetics*, 176: 865-75.

Brookes, P., and P. D. Lawley. 1961. 'The reaction of mono- and di-functional alkylating agents with nucleic acids', *Biochem J*, 80: 496-503.

Brooks, K. K., B. Liang, and J. L. Watts. 2009. 'The influence of bacterial diet on fat storage in C. elegans', *PLoS One*, 4: e7545.

Burnell, A. M., K. Houthoofd, K. O'Hanlon, and J. R. Vanfleteren. 2005. 'Alternate metabolism during the dauer stage of the nematode Caenorhabditis elegans', *Exp Gerontol*, 40: 850-6.

Chauhan, V. M., G. Orsi, A. Brown, D. I. Pritchard, and J. W. Aylott. 2013. 'Mapping the pharyngeal and intestinal pH of Caenorhabditis elegans and real-time luminal pH oscillations using extended dynamic range pH-sensitive nanosensors', *ACS Nano*, 7: 5577-87.

Chen, W. W., Y. H. Yi, C. H. Chien, K. C. Hsiung, T. H. Ma, Y. C. Lin, S. J. Lo, and T. C. Chang. 2016. 'Specific polyunsaturated fatty acids modulate lipid delivery and oocyte development in C. elegans revealed by molecular-selective label-free imaging', *Sci Rep*, 6: 32021.

Choudhary, V., N. Ojha, A. Golden, and W. A. Prinz. 2015. 'A conserved family of proteins facilitates nascent lipid droplet budding from the ER', *J Cell Biol*, 211: 261-71.

Coulondre, C., and J. H. Miller. 1977. 'Genetic studies of the lac repressor. III. Additional correlation of mutational sites with specific amino acid residues', *J Mol Biol*, 117: 525-67.

DePina, A. S., W. B. Iser, S. S. Park, S. Maudsley, M. A. Wilson, and C. A. Wolkow. 2011. 'Regulation of Caenorhabditis elegans vitellogenesis by DAF-2/IIS through separable transcriptional and posttranscriptional mechanisms', *BMC Physiol*, 11: 11.

Dirksen, P., S. A. Marsh, I. Braker, N. Heitland, S. Wagner, R. Nakad, S. Mader, C. Petersen, V. Kowallik, P. Rosenstiel, M. A. Felix, and H. Schulenburg. 2016. 'The native microbiome of the nematode Caenorhabditis elegans: gateway to a new host-microbiome model', *BMC Biol*, 14: 38.

Dourlen, P., A. Sujkowski, R. Wessells, and B. Mollereau. 2015. 'Fatty acid transport proteins in disease: New insights from invertebrate models', *Prog Lipid Res*, 60: 30-40.

Eberle, D., B. Hegarty, P. Bossard, P. Ferre, and F. Foufelle. 2004. 'SREBP transcription factors: master regulators of lipid homeostasis', *Biochimie*, 86: 839-48.

El-Yassimi, A., A. Hichami, P. Besnard, and N. A. Khan. 2008. 'Linoleic acid induces calcium signaling, Src kinase phosphorylation, and neurotransmitter release in mouse CD36-positive gustatory cells', *J Biol Chem*, 283: 12949-59.

Estevez, M., L. Attisano, J. L. Wrana, P. S. Albert, J. Massague, and D. L. Riddle. 1993. 'The daf-4 gene encodes a bone morphogenetic protein receptor controlling C. elegans dauer larva development', *Nature*, 365: 644-9.

Ewbank, J. J. 2006. 'Signaling in the immune response', *WormBook*: 1-12.

Fajas, L., D. Auboeuf, E. Raspe, K. Schoonjans, A. M. Lefebvre, R. Saladin, J. Najib, M. Laville, J. C. Fruchart, S. Deeb, A. Vidal-Puig, J. Flier, M. R. Briggs, B. Staels, H. Vidal, and J. Auwerx. 1997. 'The organization, promoter analysis, and expression of the human PPARgamma gene', *J Biol Chem*, 272: 18779-89.

Fang-Yen, C., L. Avery, and A. D. Samuel. 2009. 'Two size-selective mechanisms specifically trap bacteria-sized food particles in Caenorhabditis elegans', *Proc Natl Acad Sci U S A*, 106: 20093-6.

Feng, Y., B. G. Williams, F. Koumanov, A. J. Wolstenholme, and G. D. Holman. 2013. 'FGT-1 is the major glucose transporter in C. elegans and is central to aging pathways', *Biochem J*, 456: 219-29.

Gaglia, M. M., and C. Kenyon. 2009. 'Stimulation of movement in a quiescent, hibernation-like form of Caenorhabditis elegans by dopamine signaling', *J Neurosci*, 29: 7302-14.

Garg, A. V., N. Amatya, K. Chen, J. A. Cruz, P. Grover, N. Whibley, H. R. Conti, G. Hernandez Mir, T. Sirakova, E. C. Childs, T. E. Smithgall, P. S. Biswas, J. K. Kolls, M. J. McGeachy, P. E. Kolattukudy, and S. L. Gaffen. 2015. 'MCPIP1 Endoribonuclease Activity Negatively Regulates Interleukin-17-Mediated Signaling and Inflammation', *Immunity*, 43: 475-87.

Gems, D., A. J. Sutton, M. L. Sundermeyer, P. S. Albert, K. V. King, M. L. Edgley, P. L. Larsen, and D. L. Riddle. 1998. 'Two pleiotropic classes of daf-2 mutation affect larval arrest, adult behavior, reproduction and longevity in Caenorhabditis elegans', *Genetics*, 150: 129-55.

Georgi, L. L., P. S. Albert, and D. L. Riddle. 1990. 'daf-1, a C. elegans gene controlling dauer larva development, encodes a novel receptor protein kinase', *Cell*, 61: 635-45.

Goszczynski, B., V. V. Captan, A. M. Danielson, B. R. Lancaster, and J. D. McGhee. 2016. 'A 44 bp intestine-specific hermaphrodite-specific enhancer from the C. elegans vit-2 vitellogenin gene is directly regulated by ELT-2, MAB-3, FKH-9 and DAF-16 and indirectly regulated by the germline, by daf-2/insulin signaling and by the TGF-beta/Sma/Mab pathway', *Dev Biol*, 413: 112-27.

Goujon, M., H. McWilliam, W. Li, F. Valentin, S. Squizzato, J. Paern, and R. Lopez. 2010. 'A new bioinformatics analysis tools framework at EMBL-EBI', *Nucleic Acids Res*, 38: W695-9.

Greer, E. R., C. L. Perez, M. R. Van Gilst, B. H. Lee, and K. Ashrafi. 2008. 'Neural and molecular dissection of a C. elegans sensory circuit that regulates fat and feeding', *Cell Metab*, 8: 118-31.

Gumienny, T. L., and C. Savage-Dunn. 2013. 'TGF-beta signaling in C. elegans', *WormBook*: 1-34.

Habacher, C., Y. Guo, R. Venz, P. Kumari, A. Neagu, D. Gaidatzis, E. B. Harvald, N. J. Faergeman, H. Gut, and R. Ciosk. 2016. 'Ribonuclease-Mediated Control of Body Fat', *Dev Cell*, 39: 359-69.

Han, S., E. A. Schroeder, C. G. Silva-Garcia, K. Hebestreit, W. B. Mair, and A. Brunet. 2017. 'Mono-unsaturated fatty acids link H3K4me3 modifiers to C. elegans lifespan', *Nature*.

Happel, C., D. Ramalingam, and J. M. Ziegelbauer. 2016. 'Virus-Mediated Alterations in miRNA Factors and Degradation of Viral miRNAs by MCPIP1', *PLoS Biol*, 14: e2000998.

Hashmi, S., Q. Ji, J. Zhang, R. S. Parhar, C. H. Huang, C. Brey, and R. Gaugler. 2008. 'A Kruppel-like factor in Caenorhabditis elegans with essential roles in fat regulation, cell death, and phagocytosis', *DNA Cell Biol*, 27: 545-51.

Heinz, S., C. Benner, N. Spann, E. Bertolino, Y. C. Lin, P. Laslo, J. X. Cheng, C. Murre, H. Singh, and C. K. Glass. 2010. 'Simple combinations of lineage-determining transcription factors prime cis-regulatory elements required for macrophage and B cell identities', *Mol Cell*, 38: 576-89.

Hellerer, T., C. Axang, C. Brackmann, P. Hillertz, M. Pilon, and A. Enejder. 2007. 'Monitoring of lipid storage in Caenorhabditis elegans using coherent anti-Stokes Raman scattering (CARS) microscopy', *Proc Natl Acad Sci U S A*, 104: 14658-63.

Hills, T., P. J. Brockie, and A. V. Maricq. 2004. 'Dopamine and glutamate control area-restricted search behavior in Caenorhabditis elegans', *J Neurosci*, 24: 1217-25.

Huang, S., S. Liu, J. J. Fu, T. Tony Wang, X. Yao, A. Kumar, G. Liu, and M. Fu. 2015. 'Monocyte Chemotactic Protein-induced Protein 1 and 4 Form a Complex but Act Independently in Regulation of Interleukin-6 mRNA Degradation', *J Biol Chem*, 290: 20782-92.

Hudson, B. P., M. A. Martinez-Yamout, H. J. Dyson, and P. E. Wright. 2004. 'Recognition of the mRNA AU-rich element by the zinc finger domain of TIS11d', *Nat Struct Mol Biol*, 11: 257-64.

Irazoqui, J. E., J. M. Urbach, and F. M. Ausubel. 2010. 'Evolution of host innate defence: insights from Caenorhabditis elegans and primitive invertebrates', *Nat Rev Immunol*, 10: 47-58.

Iwasaki, H., O. Takeuchi, S. Teraguchi, K. Matsushita, T. Uehata, K. Kuniyoshi, T. Satoh, T. Saitoh, M. Matsushita, D. M. Standley, and S. Akira. 2011. 'The IkappaB kinase complex regulates the stability of cytokine-encoding mRNA induced by TLR-IL-1R by controlling degradation of regnase-1', *Nat Immunol*, 12: 1167-75.

Jeltsch, K. M., D. Hu, S. Brenner, J. Zoller, G. A. Heinz, D. Nagel, K. U. Vogel, N. Rehage, S. C. Warth, S. L. Edelmann, R. Gloury, N. Martin, C. Lohs, M. Lech, J. E. Stehklein, A. Geerlof, E. Kremmer, A. Weber, H. J. Anders, I. Schmitz, M. Schmidt-Supprian, M. Fu, H. Holtmann, D. Krappmann, J. Ruland, A. Kallies, M. Heikenwalder, and V. Heissmeyer. 2014. 'Cleavage of roquin and regnase-1 by the paracaspase MALT1 releases their cooperatively repressed targets to promote T(H)17 differentiation', *Nat Immunol*, 15: 1079-89.

Jo, H., J. Shim, J. H. Lee, J. Lee, and J. B. Kim. 2009. 'IRE-1 and HSP-4 contribute to energy homeostasis via fasting-induced lipases in C. elegans', *Cell Metab*, 9: 440-8.

Johnson, A. R., J. J. Milner, and L. Makowski. 2012. 'The inflammation highway: metabolism accelerates inflammatory traffic in obesity', *Immunol Rev*, 249: 218-38.

Juozaityte, V., D. Pladevall-Morera, A. Podolska, S. Norgaard, B. Neumann, and R. Pocock. 2017. 'The ETS-5 transcription factor regulates activity states in Caenorhabditis elegans by controlling satiety', *Proc Natl Acad Sci U S A*, 114: E1651-e58.

Jura, J., L. Skalniak, and A. Koj. 2012. 'Monocyte chemotactic protein-1-induced protein-1 (MCPIP1) is a novel multifunctional modulator of inflammatory reactions', *Biochim Biophys Acta*, 1823: 1905-13.

Kage-Nakadai, E., H. Kobuna, M. Kimura, K. Gengyo-Ando, T. Inoue, H. Arai, and S. Mitani. 2010. 'Two very long chain fatty acid acyl-CoA synthetase genes, acs-20 and acs-22, have roles in the cuticle surface barrier in Caenorhabditis elegans', *PLoS One*, 5: e8857.

Kenyon, C., J. Chang, E. Gensch, A. Rudner, and R. Tabtiang. 1993. 'A C. elegans mutant that lives twice as long as wild type', *Nature*, 366: 461-4.

Kenyon, C. J. 2010. 'The genetics of ageing', *Nature*, 464: 504-12.

Kim, J. B., G. D. Spotts, Y. D. Halvorsen, H. M. Shih, T. Ellenberger, H. C. Towle, and B. M. Spiegelman. 1995. 'Dual DNA binding specificity of ADD1/SREBP1 controlled by a single amino acid in the basic helix-loop-helix domain', *Mol Cell Biol*, 15: 2582-8.

Kim, V. N., J. Han, and M. C. Siomi. 2009. 'Biogenesis of small RNAs in animals', *Nat Rev Mol Cell Biol*, 10: 126-39.

Kimble, J., and W. J. Sharrock. 1983. 'Tissue-specific synthesis of yolk proteins in Caenorhabditis elegans', *Dev Biol*, 96: 189-96.

Kimura, K. D., H. A. Tissenbaum, Y. Liu, and G. Ruvkun. 1997. 'daf-2, an insulin receptor-like gene that regulates longevity and diapause in Caenorhabditis elegans', *Science*, 277: 942-6.

Kitaoka, S., A. D. Morielli, and F. Q. Zhao. 2013. 'FGT-1 is a mammalian GLUT2-like facilitative glucose transporter in Caenorhabditis elegans whose malfunction induces fat accumulation in intestinal cells', *PLoS One*, 8: e68475. 2016. 'FGT-1-mediated glucose uptake is defective in insulin/IGF-like signaling mutants in Caenorhabditis elegans', *FEBS Open Bio*, 6: 576-85.

Klass, M., and D. Hirsh. 1976. 'Non-ageing developmental variant of Caenorhabditis elegans', *Nature*, 260: 523-5.

Klemm, R. W., J. P. Norton, R. A. Cole, C. S. Li, S. H. Park, M. M. Crane, L. Li, D. Jin, A. Boye-Doe, T. Y. Liu, Y. Shibata, H. Lu, T. A. Rapoport, R. V. Farese, Jr., C. Blackstone, Y. Guo, and H. Y. Mak. 2013. 'A conserved role for atlastin GTPases in regulating lipid droplet size', *Cell Rep*, 3: 1465-75.

Kniazeva, M., M. Sieber, S. McCauley, K. Zhang, J. L. Watts, and M. Han. 2003. 'Suppression of the ELO-2 FA elongation activity results in alterations of the fatty acid composition and multiple physiological defects, including abnormal ultradian rhythms, in Caenorhabditis elegans', *Genetics*, 163: 159-69.

Kobayashi, H., and Y. Tomari. 2016. 'RISC assembly: Coordination between small RNAs and Argonaute proteins', *Biochim Biophys Acta*, 1859: 71-81.

Koopman, M., H. Michels, B. M. Dancy, R. Kamble, L. Mouchiroud, J. Auwerx, E. A. Nollen, and R. H. Houtkooper. 2016. 'A screening-based platform for the assessment of cellular respiration in Caenorhabditis elegans', *Nat Protoc*, 11: 1798-816.

Labrousse, A., S. Chauvet, C. Couillault, C. L. Kurz, and J. J. Ewbank. 2000. 'Caenorhabditis elegans is a model host for Salmonella typhimurium', *Curr Biol*, 10: 1543-5.

Lai, W. S., E. A. Kennington, and P. J. Blackshear. 2002. 'Interactions of CCCH zinc finger proteins with mRNA: non-binding tristetraprolin mutants exert an inhibitory effect on degradation of AU-rich element-containing mRNAs', *J Biol Chem*, 277: 9606-13.

Lapierre, L. R., M. J. Silvestrini, L. Nunez, K. Ames, S. Wong, T. T. Le, M. Hansen, and A. Melendez. 2013. 'Autophagy genes are required for normal lipid levels in C. elegans', *Autophagy*, 9: 278-86.

Larance, M., E. Pourkarimi, B. Wang, A. Brenes Murillo, R. Kent, A. I. Lamond, and A. Gartner. 2015. 'Global Proteomics Analysis of the Response to Starvation in C. elegans', *Mol Cell Proteomics*, 14: 1989-2001.

Le Foll, C., A. A. Dunn-Meynell, and B. E. Levin. 2015. 'Role of FAT/CD36 in fatty acid sensing, energy, and glucose homeostasis regulation in DIO and DR rats', *Am J Physiol Regul Integr Comp Physiol*, 308: R188-98.

Le Foll, C., A. Dunn-Meynell, S. Musatov, C. Magnan, and B. E. Levin. 2013. 'FAT/CD36: a major regulator of neuronal fatty acid sensing and energy homeostasis in rats and mice', *Diabetes*, 62: 2709-16.

Lee, J. H., J. Kong, J. Y. Jang, J. S. Han, Y. Ji, J. Lee, and J. B. Kim. 2014. 'Lipid droplet protein LID-1 mediates ATGL-1-dependent lipolysis during fasting in Caenorhabditis elegans', *Mol Cell Biol*, 34: 4165-76.

Lee, K., G. Y. Goh, M. A. Wong, T. L. Klassen, and S. Taubert. 2016. 'Gain-of-Function Alleles in Caenorhabditis elegans Nuclear Hormone Receptor nhr-49 Are Functionally Distinct', *PLoS One*, 11: e0162708.

Lemieux, G. A., and K. Ashrafi. 2015. 'Insights and challenges in using C. elegans for investigation of fat metabolism', *Crit Rev Biochem Mol Biol*, 50: 69-84.

Lesa, G. M., M. Palfreyman, D. H. Hall, M. T. Clandinin, C. Rudolph, E. M. Jorgensen, and G. Schiavo. 2003. 'Long chain polyunsaturated fatty acids are required for efficient neurotransmission in C. elegans', *J Cell Sci*, 116: 4965-75.

Li, M., W. Cao, H. Liu, W. Zhang, X. Liu, Z. Cai, J. Guo, X. Wang, Z. Hui, H. Zhang, J. Wang, and L. Wang. 2012. 'MCPIP1 down-regulates IL-2 expression through an ARE-independent pathway', *PLoS One*, 7: e49841.

Li, S., S. Xu, Y. Ma, S. Wu, Y. Feng, Q. Cui, L. Chen, S. Zhou, Y. Kong, X. Zhang, J. Yu, M. Wu, and S. O. Zhang. 2016. 'A Genetic Screen for Mutants with Supersized Lipid Droplets in Caenorhabditis elegans', *G3 (Bethesda)*, 6: 2407-19.

Li, W., B. Gao, S. M. Lee, K. Bennett, and D. Fang. 2007. 'RLE-1, an E3 ubiquitin ligase, regulates C. elegans aging by catalyzing DAF-16 polyubiquitination', *Dev Cell*, 12: 235-46.

Li, Y., B. Chen, W. Zou, X. Wang, Y. Wu, D. Zhao, Y. Sun, Y. Liu, L. Chen, L. Miao, C. Yang, and X. Wang. 2016. 'The lysosomal membrane protein SCAV-3 maintains lysosome integrity and adult longevity', *J Cell Biol*, 215: 167-85.

Li, Y., Y. Zhao, X. Huang, X. Lin, Y. Guo, D. Wang, C. Li, and D. Wang. 2013. 'Serotonin control of thermotaxis memory behavior in nematode Caenorhabditis elegans', *PLoS One*, 8: e77779.

Liang, J., Y. Saad, T. Lei, J. Wang, D. Qi, Q. Yang, P. E. Kolattukudy, and M. Fu. 2010. 'MCP-induced protein 1 deubiquitinates TRAF proteins and negatively regulates JNK and NF-kappaB signaling', *J Exp Med*, 207: 2959-73.

Lin, R. J., H. L. Chien, S. Y. Lin, B. L. Chang, H. P. Yu, W. C. Tang, and Y. L. Lin. 2013. 'MCPIP1 ribonuclease exhibits broad-spectrum antiviral effects through viral RNA binding and degradation', *Nucleic Acids Res*, 41: 3314-26.

Lin, R. J., J. S. Chu, H. L. Chien, C. H. Tseng, P. C. Ko, Y. Y. Mei, W. C. Tang, Y. T. Kao, H. Y. Cheng, Y. C. Liang, and S. Y. Lin. 2014. 'MCPIP1 suppresses hepatitis C virus replication and negatively regulates virus-induced proinflammatory cytokine responses', *J Immunol*, 193: 4159-68.

Ling, J., C. Brey, M. Schilling, F. Lateef, Z. P. Lopez-Dee, K. Fernandes, K. Thiruchelvam, Y. Wang, K. Chandel, K. Rau, R. Parhar, F. Al-Mohanna, R. Gaugler, and S. Hashmi. 2017. 'Defective lipid metabolism associated with mutation in klf-2 and klf-3: important roles of essential dietary salts in fat storage', *Nutr Metab (Lond)*, 14: 22.

Lipert, B., P. Wegrzyn, H. Sell, J. Eckel, M. Winiarski, A. Budzynski, M. Matlok, J. Kotlinowski, L. Ramage, M. Malecki, W. Wilk, J. Mitus, and J. Jura. 2014. 'Monocyte chemoattractant protein-induced protein 1 impairs adipogenesis in 3T3-L1 cells', *Biochim Biophys Acta*, 1843: 780-8.

Liu, F., Y. Xiao, X. L. Ji, K. Q. Zhang, and C. G. Zou. 2017. 'The cAMP-PKA pathway-mediated fat mobilization is required for cold tolerance in C. elegans', *Sci Rep*, 7: 638.

Liu, L., Z. Zhou, S. Huang, Y. Guo, Y. Fan, J. Zhang, J. Zhang, M. Fu, and Y. E. Chen. 2013. 'Zc3h12c inhibits vascular inflammation by repressing NF-kappaB activation and pro-inflammatory gene expression in endothelial cells', *Biochem J*, 451: 55-60.

Liu, Z., X. Li, Q. Ge, M. Ding, and X. Huang. 2014. 'A lipid droplet-associated GFP reporter-based screen identifies new fat storage regulators in C. elegans', *J Genet Genomics*, 41: 305-13.

Luedtke, S., V. O'Connor, L. Holden-Dye, and R. J. Walker. 2010. 'The regulation of feeding and metabolism in response to food deprivation in Caenorhabditis elegans', *Invert Neurosci*, 10: 63-76.

Luz, A. L., L. L. Smith, J. P. Rooney, and J. N. Meyer. 2015. 'Seahorse Xfe 24 Extracellular Flux Analyzer-Based Analysis of Cellular Respiration in Caenorhabditis elegans', *Curr Protoc Toxicol*, 66: 25.7.1-15.

Mao, R., R. Yang, X. Chen, E. W. Harhaj, X. Wang, and Y. Fan. 2017. 'Regnase-1, a rapid response ribonuclease regulating inflammation and stress responses', *Cell Mol Immunol*.

Matsushita, K., O. Takeuchi, D. M. Standley, Y. Kumagai, T. Kawagoe, T. Miyake, T. Satoh, H. Kato, T. Tsujimura, H. Nakamura, and S. Akira. 2009. 'Zc3h12a is an RNase essential for controlling immune responses by regulating mRNA decay', *Nature*, 458: 1185-90.

McGhee, J. D., M. C. Sleumer, M. Bilenky, K. Wong, S. J. McKay, B. Goszczynski, H. Tian, N. D. Krich, J. Khattra, R. A. Holt, D. L. Baillie, Y. Kohara, M. A. Marra, S. J. Jones, D. G. Moerman, and A. G. Robertson. 2007. 'The ELT-2 GATA-factor and the global regulation of transcription in the C. elegans intestine', *Dev Biol*, 302: 627-45.

McKay, R. M., J. P. McKay, L. Avery, and J. M. Graff. 2003. 'C elegans: a model for exploring the genetics of fat storage', *Dev Cell*, 4: 131-42.

McKay, S. J., R. Johnsen, J. Khattra, J. Asano, D. L. Baillie, S. Chan, N. Dube, L. Fang, B. Goszczynski, E. Ha, E. Halfnight, R. Hollebakken, P. Huang, K. Hung, V. Jensen, S. J. Jones, H. Kai, D. Li, A. Mah, M. Marra, J. McGhee, R. Newbury, A. Pouzyrev, D. L. Riddle, E. Sonnhammer, H. Tian, D. Tu, J. R. Tyson, G. Vatcher, A. Warner, K. Wong, Z. Zhao, and D. G. Moerman. 2003. 'Gene expression profiling of cells, tissues, and developmental stages of the nematode C. elegans', *Cold Spring Harb Symp Quant Biol*, 68: 159-69.

McWilliam, H., W. Li, M. Uludag, S. Squizzato, Y. M. Park, N. Buso, A. P. Cowley, and R. Lopez. 2013. 'Analysis Tool Web Services from the EMBL-EBI', *Nucleic Acids Res*, 41: W597-600.

Mendenhall, A., M. M. Crane, S. Leiser, G. Sutphin, P. M. Tedesco, M. Kaeberlein, T. E. Johnson, and R. Brent. 2017. 'Environmental Canalization of Life Span and Gene Expression in Caenorhabditis elegans', *J Gerontol A Biol Sci Med Sci*.

Miao, R., S. Huang, Z. Zhou, T. Quinn, B. Van Treeck, T. Nayyar, D. Dim, Z. Jiang, C. J. Papasian, Y. Eugene Chen, G. Liu, and M. Fu. 2013. 'Targeted disruption of MCPIP1/Zc3h12a results in fatal inflammatory disease', *Immunol Cell Biol*, 91: 368-76.

Miltsch, S. M., P. H. Seeberger, and B. Lepenies. 2014. 'The C-type lectin-like domain containing proteins Clec-39 and Clec-49 are crucial for Caenorhabditis elegans immunity against Serratia marcescens infection', *Dev Comp Immunol*, 45: 67-73.

Milward, K., K. E. Busch, R. J. Murphy, M. de Bono, and B. Olofsson. 2011. 'Neuronal and molecular substrates for optimal foraging in Caenorhabditis elegans', *Proc Natl Acad Sci U S A*, 108: 20672-7.

Min, J., D. T. Chiu, and Y. Wang. 2013. 'Variation in the heritability of body mass index based on diverse twin studies: a systematic review', *Obes Rev*, 14: 871-82.

Mino, T., Y. Murakawa, A. Fukao, A. Vandenbon, H. H. Wessels, D. Ori, T. Uehata, S. Tartey, S. Akira, Y. Suzuki, C. G. Vinuesa, U. Ohler, D. M. Standley, M. Landthaler, T. Fujiwara, and O. Takeuchi. 2015. 'Regnase-1 and Roquin Regulate a Common Element in Inflammatory mRNAs by Spatiotemporally Distinct Mechanisms', *Cell*, 161: 1058-73.

Mizgalska, D., P. Wegrzyn, K. Murzyn, A. Kasza, A. Koj, J. Jura, B. Jarzab, and J. Jura. 2009. 'Interleukin-1-inducible MCPIP protein has structural and functional properties of RNase and participates in degradation of IL-1beta mRNA', *FEBS J*, 276: 7386-99.

Monin, L., J. E. Gudjonsson, E. E. Childs, N. Amatya, X. Xing, A. H. Verma, B. M. Coleman, A. V. Garg, M. Killeen, A. Mathers, N. L. Ward, and S. L. Gaffen. 2017. 'MCPIP1/Regnase-1 Restricts IL-17A- and IL-17C-Dependent Skin Inflammation', *J Immunol*, 198: 767-75.

Moulle, V. S., C. Le Foll, E. Philippe, N. Kassis, C. Rouch, N. Marsollier, L. C. Bui, C. Guissard, J. Dairou, A. Lorsignol, L. Penicaud, B. E. Levin, C. Cruciani-Guglielmacci, and C. Magnan. 2013. 'Fatty acid transporter CD36 mediates hypothalamic effect of fatty acids on food intake in rats', *PLoS One*, 8: e74021.

Mullaney, B. C., and K. Ashrafi. 2009. 'C. elegans fat storage and metabolic regulation', *Biochim Biophys Acta*, 1791: 474-8.

Munir, S., S. ber Rahman, S. Rehman, N. Saba, W. Ahmad, S. Nilsson, K. Mazhar, and A. T. Naluai. 2015. 'Association analysis of GWAS and candidate gene loci in a Pakistani population with psoriasis', *Mol Immunol*, 64: 190-4.

Murphy, C. T., and P. J. Hu. 2013. 'Insulin/insulin-like growth factor signaling in C. elegans', *WormBook*: 1-43.

Narbonne, P., and R. Roy. 2009. 'Caenorhabditis elegans dauers need LKB1/AMPK to ration lipid reserves and ensure long-term survival', *Nature*, 457: 210-4.

Nehrke, K. 2003. 'A reduction in intestinal cell pHi due to loss of the Caenorhabditis elegans Na+/H+ exchanger NHX-2 increases life span', *J Biol Chem*, 278: 44657-66.

Ng, M., T. Fleming, M. Robinson, B. Thomson, N. Graetz, C. Margono, et al. 2014. 'Global, regional, and national prevalence of overweight and obesity in children and adults during 1980-2013: a systematic analysis for the Global Burden of Disease Study 2013', *Lancet*, 384: 766-81.

Noble, T., J. Stieglitz, and S. Srinivasan. 2013. 'An integrated serotonin and octopamine neuronal circuit directs the release of an endocrine signal to control C. elegans body fat', *Cell Metab*, 18: 672-84.

O'Rourke, E. J., and G. Ruvkun. 2013. 'MXL-3 and HLH-30 transcriptionally link lipolysis and autophagy to nutrient availability', *Nat Cell Biol*, 15: 668-76.

O'Rourke, E. J., A. A. Soukas, C. E. Carr, and G. Ruvkun. 2009. 'C. elegans major fats are stored in vesicles distinct from lysosome-related organelles', *Cell Metab*, 10: 430-5.

Oberst, A., M. Malatesta, R. I. Aqeilan, M. Rossi, P. Salomoni, R. Murillas, P. Sharma, M. R. Kuehn, M. Oren, C. M. Croce, F. Bernassola, and G. Melino. 2007. 'The Nedd4-binding partner 1 (N4BP1) protein is an inhibitor of the E3 ligase Itch', *Proc Natl Acad Sci U S A*, 104: 11280-5.

Ogg, S., S. Paradis, S. Gottlieb, G. I. Patterson, L. Lee, H. A. Tissenbaum, and G. Ruvkun. 1997. 'The Fork head transcription factor DAF-16 transduces insulin-like metabolic and longevity signals in C. elegans', *Nature*, 389: 994-9.

Ogg, S., and G. Ruvkun. 1998. 'The C. elegans PTEN homolog, DAF-18, acts in the insulin receptor-like metabolic signaling pathway', *Mol Cell*, 2: 887-93.

Palamiuc, L., T. Noble, E. Witham, H. Ratanpal, M. Vaughan, and S. Srinivasan. 2017. 'A tachykinin-like neuroendocrine signalling axis couples central serotonin action and nutrient sensing with peripheral lipid metabolism', *Nat Commun*, 8: 14237.

Palikaras, K., M. Mari, B. Petanidou, A. Pasparaki, G. Filippidis, and N. Tavernarakis. 2017. 'Ectopic fat deposition contributes to age-associated pathology in Caenorhabditis elegans', *J Lipid Res*, 58: 72-80.

Pathare, P. P., A. Lin, K. E. Bornfeldt, S. Taubert, and M. R. Van Gilst. 2012. 'Coordinate regulation of lipid metabolism by novel nuclear receptor partnerships', *PLoS Genet*, 8: e1002645.

Patterson, G. I., A. Koweek, A. Wong, Y. Liu, and G. Ruvkun. 1997. 'The DAF-3 Smad protein antagonizes TGF-beta-related receptor signaling in the Caenorhabditis elegans dauer pathway', *Genes Dev*, 11: 2679-90.

Pees, B., W. Yang, A. Zarate-Potes, H. Schulenburg, and K. Dierking. 2016. 'High Innate Immune Specificity through Diversified C-Type Lectin-Like Domain Proteins in Invertebrates', *J Innate Immun*, 8: 129-42.

Perez, C. L., and M. R. Van Gilst. 2008. 'A 13C isotope labeling strategy reveals the influence of insulin signaling on lipogenesis in C. elegans', *Cell Metab*, 8: 266-74.

Plenefisch, J., H. Xiao, B. Mei, J. Geng, P. R. Komuniecki, and R. Komuniecki. 2000. 'Secretion of a novel class of iFABPs in nematodes: coordinate use of the Ascaris/Caenorhabditis model systems', *Mol Biochem Parasitol*, 105: 223-36.

Pradel, E., and J. J. Ewbank. 2004. 'Genetic models in pathogenesis', *Annu Rev Genet*, 38: 347-63.

Raizen, D. M., R. Y. Lee, and L. Avery. 1995. 'Interacting genes required for pharyngeal excitation by motor neuron MC in Caenorhabditis elegans', *Genetics*, 141: 1365-82.

Ramiscal, R. R., I. A. Parish, R. S. Lee-Young, J. J. Babon, J. Blagih, A. Pratama, J. Martin, N. Hawley, J. Y. Cappello, P. F. Nieto, J. I. Ellyard, N. J. Kershaw, R. A. Sweet, C. C. Goodnow, R. G. Jones, M. A. Febbraio, C. G. Vinuesa, and V. Athanasopoulos. 2015. 'Attenuation of AMPK signaling by ROQUIN promotes T follicular helper cell formation', *Elife*, 4.

Ranganathan, R., S. C. Cannon, and H. R. Horvitz. 2000. 'MOD-1 is a serotonin-gated chloride channel that modulates locomotory behaviour in C. elegans', *Nature*, 408: 470-5.

Ren, P., C. S. Lim, R. Johnsen, P. S. Albert, D. Pilgrim, and D. L. Riddle. 1996. 'Control of C. elegans larval development by neuronal expression of a TGF-beta homolog', *Science*, 274: 1389-91.

Roy, A., M. Zhang, Y. Saad, and P. E. Kolattukudy. 2013. 'Antidicer RNAse activity of monocyte chemotactic protein-induced protein-1 is critical for inducing angiogenesis', *Am J Physiol Cell Physiol*, 305: C1021-32.

Ruiz-Romeu, E., M. Ferran, A. Gimenez-Arnau, B. Bugara, B. Lipert, J. Jura, E. F. Florencia, E. P. Prens, A. Celada, R. M. Pujol, and L. F. Santamaria-Babi. 2016. 'MCPIP1 RNase Is Aberrantly Distributed in Psoriatic Epidermis and Rapidly Induced by IL-17A', *J Invest Dermatol*, 136: 1599-607.

Ruvkun, G., and O. Hobert. 1998. 'The taxonomy of developmental control in Caenorhabditis elegans', *Science*, 282: 2033-41.

Satouchi, K., K. Hirano, M. Sakaguchi, H. Takehara, and F. Matsuura. 1993. 'Phospholipids from the free-living nematode Caenorhabditis elegans', *Lipids*, 28: 837-40.

Sawin, E. R., R. Ranganathan, and H. R. Horvitz. 2000. 'C. elegans locomotory rate is modulated by the environment through a dopaminergic pathway and by experience through a serotonergic pathway', *Neuron*, 26: 619-31.

Schneider, W. J. 1996. 'Vitellogenin receptors: oocyte-specific members of the low-density lipoprotein receptor supergene family', *Int Rev Cytol*, 166: 103-37.

Sell, H., C. Habich, and J. Eckel. 2012. 'Adaptive immunity in obesity and insulin resistance', *Nat Rev Endocrinol*, 8: 709-16.

Sharrock, W. J., M. E. Sutherlin, K. Leske, T. K. Cheng, and T. Y. Kim. 1990. 'Two distinct yolk lipoprotein complexes from Caenorhabditis elegans', *J Biol Chem*, 265: 14422-31.

Sheng, M., A. Hosseinzadeh, S. V. Muralidharan, R. Gaur, E. Selstam, and S. Tuck. 2015. 'Aberrant fat metabolism in Caenorhabditis elegans mutants with defects in the defecation motor program', *PLoS One*, 10: e0124515.

Sievers, F., A. Wilm, D. Dineen, T. J. Gibson, K. Karplus, W. Li, R. Lopez, H. McWilliam, M. Remmert, J. Soding, J. D. Thompson, and D. G. Higgins. 2011. 'Fast, scalable generation of high-quality protein multiple sequence alignments using Clustal Omega', *Mol Syst Biol*, 7: 539.

Simmer, F., C. Moorman, A. M. van der Linden, E. Kuijk, P. V. van den Berghe, R. S. Kamath, A. G. Fraser, J. Ahringer, and R. H. Plasterk. 2003. 'Genome-wide RNAi of C. elegans using the hypersensitive rrf-3 strain reveals novel gene functions', *PLoS Biol*, 1: E12.

Smolenaars, M. M., O. Madsen, K. W. Rodenburg, and D. J. Van der Horst. 2007. 'Molecular diversity and evolution of the large lipid transfer protein superfamily', *J Lipid Res*, 48: 489-502.

So, S., K. Miyahara, and Y. Ohshima. 2011. 'Control of body size in C. elegans dependent on food and insulin/IGF-1 signal', *Genes Cells*, 16: 639-51.

So, S., T. Tokumaru, K. Miyahara, and Y. Ohshima. 2011. 'Control of lifespan by food bacteria, nutrient limitation and pathogenicity of food in C. elegans', *Mech Ageing Dev*, 132: 210-2.

Somma, D., P. Mastrovito, M. Grieco, A. Lavorgna, A. Pignalosa, L. Formisano, A. M. Salzano, A. Scaloni, F. Pacifico, U. Siebenlist, and A. Leonardi. 2015. 'CIKS/DDX3X interaction controls the stability of the Zc3h12a mRNA induced by IL-17', *J Immunol*, 194: 3286-94.

Spanier, B., K. Lasch, S. Marsch, J. Benner, W. Liao, H. Hu, H. Kienberger, W. Eisenreich, and H. Daniel. 2009. 'How the intestinal peptide transporter PEPT-1 contributes to an obesity phenotype in Caenorhabditits elegans', *PLoS One*, 4: e6279.

Spieth, J., M. Nettleton, E. Zucker-Aprison, K. Lea, and T. Blumenthal. 1991. 'Vitellogenin motifs conserved in nematodes and vertebrates', *J Mol Evol*, 32: 429-38.

Srinivasan, S. 2015. 'Regulation of body fat in Caenorhabditis elegans', *Annu Rev Physiol*, 77: 161-78.

Srinivasan, S., L. Sadegh, I. C. Elle, A. G. Christensen, N. J. Faergeman, and K. Ashrafi. 2008. 'Serotonin regulates C. elegans fat and feeding through independent molecular mechanisms', *Cell Metab*, 7: 533-44.

Suzuki, H. I., M. Arase, H. Matsuyama, Y. L. Choi, T. Ueno, H. Mano, K. Sugimoto, and K. Miyazono. 2011. 'MCPIP1 ribonuclease antagonizes dicer and terminates microRNA biogenesis through precursor microRNA degradation', *Mol Cell*, 44: 424-36.

Sze, J. Y., M. Victor, C. Loer, Y. Shi, and G. Ruvkun. 2000. 'Food and metabolic signalling defects in a Caenorhabditis elegans serotonin-synthesis mutant', *Nature*, 403: 560-4.

Tanaka, T., K. Ikita, T. Ashida, Y. Motoyama, Y. Yamaguchi, and K. Satouchi. 1996. 'Effects of growth temperature on the fatty acid composition of the free-living nematode Caenorhabditis elegans', *Lipids*, 31: 1173-8.

Taubert, S., M. Hansen, M. R. Van Gilst, S. B. Cooper, and K. R. Yamamoto. 2008. 'The Mediator subunit MDT-15 confers metabolic adaptation to ingested material', *PLoS Genet*, 4: e1000021.

Taubert, S., M. R. Van Gilst, M. Hansen, and K. R. Yamamoto. 2006. 'A Mediator subunit, MDT-15, integrates regulation of fatty acid metabolism by NHR-49-dependent and -independent pathways in C. elegans', *Genes Dev*, 20: 1137-49.

Thomas, J. H. 1990. 'Genetic analysis of defecation in Caenorhabditis elegans', *Genetics*, 124: 855-72.

Tocchini, C., J. J. Keusch, S. B. Miller, S. Finger, H. Gut, M. B. Stadler, and R. Ciosk. 2014. 'The TRIM-NHL protein LIN-41 controls the onset of developmental plasticity in Caenorhabditis elegans', *PLoS Genet*, 10: e1004533.

Tontonoz, P., E. Hu, and B. M. Spiegelman. 1994. 'Stimulation of adipogenesis in fibroblasts by PPAR gamma 2, a lipid-activated transcription factor', *Cell*, 79: 1147-56.

Tsai, H. Y., C. C. Chen, D. Conte, Jr., J. J. Moresco, D. A. Chaves, S. Mitani, J. R. Yates, 3rd, M. D. Tsai, and C. C. Mello. 2015. 'A ribonuclease coordinates siRNA amplification and mRNA cleavage during RNAi', *Cell*, 160: 407-19.

Tserevelakis, G. J., E. V. Megalou, G. Filippidis, B. Petanidou, C. Fotakis, and N. Tavernarakis. 2014. 'Label-free imaging of lipid depositions in C. elegans using third-harmonic generation microscopy', *PLoS One*, 9: e84431.

Tsoi, L. C., S. L. Spain, J. Knight, E. Ellinghaus, P. E. Stuart, F. Capon, J. Ding, Y. Li, T. Tejasvi, et al.2012. 'Identification of 15 new psoriasis susceptibility loci highlights the role of innate immunity', *Nat Genet*, 44: 1341-8.

Uehata, T., and S. Akira. 2013. 'mRNA degradation by the endoribonuclease Regnase-1/ZC3H12a/MCPIP-1', *Biochim Biophys Acta*, 1829: 708-13.

Uehata, T., H. Iwasaki, A. Vandenbon, K. Matsushita, E. Hernandez-Cuellar, K. Kuniyoshi, T. Satoh, T. Mino, Y. Suzuki, D. M. Standley, T. Tsujimura, H. Rakugi, Y. Isaka, O. Takeuchi, and S. Akira. 2013. 'Malt1-induced cleavage of regnase-1 in CD4(+) helper T cells regulates immune activation', *Cell*, 153: 1036-49.

Van Gilst, M. R., H. Hadjivassiliou, A. Jolly, and K. R. Yamamoto. 2005. 'Nuclear hormone receptor NHR-49 controls fat consumption and fatty acid composition in C. elegans', *PLoS Biol*, 3: e53.

Van Gilst, M. R., H. Hadjivassiliou, and K. R. Yamamoto. 2005. 'A Caenorhabditis elegans nutrient response system partially dependent on nuclear receptor NHR-49', *Proc Natl Acad Sci U S A*, 102: 13496-501.

von Reuss, S. H., and F. C. Schroeder. 2015. 'Combinatorial chemistry in nematodes: modular assembly of primary metabolism-derived building blocks', *Nat Prod Rep*, 32: 994-1006.

Wahlby, C., A. L. Conery, M. A. Bray, L. Kamentsky, J. Larkins-Ford, K. L. Sokolnicki, M. Veneskey, K. Michaels, A. E. Carpenter, and E. J. O'Rourke. 2014. 'High- and low-throughput scoring of fat mass and body fat distribution in C. elegans', *Methods*, 68: 492-9.

Wang, H., X. Jiang, J. Wu, L. Zhang, J. Huang, Y. Zhang, X. Zou, and B. Liang. 2016. 'Iron Overload Coordinately Promotes Ferritin Expression and Fat Accumulation in Caenorhabditis elegans', *Genetics*, 203: 241-53.

Watts, J. L. 2009. 'Fat synthesis and adiposity regulation in Caenorhabditis elegans', *Trends Endocrinol Metab*, 20: 58-65.

Watts, J. L., and J. Browse. 2000. 'A palmitoyl-CoA-specific delta9 fatty acid desaturase from Caenorhabditis elegans', *Biochem Biophys Res Commun*, 272: 263-9.2002. 'Genetic dissection of polyunsaturated fatty acid synthesis in Caenorhabditis elegans', *Proc Natl Acad Sci U S A*, 99: 5854-9.

Watts, J. L., E. Phillips, K. R. Griffing, and J. Browse. 2003. 'Deficiencies in C20 polyunsaturated fatty acids cause behavioral and developmental defects in Caenorhabditis elegans fat-3 mutants', *Genetics*, 163: 581-9.

Wawro, M., J. Kochan, and A. Kasza. 2016. 'The perplexities of the ZC3H12A self-mRNA regulation', *Acta Biochim Pol*, 63: 411-5.

Wawro, M., J. Kochan, S. Krzanik, J. Jura, and A. Kasza. 2017. 'Intact NYN/PIN-Like Domain is Crucial for the Degradation of Inflammation-Related Transcripts by ZC3H12D', *J Cell Biochem*, 118: 487-98.

Wensveen, F. M., S. Valentic, M. Sestan, T. Turk Wensveen, and B. Polic. 2015. 'The "Big Bang" in obese fat: Events initiating obesity-induced adipose tissue inflammation', *Eur J Immunol*, 45: 2446-56.

Witting, M., and P. Schmitt-Kopplin. 2016. 'The Caenorhabditis elegans lipidome: A primer for lipid analysis in Caenorhabditis elegans', *Arch Biochem Biophys*, 589: 27-37.

Wu, Z., and S. Wang. 2013. 'Role of kruppel-like transcription factors in adipogenesis', *Dev Biol*, 373: 235-43.

Xie, M., and R. Roy. 2015. 'AMP-Activated Kinase Regulates Lipid Droplet Localization and Stability of Adipose Triglyceride Lipase in C. elegans Dauer Larvae', *PLoS One*, 10: e0130480.

Xu, J., W. Peng, Y. Sun, X. Wang, Y. Xu, X. Li, G. Gao, and Z. Rao. 2012. 'Structural study of MCPIP1 N-terminal conserved domain reveals a PIN-like RNase', *Nucleic Acids Res*, 40: 6957-65.

Xu, M., E. Y. Choi, and Y. K. Paik. 2014. 'Mutation of the lbp-5 gene alters metabolic output in Caenorhabditis elegans', *BMB Rep*, 47: 15-20.

Xu, M., H. J. Joo, and Y. K. Paik. 2011. 'Novel functions of lipid-binding protein 5 in Caenorhabditis elegans fat metabolism', *J Biol Chem*, 286: 28111-8.

Xu, N., S. O. Zhang, R. A. Cole, S. A. McKinney, F. Guo, J. T. Haas, S. Bobba, R. V. Farese, Jr., and H. Y. Mak. 2012. 'The FATP1-DGAT2 complex facilitates lipid droplet expansion at the ER-lipid droplet interface', *J Cell Biol*, 198: 895-911.

Yang, F., B. W. Vought, J. S. Satterlee, A. K. Walker, Z. Y. Jim Sun, J. L. Watts, R. DeBeaumont, R. M. Saito, S. G. Hyberts, S. Yang, C. Macol, L. Iyer, R. Tjian, S. van den Heuvel, A. C. Hart, G. Wagner, and A. M. Naar. 2006. 'An ARC/Mediator subunit required for SREBP control of cholesterol and lipid homeostasis', *Nature*, 442: 700-4.

Yazdi, F. T., S. M. Clee, and D. Meyre. 2015. 'Obesity genetics in mouse and human: back and forth, and back again', *PeerJ*, 3: e856.

Yen, K., T. T. Le, A. Bansal, S. D. Narasimhan, J. X. Cheng, and H. A. Tissenbaum. 2010. 'A comparative study of fat storage quantitation in nematode Caenorhabditis elegans using label and label-free methods', *PLoS One*, 5.

Yokogawa, M., T. Tsushima, N. N. Noda, H. Kumeta, Y. Enokizono, K. Yamashita, D. M. Standley, O. Takeuchi, S. Akira, and F. Inagaki. 2016. 'Structural basis for the regulation of enzymatic activity of Regnase-1 by domain-domain interactions', *Sci Rep*, 6: 22324.

You, Y. J., J. Kim, D. M. Raizen, and L. Avery. 2008. 'Insulin, cGMP, and TGF-beta signals regulate food intake and quiescence in C. elegans: a model for satiety', *Cell Metab*, 7: 249-57.

Younce, C., and P. Kolattukudy. 2012. 'MCP-1 induced protein promotes adipogenesis via oxidative stress, endoplasmic reticulum stress and autophagy', *Cell Physiol Biochem*, 30: 307-20.

Zhang, H., W. C. Wang, J. K. Chen, L. Zhou, M. Wang, Z. D. Wang, B. Yang, Y. M. Xia, S. Lei, E. Q. Fu, and T. Jiang. 2015. 'ZC3H12D attenuated inflammation responses by reducing mRNA stability of proinflammatory genes', *Mol Immunol*, 67: 206-12.

Zhang, L., J. D. Ward, Z. Cheng, and A. F. Dernburg. 2015. 'The auxin-inducible degradation (AID) system enables versatile conditional protein depletion in C. elegans', *Development*, 142: 4374-84.

Zhang, P., H. Na, Z. Liu, S. Zhang, P. Xue, Y. Chen, J. Pu, G. Peng, X. Huang, F. Yang, Z. Xie, T. Xu, P. Xu, G. Ou, S. O. Zhang, and P. Liu. 2012. 'Proteomic study and marker protein identification of Caenorhabditis elegans lipid droplets', *Mol Cell Proteomics*, 11: 317-28.

Zhang, Q., L. Fan, F. Hou, A. Dong, Y. X. Wang, and Y. Tong. 2015. 'New Insights into the RNA-Binding and E3 Ubiquitin Ligase Activities of Roquins', *Sci Rep*, 5: 15660.

Zhang, S. O., A. C. Box, N. Xu, J. Le Men, J. Yu, F. Guo, R. Trimble, and H. Y. Mak. 2010. 'Genetic and dietary regulation of lipid droplet expansion in Caenorhabditis elegans', *Proc Natl Acad Sci U S A*, 107: 4640-5.

Zhang, S. O., R. Trimble, F. Guo, and H. Y. Mak. 2010. 'Lipid droplets as ubiquitous fat storage organelles in C. elegans', *BMC Cell Biol*, 11: 96.

Zheng, J., and F. L. Greenway. 2012. 'Caenorhabditis elegans as a model for obesity research', *Int J Obes (Lond)*, 36: 186-94.

Zhou, Z., R. Miao, S. Huang, B. Elder, T. Quinn, C. J. Papasian, J. Zhang, D. Fan, Y. E. Chen, and M. Fu. 2013. 'MCPIP1 deficiency in mice results in severe anemia related to autoimmune mechanisms', *PLoS One*, 8: e82542.

Zhu, H. J., and A. W. Burgess. 2001. 'Regulation of transforming growth factor-beta signaling', *Mol Cell Biol Res Commun*, 4: 321-30.

Zimmermann, R., J. G. Strauss, G. Haemmerle, G. Schoiswohl, R. Birner-Gruenberger, M. Riederer, A. Lass, G. Neuberger, F. Eisenhaber, A. Hermetter, and R. Zechner. 2004. 'Fat mobilization in adipose tissue is promoted by adipose triglyceride lipase', *Science*, 306: 1383-6.